ROBUST CONTROL STRATEGIES FOR A FIXED BED CHEMICAL REACTOR

Thesis by

Christopher J. Webb

In Partial Fulfillment of the Requirements

for the Degree of

Doctor of Philosophy

California Institute of Technology

Pasadena, California

1990

(Submitted September 28, 1989)

To my beautiful wife, Linda. May our next 76 be even more enjoyable.

Acknowledgements

I am grateful to my advisor Manfred Morari for his support and guidance during this project. I appreciate the many hours he devoted to me discussing this work and directing my education in process control.

I am thankful to John Seinfeld for support and advice especially during the the initial phases of this project.

I am grateful to Dave Strand, Rohit Khanna, Jorge Mandler, Eric Hancyzc, and especially Hector Budman. Without your help, I would never have finished this phase of the project.

To the staff and especially Jan, Helen, Chic, George, Floyd, and Evangelos, thank you for help and advice throughout the years.

I am grateful to my family, friends, and coworkers who kept me from going crazy over the years. I wish you the best of luck in the future and smooth sailing in your endeavors. May we both look back at these times with some fond memories. I will treasure your friendship.

I wish to thank George and Jean for your special friendship. I hope the future is brighter than the present.

Special thanks to Ilona and Linda. I pray your special patience will be justly rewarded in the future.

Lastly, I wish to thank Caltech and the National Science Foundation for their financial support.

Abstract

This thesis addresses the practical application of robust control design to an experimental fixed bed reactor. Controllers are designed using robust control theory, specifically, Structured Singular Value analysis and Internal Model Control theory. These controllers are guaranteed to be stable and have good performance even when there is plant-model mismatch. To understand the sources of model mismatch and how model mismatch affects a fixed bed reactor's control design, an experimental methanation reactor was constructed.

The reactor is non-adiabatic with a constant wall temperature. A series of thermocouples located inside an axial thermowell are used to measure bed temperatures, and a gas chromatograph is used to measure gas concentrations. The pilot plant includes a feed-effluent heat exchanger and a product recycle line for positive feedback of both mass and energy.

A mathematical model of the reactor is developed from first principles. This dynamic model is a three dimensional heterogenous model. It consists of four nonlinear coupled partial differential equations. Finite difference methods are used to approximate these equations with a series of ordinary differential equations. The temperature profiles simulated using the model compare favorably with the profiles obtained from the experimental reactor.

Two control configurations are studied: the control of the hot spot temperature using the flow rate of an inert gas, and the control of the outlet concentration and temperature by manipulating the recycle flow rate and power supplied to an inlet heater. For both of these experiments, the control objective is to maintain stability and acceptable performance for a variety of operating conditions. Bounds of the amount of model uncertainty are explicitly incorporated in the controller design.

A new methodology for computing frequency domain uncertainty bounds for single-input single-output systems is presented. This new methodology uses spec-

tral analysis to identify a series of non-parametric frequency domain models and a "regions-mapping" technique to bound the frequency by frequency description of these models in the complex plane. The methodology is compared to existing non-parametric techniques and shown to be superior for identifying the uncertainty bound associated with a nonlinear system. This methodology is then applied to the hot spot temperature identification problem of the fixed bed reactor. A robust controller with a single adjustable parameter is designed for the reactor using Internal Model Control (IMC) theory. The computed uncertainty bounds are experimentally validated using the IMC controller.

A simple procedure is presented for designing a robust controller when one or more of the control variables must be inferred from other process measurements. As part of this procedure, a robust measurement selection scheme determines which process measurements should be used for inference. The measurement selection scheme is based on Structured Singular Value analysis. This procedure is successfully applied to the outlet concentration control for the experimental methanation reactor.

Contents

List of Figures

List of Tables

Chapter 1

Introduction

This thesis addresses robust control system design for an experimental fixed bed methanation reactor. The design of control systems for fixed bed reactors has traditionally been complex and arduous. These reactors are known to exhibit a number of characteristics which limit one's ability to control them. These characteristics include:

- nonlinear coupling of the kinetic and thermal processes
- physical parameters which are distributed in space and vary with time
- steady state multiplicity
- unavailability of important continuous on-line measurements most notably concentration measurements
- "wrong way" (inverse) response of some controlled variables (e.g., outlet temperature) to changes in certain manipulated variables (e.g., inlet flow rate, or inlet temperature)
- time delay caused by the slow propagation of the thermal wave through the catalyst bed

Although many papers have been written in recent years on the control of these reactors, most have been limited to the analysis of a mathematical model or to computer simulation. Those studies that have applied modern control design methods to an experimental system have had varying degrees of success. Often, these authors report that very good control is obtained if the system is operated close to the operating condition for which the controller is designed. However, when the true operating conditions are different, there is a significant degradation in the controller performance [121,108,134,133].

The difference between the model used in the design of the controller and the real system is called the model mismatch or model uncertainty. The reasons for model

uncertainty include incorrect model structure, parameter inaccuracies, unmodelled dynamics, and neglected nonlinearities. Recently, a number of control paradigms have been developed which explicitly account for model uncertainty in the design of the controller. These control paradigms are collectively referred to as robust control theory. By definition, a control system is said to be robust if in the face of model uncertainty, stability and acceptable performance are maintained.

This thesis represents the first application of robust control theory to the control system design for an experimental fixed bed reactor. It addresses several important implementational questions of major concern to the practicing engineer and as such helps to bridge the gap between theory and practice. The controllers presented in this thesis are designed in a straightforward manner and are parameterized in terms of variables understood by practitioners (e.g., speed of response). It is hoped that the techniques derived from this study will be of great use to this group.

A greater appreciation for the power of these techniques and a broader understanding of the problems addressed is obtained if we look at a brief history of fixed bed reactor control.

1.1 Historical Background

During the early seventies, modern control theory and its chief component Linear Quadratic Gaussian, LQG, control were stressed in academia. Several researchers successfully synthesized LQG controller and applied them to different fixed bed reactors [121,63,114]. When compared to the other control methodologies available at that time and specifically to multivariable PI control, the LQG controllers offered better setpoint regulation and disturbance rejection. However, to obtain these improvements, a considerable effort was required for the development of the system model.

In most cases, the researchers started from first principles and developed a series

of partial differential equations relating to the unsteady heat and material balances. These distributed parameter models were then lumped to obtain a finite number of ordinary differential equations using a reduction technique such as orthogonal collocation. From this point, the equations were rearranged to fit into state space format, and the resulting equations were linearized about an operating point before they could be used in the LQG design. For this method to be effective, accurate estimates of the reactor parameters were needed. When these parameters changed either with time or with the operating condition there was a significant degradation in the system performance. As pointed out by Wallman [133], this approach "does little to help the engineer who is uncertain about his process model and who has no hope of improving that model."

During this period, a number of other methods were applied to fixed bed reactor control including Direct Nyquist Array, characteristic loci, and pole placement. Since these method do not explicitly account for model uncertainty, they suffer from some of the same drawbacks as LQG. In fact, in the experimental studies where these controllers were compared to a LQG controller, the LQG controller usually performed better [46,19].

At this point in time, control researchers began to develop schemes which allowed for larger changes in the operating parameters. One approach taken was to adapt the controller to different operating conditions. A number of applications of both model reference adaptive control and self-tuning control to fixed bed reactor control were reported in the literature [46,19]. Unfortunately, due to their nonlinear nature, these adaptive control schemes are difficult to analyze.

An alternative approach is to design a single linear time invariant controller which will simultaneously stabilize the reactor for a variety of different operating condition. This concept of designing the controller for a "family" of plants is the premise behind the design techniques of robust control theory.

Robust control theory first started in the late 1970's when control researchers returned to frequency domain analysis techniques. As pointed out by Horowitz the issue of model uncertainty cannot be clearly addressed in the state space format [55]. A number of new, and not so new, techniques were espoused including Quantitative Feedback theory and Linear Quadratic Gaussian Control with Loop Transfer Recovery. Much attention has gone to H_∞ optimal control, to the Structured Singular Value, μ, and in chemical process control, to Internal Model Control.

Zames and coworkers [147,32] introduced optimal control methods for minimizing the ∞-norm of a transfer function related to performance. This is based in part on the fact that when model uncertainty is described as a norm bounded perturbation, conditions which guarantee closed-loop stability in light of the model uncertainty are expressed in terms of the ∞-norm. In parallel with this work was the development of singular value analysis [26] and the singular value loop shaping synthesis technique [27].

These techniques require a rather restrictive assumption that plant uncertainty has to be modelled as a single "unstructured perturbation" [25]. This shortcoming in the theory was addressed by Doyle [24] with the development of the Structured Singular Value, μ. Using μ, Doyle has shown that performance specifications can be included in the design to yield a controller which is not only robust to modelling uncertainty but also guarantees to provide a minimum level of performance.

In the chemical process industries, the emphasis has been more on the development of IMC [92]. By including an internal model in the feedback path, Garcia and Morari [34] constructed a convenient parameterization of all stabilizing controllers for an open-loop stable system. Furthermore, using IMC they were able to show clearly why non-minimum phase effects are detrimental to control system design. Finally and most importantly, they advocated the use of a simple filter to account for modelling uncertainty. This filter is used to detune the closed-loop system so

that modelling uncertainty does not cause stability problems.

1.2 Experimental Methanation Reactor

Armed with this new robust control theory, we decided to examine how robust control strategies can be applied to a fixed bed reactor. We chose to examine the control of fixed bed reactors because of their importance to the chemical process industries and because of the difficulties with control which have been observed in the past.

In order to fully appreciate the effects of model uncertainty, an experimental methanation reactor was constructed. As noted by Wallman [134], "Model mismatching has been the most significant problem (in control system design) and although certain aspects of it (can be) investigated by simulation, the full effect of manifold (model) mismatching (can) only be reliably determined by experiment."

The pilot plant is designed to include a number of features commonly found in industrial reactors. These are:

- a cooling jacket which surrounds the reactor tube and maintain a constant reactor wall temperature
- an axial thermowell
- a feed-effluent heat exchanger used for heat integration
- a product recycle stream

By designing the system in this manner, we are able to more accurately represent industrial reactors. This is an important requirement if the work presented in this thesis is to be accepted in industry.

This reactor can be operated in four different modes each leading to its own set of control problems.

1. reaction with neither energy nor product recycle

2. reaction with energy recycle only

3. reaction with product recycle only

4. reaction with both energy and product recycle

The primary control objective is to keep the concentration and flow rate at the outlet of the reactor at their operating specifications while maintaining the temperatures inside the reactor within some operating window. This operating window is defined to eliminate undesirable side reactions, to avoid the sintering of the catalyst, and to insure the safety of the system. It is also important that the controller perform well for a variety of operating conditions and when there are large upsets in the reactor. This definition of the control objective is quite general and includes most control configurations stated in the literature.

For the experiments mentioned in this study, we operate the reactor with two different control configurations:

Type of Control Problem	Controlled Variable	Manipulated Variable	Disturbance Variable
SISO Control	Hot Spot Temperature	N_2 Flow Rate	Inlet CO_2 Concentration
MIMO Control	Hot Spot Temperature	Recycle Flowrate	Wall Temperature
	Outlet CO_2 Concentration	Power Supplied to Inlet Heater	

1.3 Control Problems

1.3.1 Single-Input Single-Output (SISO) Control

In the first control problem, we examine the control of the hot spot temperature using the flow rate of an inert gas as the manipulated variable. The control objective

is to regulate the hot spot temperature using a single controller over a variety of operating conditions. For the operating conditions chosen, the hot spot temperature dynamics change significantly as the inerts flow rate varies. It is necessary to incorporate this change in the system dynamics as part of a bound on the model uncertainty.

A new technique is proposed whereby a frequency domain model and a bound on the model uncertainty are identified from input-output experiments. Using closed-loop setpoint experiments with a robust controller (IMC design), uncertainty bounds obtained from the identification experiments are shown to accurately describe the changes in the hot spot dynamics. The closed-loop hot spot temperature is also monitored for moderate changes in the inlet concentration, a disturbance. While the robust controller has not been explicitly designed to incorporate the hot spot dynamics at this new operating condition, the controller rejects the disturbance well.

1.3.2 Multiple-Input Multiple-Output (MIMO) Control

Extending the robust control design methods, we studied the control of the reactor under conditions of partial conversion. For this experiment, the controller variables are the outlet concentration and the hot spot temperature; the manipulated variables are the recycle flow rate and the amount of power applied to an inlet heater. As in the previous experiment, the objective is to obtain good closed-loop performance over a range of operating conditions.

While it is desired to control the outlet concentration, in practice, the closed-loop performance is limited by the rate at which the concentration can be measured. Concentration measurements are made using a gas chromatograph which is inherently slow. To increase this performance, the concentration is inferred from other system measurements, specifically temperature measurements. One of the main issues in the design of an inferential control scheme is in the selection of both the number of

thermocouples and their position in order to optimize the system performance. A robust measurement selection scheme based on Structured Singular Value analysis is applied. The measurements used in control are obtained from uncertain steady state gain information.

Using these temperature measurements, we identify the transfer functions relating to changes in the manipulated and disturbance variables to changes in the measured variables. In this experiment we regard changes in the reactor wall temperature as the disturbances. A robust controller is then designed and implemented on the reactor. This controller meets the control objectives.

1.4 First Principles Model of Reactor

In parallel with the design of the control system for the reactor is the development of a mathematical model suitable for process control. This model characterizes the essential dynamics found in the experimental system. A nonlinear distributed parameter first principles model of the reactor is developed from unsteady mass and energy balances. Several features are included in the model to more accurately represent the experimental system. These features include:

- heterogenous (two phase) model
- spatial derivatives in axial and radial directions
- nonlinear and time varying reaction rate
- dynamical model

This model is lumped using a finite difference method, and the resulting set of ordinary differential equations are solved using a numerically robust differential-algebraic solver. Simulated steady state temperature profiles are compared to experimental results and are found to be in good agreement. Due to the complexity

of this model, we choose to use a much simpler input-output model for the control system design. Though it is not directly used for control design the reactor model is used to:

- predict the steady state concentration and temperature profiles for new operating conditions
- understand the dynamical interactions occurring in the system
- provide a safe way to test control strategies before they are implemented on the pilot plant

1.5 Organization of Thesis

Chapter 2 presents a summary of the literature associated with experimental fixed bed reactor control. Particular attention is placed on the reactor design, the identification of the system variables, and the type of control synthesis techniques studied. Chapter 3 examines the experimental equipment and addresses the issues of reaction selection, equipment design, instrumentation, computer control, and the selection of manipulated, controlled and disturbance variables. Chapter 4 addresses the mathematical modelling of the experimental system and formulates two models: one for a feed-effluent heat exchanger, and one for the reactor. Chapter 5 addresses the SISO control problem and the problem of identifying the size of the uncertainty bound associated with a given model. A new methodology for computing frequency domain uncertainty bounds for SISO systems is presented. This method is compared to existing techniques and shown to be superior to these other methods when dealing with nonlinear plants such as the reactor. Using an IMC controller with a single adjustable filter parameter, the computed uncertainty bounds associated with a fixed bed reactor model are experimentally validated. Chapter 6 addresses the MIMO problem. In this design one of the controlled variables must be inferred

from other process measurements. A robust measurement selection scheme is presented for determining which measurements should be used for inferential control. Using this scheme, a robust controller is designed for the fixed bed reactor. This controller is shown to robustly stabilize the system. Finally, Chapter 7 summarizes the conclusions from this work and presents a number of suggestions for future research.

Chapter 2

Literature Review

A number of review papers have been written on the control of reactors and in particular the experimental control of fixed bed reactors [22,95,106,101,58]. Of these papers, the review of Jorgensen [58] is the most current and the most applicable to the current research. Instead of giving a number of broad references concerning all aspects of chemical reactors, this literature review concentrates specifically on experimental fixed bed control studies and will go into detail on these studies. For convenience, most of this detail is condensed into Tables 2.1–2.4. The reader with less specific needs should consult one of the previous references.

This author is aware of seven different research groups doing active research in experimental fixed bed reactor control.

2.1 Berkeley Group

The oldest of these groups, the Berkeley Group, investigates the control of a two bed adiabatic reactor originally designed by Hoiberg and Foss [52] in 1971 (Table 2.1). Each bed of this reactor contains a number of thermocouples running down the axis of the reactor for measuring catalyst temperatures, and several gas taps for measuring oxygen concentrations with a paramagnetic analyzer. The reaction considered is the oxidization ($\sim$ 1% O_2) of hydrogen. A quench stream between the two beds is used to modulate the inter-bed temperature and concentration. The manipulated variables consist of the quench stream flow rate and temperature. The control objective is to maintain the effluent gas concentration as inferred from one or more axial temperatures when there are disturbances in the feed temperature or concentration. The various control schemes studied include LQG, characteristic loci, time optimal control, and steady state optimization. These last two schemes are applied to an energy recovery problem in which the main concern is the control of the reactor inlet temperature.

2.2 McMasters Group

The McMasters group examines a butane hydrogenolysis reactor originally constructed by Tremblay and Wright [120] (Table 2.2). Nine thermocouples measure the axial temperatures and a gas chromatograph monitors the outlet concentration. Direct digital control maintains proper inlet hydrogen and butane flow rates — either of which may be a manipulated variable. The controlled variable varies with the experiment but is either the outlet gas concentration as inferred from internal temperatures or the hot spot temperature. In either case, the control objective is the rejection of disturbances in the reactor wall temperature. This is one of the more comprehensive studies with controllers from several different design methodologies tested. These include LQG, PI, model reference adaptive control, self-tuning control, and IMC. The last paper in this table advocates the use of the logarithm of the deviation of the hot spot from the wall temperature as the controlled variable. The author points out that this quantity is linear over a much larger operating range.

2.3 Lyngby (Denmark) Group

The Lyngby group investigates the controller design of a single bed adiabatic reactor for the oxidation of hydrogen on platinum. This reactor was constructed by Hansen and Jorgensen [44] and is discussed in [44,43,45] (Table 2.3). The reactor contains several ports along its axis for the measurement of temperatures and concentrations. The manipulated variables include the inlet temperature, concentration and flow rate. A disturbance stream downstream from the inlet (manipulated) stream modifies the gas characteristics before it reaches the reactor bed. The control objective is to maintain the entire temperature profile and outlet concentration at it desired value. Synthesis techniques investigated include LQG, direct Nyquist array, and self-tuning control. Although it is only a simulation study, Terndrup, Clement,

and Jorgensen [118] give a nice comparison of PI, direct Nyquist array, and LQG control for this system.

2.4 Santa Barbara Group

The Santa Barbara group examines the control of an autothermal reactor described in great detail by Bonvin, et al. [10,8,9] and Wong, et al. [144] (Table 2.4). This reactor consists of two concentric tubes with the inner tube is filled with a water-gas shift catalyst. The feed gas enters the annular space near the exit of the reactor bed and flows toward the top of the reactor. As it moves through the annular space, it exchanges heat with the reacting gases inside the reactor. Depending on the temperature profile inside the reactor, the feed gases can either heat or cool the catalyst bed. A heater at the inlet of the reactor bed is the manipulated variable, and three temperatures inside the catalyst bed are the measured variables [144]. The control objective is to regulate the reactor at an open-loop unstable operating point.

Using this same reactor, McDermott, Mellichamp and Rinker, show how a simple pole placement STC can be used to control the temperature immediately before the reactor hot spot at its upper steady state value or at an intermediate value corresponding to unstable steady state. By adding a second controlled variable, the exit temperature, and a second manipulated variable, the feed temperature or flow rate, the complete temperature profile of the catalyst bed is controlled [87].

2.5 Other Groups

A number of other groups have conducted much smaller studies. These include Lee and Lee who [79] investigate the control of a constant wall temperature reactor for the partial oxidation of n-butane to maleic anhydride, Chylla and Cinar [18] who

use inferential internal model control to control the exit concentrations of a tubular autothermal carbon monoxide oxidation reactor and Windes, Schwedock, and Ray [143,107] who have extensively modelled and observed the dynamic behavior of a cooled packed bed reactor for on-line estimation and optimizing control. This last group is studing the partial oxidation of methanol to formaldehyde.

Bed Type	A two bed adiabatic reactor
Reaction	Oxidization of hydrogen
Controlled Variables	Effluent gas concentration as inferred from one or more axial temperatures
Maniulated Variables	Quench stream flow rate and temperature
Disturbances	Feed temperature or concentration

Reference	Model Type	Control Strategy
Vakil, Michelsen, and Foss [121]	state	LQG
Silva, Wallman, and Foss [108]	state	LQG
Wallman, Silva, and Foss [134]	state	LQG
Wallman and Foss [133]	state	LQG
Foss, Edmunds, and Kouvaritakis [30]	transfer function	characteristic loci
Lappinga and Foss [73]	time model	time optimal control
Metchis and Foss [90]	—	on-line estimation

Table 2.1: Synopsis of work performed by Berkeley group

Bed Type	Constant wall temperature
Reaction	Butane hydrogenolysis
Controlled Variables	Either the outlet gas concentration as inferred from internal temperatures or the hot spot temperature
Maniulated Variables	Inlet feed flow rate
Disturbances	Reactor wall temperature

Reference	Model Type	Control Strategy
Jutan, et al. [61,63]	state	LQG
Wright, et al. [145]	state	MRAC
Harris, MacGregor, and Wright [46,47]	ARMAX	minimum var
Jutan, Wright and MacGregor [62]	state	LQ
Kozub, MacGregor and Wright [70]	state	LQ, IMC
Onderwater, MacGregor, and Wright [93]	state	STC

Table 2.2: Synopsis of work performed by McMasters group

Bed Type	Single bed adiabatic reactor
Reaction	Oxidation of hydrogen
Controlled Variables	Several temperature measurements
Maniulated Variables	Inlet temperature, concentration, flow rate
Disturbances	Downstream temperature, concentration, flow rate

Reference	Model Type	Control Strategy
Sorensen [113,114]	state	LQG
Sorensen, Jorgensen, and Clement [115]	state	LQG
Clement and Jorgensen [19]	state	inverse Nyquist
Hallager and Jorgensen [41]	ARMAX	LQ,STC
Goldschmidt, Hallager, and Jorgensen [39]	ARMAX	LQ,STC

Table 2.3: Synopsis of work performed by Lyngby group

Bed Type	Autothermal reactor
Reaction	Water-gas reaction
Controlled Variables	Internal temperatures
Maniulated Variables	Reactor inlet or feed temperature
Disturbances	Flow rate or heat

Reference	Model Type	Control Strategy
Wong, et al. [144]	state	pole placement
McDermott, Mellichamp, Rinker [88]	ARMAX	pole placement
McDermott, Mellichamp, Rinker [87]	ARMAX	pole placement

Table 2.4: Synopsis of work performed by Santa Barbara group

Chapter 3

Description of Experimental Reactor

Introduction

In this chapter, an experimental fixed bed reactor is described and its various components analyzed. This reactor, originally constructed by Strand [117] to study multi-variable computer control, has been extensively modified for the current control experiments. When modifying the equipment, three design goals are stressed: keep the system modular, design the equipment with the same features found in the chemical industries, and preserve the interesting reactor dynamics.

Modularity is achieved by building the reactor in separate units. Each unit, such as the reactor tube, Section 3.2.3; cooling jacket, Section 3.2.3; or feed-effluent heat exchanger, Section 3.2.2, performs a single task and is independent of the other units. This means that modifications can be made easily to any one unit without affecting the other units. Using this modular approach, the system is easier to build, modify and operate.

By designing the equipment with the same features found in industrial fixed bed catalytic reactors, it is hoped that the behavior of this pilot plant reactor will be similar to the behavior of industrial reactors. One example of this design strategy is in the use of a cooling jacket, Section 3.2.3, to cool the reactor at the tube wall. This design imitates certain industrial reactors used for the production of specialty chemicals [50,33,49].

Fixed bed chemical reactors are known to have a rich and varied behavior [58]. This behavior is often spatially dependent, nonlinear, time varying, and non-minimum phase. Furthermore, the system may have several steady states and must be operated at one of the unstable states (e.g., [144]). This dynamic behavior should be preserved in the design of the pilot plant. Equipment should not be intentionally altered to avoid control problems unless such an alteration seems reasonable in an industrial situation.

This chapter is divided into five sections: reaction, processing equipment, in-

strumentation, computer systems and software, and system variables. The reaction section describes the reactions under study and their industrial applicability, thermodynamic properties, and kinetics. The processing equipment section gives a complete physical and functional description of the processing equipment. The instrumentation section describes which measurements are made as well as how they are made. The computer systems and software section describes the computers used to analyze the system and the software which runs on them. Finally, the system variables section examines the various measured, manipulated and disturbance variables and determines which are the most likely candidates for control.

3.1 Reaction

This section describes the reactions under study, the methanation of carbon oxide. In this thesis, the term carbon oxide is defined as any mixture of carbon monoxide and carbon dioxide. These reactions are the simplest of the Fisher-Tropsch reactions in which alkanes are built from carbon oxide and hydrogen [13]. The methanation reaction is catalyzed by a number of metals including iron, cobalt, rhodium, and ruthenium [84,13], but a nickel catalyst, United Catalysts G-65RS, is used in these experiments.

Table 3.1 lists the reactions occurring in this chemical system. The top two reactions, the methanation reactions, are the desired reactions in which carbon oxide is converted to methane. The third reaction, the steam shift reaction, converts carbon monoxide to carbon dioxide. Of these three reactions, only two are independent. The other reactions are detrimental reactions and should be avoided. The first of these detrimental reactions is the carbonylization of nickel. Nickel carbonyl, $Ni(CO)_4$, is an extremely toxic gas with a exposure limit of 1 ppb [136], and its production must be avoided for safe operation. This carbonylization reaction not only produces a lethal product, it also removes the nickel from the catalyst increasing

the rate of catalyst deactivation. The other reactions listed involve the production of solid carbon, graphite. Graphite blocks the pores of the catalyst and reacts with the catalyst to form nickel carbide, NiC_3. Both of these actions slowly deactivate the catalyst. In addition, there are a number of trace elements which are known to deactivate the catalyst. These include sulfur, selenium, and the reactive metal ions especially sodium and potassium. Luckily, choosing the proper operating conditions avoids the detrimental reactions.

There are several reasons for studying this chemical system:

- Important industrial applications exist
- Reactions are well characterized thermodynamically and kinetically
- Highly exothermic reactions are known to lead to control problems
- Operating costs are minimal

The first two points will be discussed in more detail.

3.1.1 Industrial Applications

Methanation has two primary industrial applications: the clean up of feed gases in ammonia synthesis [67] and the generation of synthetic natural gas [67,129].

Ammonia Synthesis

In ammonia synthesis, the reactor is designed to convert small levels, <1%, of carbon monoxide in a feed stream containing mostly nitrogen and hydrogen to methane before this stream reaches an ammonia catalyst. Carbon monoxide is a poison to this catalyst and must be removed to prolong the catalyst life.

Synthetic Natural Gas

In synthetic natural gas production, the reactor is designed to convert a low calorific synthesis gas generated by the partial oxidation of coal to a high calorific fuel which can be used in place of natural gas. In this application, the synthesis gas starts with a relatively high concentration of carbon monoxide, 6–18%, depending on the process.

3.1.2 Thermodynamics

Table 3.2 lists the various reactions, their heats of reaction and their equilibrium constants. This table shows that both methanation reactions are highly exothermic and have large equilibrium constants, even at elevated temperatures. A large equilibrium constant implies that the reaction is nearly irreversible. This tends to simplify the modelling of this system since the reverse reactions can be safely ignored.

To promote the methanation reactions and reduce the side reactions, Vatcha [129], White [142] and Lunde [84] developed a number of thermodynamically based operating constraints. To eliminate the production of graphite, the operator has three options: increase the oxygen to carbon ratio (i.e., use carbon dioxide instead of carbon monoxide), increase the ratio of hydrogen to carbon oxide, or decrease the operating temperature to $< 900°C$. Likewise, to eliminate nickel carbonyl the reactor temperature must be kept above 210°C. Using these guidelines, carbon dioxide is chosen as the feed gas, and the system operates at temperatures above 220°C. Part of this decision is due to the formation of graphite inside the furnace, Section 3.2.2, when carbon monoxide is used as the feed; graphite does not form if carbon dioxide is used.

3.1.3 Kinetics

The kinetics of the methanation reactions have been studied by a number of authors including [68,51,127,135,128,137,84], but the studies considered most relevant to this work are those of Wedel [140], Van Herwijnen [126], and Chiang [17]. These authors used the G-65 catalyst in their experiments, and came up with the same functional form for the rate of the reaction. This functional form, which is based on a Langmuir-Hinshelwood kinetic model, is:

CO Methanation

$$\text{rate} = \frac{k_1 e^{-\frac{A_1}{RT}} P_{CO}}{\left[1 + k_2 e^{\frac{A_2}{RT}} P_{CO}\right]^2} [=] \frac{mols\ \text{CO}}{s \cdot g_{cat}} \tag{3.1}$$

CO_2 Methanation

$$\text{rate} = \frac{k_3 e^{-\frac{A_3}{RT}} P_{CO_2}}{\left[1 + k_4 e^{\frac{A_4}{RT}} P_{CO_2}\right]} [=] \frac{mols\ \text{CO}_2}{s \cdot g_{cat}} \tag{3.2}$$

Table 3.3 shows the coefficients identified by these authors.

Employing these rate expressions, it is observed that carbon monoxide methanation is first order in CO for low concentrations of CO and minus first order for high concentrations. Likewise, the carbon dioxide methanation is first order in CO_2 for low concentrations of CO_2 and independent of the concentration for high concentrations. For the operating conditions prevalent in the control experiments, this change in reaction order occurs at reactant concentrations $\ll 1\%$ which is far below the anticipated inlet concentration of 6%.

When mixtures of carbon monoxide and carbon dioxide are fed to a fixed bed reactor, Van Doesburg [123] has shown that the carbon monoxide will react preferentially and exclude the reaction of carbon dioxide. The carbon dioxide will not react until the level of CO is below 300 ppm [123]. Therefore, these two reactions

Reaction	Formula
CO Methanation	$CO + 3H_2 \rightleftharpoons CH_4 + H_2O$
CO_2 Methanation	$CO_2 + 4H_2 \rightleftharpoons CH_4 + 2H_2O$
Steam Shift	$CO + H_2O \rightleftharpoons CO_2 + H_2$
Nickel Carbonylization	$Ni + 4CO \rightleftharpoons Ni(CO)_4$
Coking	$2CO \rightleftharpoons C_s + CO_2$
Nickel Carbide	$3Ni + C_s \rightleftharpoons Ni_3C$

Table 3.1: List of reactions

Reaction	ΔH_r^0 (kcal/mol)	$\log K_p^0$	ΔH_r (300°C) (kcal/mol)	$\log K_p$ (300°C)
CO Methanation	-49.3	24.9	-51.8	7.2
CO_2 Methanation	-39.4	19.9	-42.4	5.6
Steam Shift	-9.9	5.0	-9.4	1.6
Nickel Carbonylization	-38.4	6.3	-37.5	-7.8
Coking	-41.2	21.0	-41.5	6.4
Nickel Carbide	9.0	-6.0	9.6	-2.6

Table 3.2: Thermodynmic properties of reactions

Parameter	Widel*	van Herwijnen	Chiang†	Units
CO Methanation				
k_1	1.31×10^7	58.1	1.34	mol CO/(s g atm)
A_1	23.2	10.1	37	kcal/mol
k_2	5.92	4.56×10^{-4}	110	atm^{-1}
A_2	2.52	12.4	0	kcal/mol
CO_2 Methanation				
k_3	8.66×10^4	3.78×10^8		mol CO_2/(s g atm)
A_3	19.1	25.3		kcal/mol
k_4	2.30	1,270		atm^{-1}
A_4	4.54	0		kcal/mol

*Coefficients are based on mole fraction not partial pressure
†Chiang also includes hydrogen dependency

Table 3.3: Reaction rate coefficients for methanation reactions

are decoupled from each other, and selectivity is not an issue.

3.2 Processing Equipment

In this section, the processing equipment used in the control experiments is described. As shown in the Figure 3.1, the equipment can be divided into five processing units: gas delivery, gas heating, reactor, gas cooling, and mass recycle. Each of these units specializes at a different task keeping the system modular. Each of these units will be discussed separately. Further details about the equipment can be found in [117,138].

Carefully regulated feed gases are introduced to the system and mixed with a recycle stream in the gas delivery unit. The combined gas stream is then heated in the gas heating unit before it arrives at the reactor. In the reactor, the feed gases are catalytically transformed into the products, methane and water. After the reactor, the product gases are cooled in the gas cooling unit and the condensed water is removed from the gas. Finally, the dry gas stream is recompressed and recycled back through the reactor. All of this occurs as a computer monitors the system and controls the appropriate inputs.

3.2.1 Gas Delivery Unit

The first processing unit is the gas delivery unit, Figure 3.2. The purpose of this unit is to regulate, filter and deliver the reactant gases. This unit can be divided into four parts: pressure regulation, filtration, flow control, and mixing. The feed gas is supplied in gas cylinders and passes through a series of pressure regulators before it enters the filtration area where several impurities are filtered from the gas. Then the flow rate of the filtered gas is regulated using electronic mass flow controllers, and the resultant gas streams are mixed together and with a recycle stream.

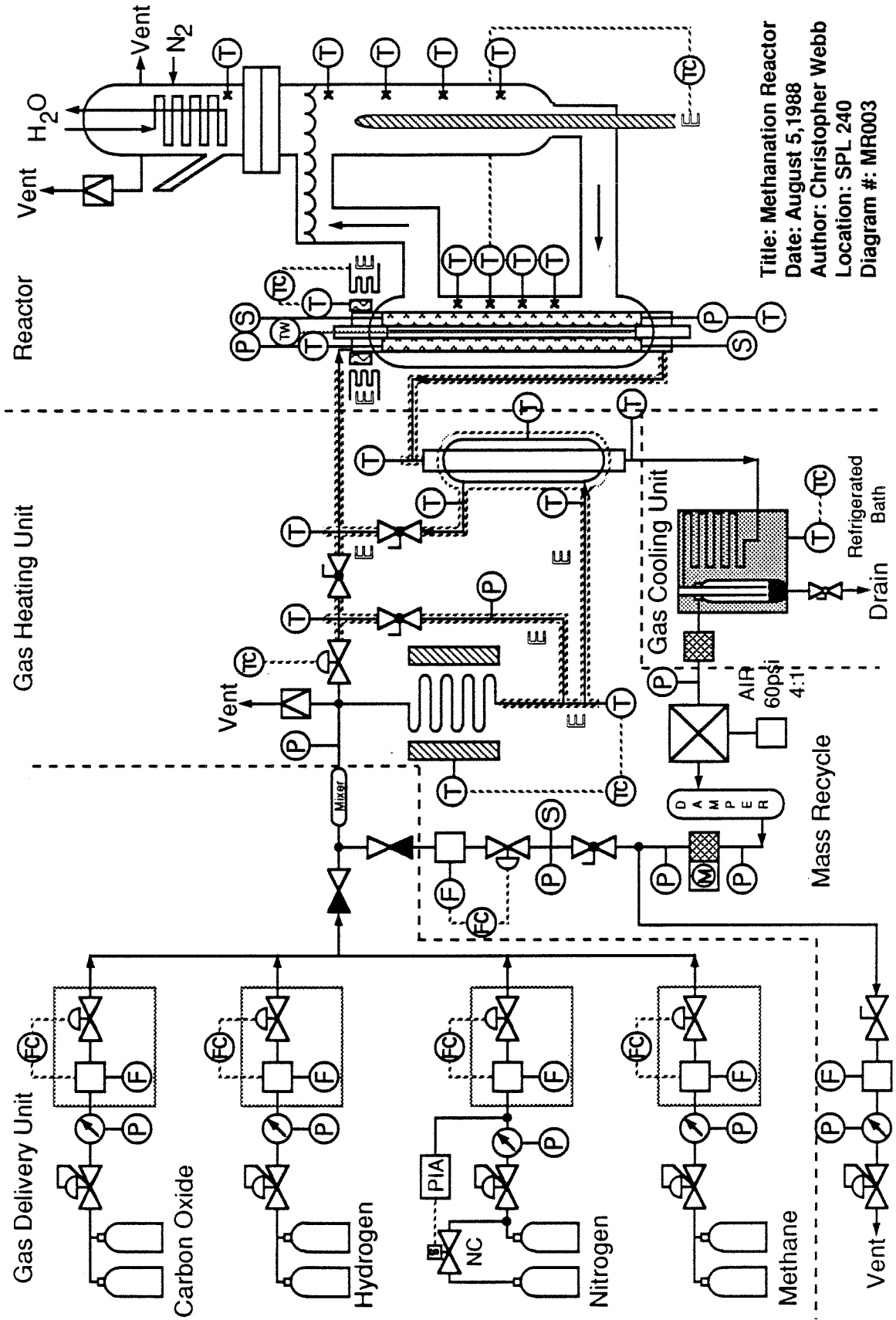

Figure 3.1: Process flowsheet for methanation reactor

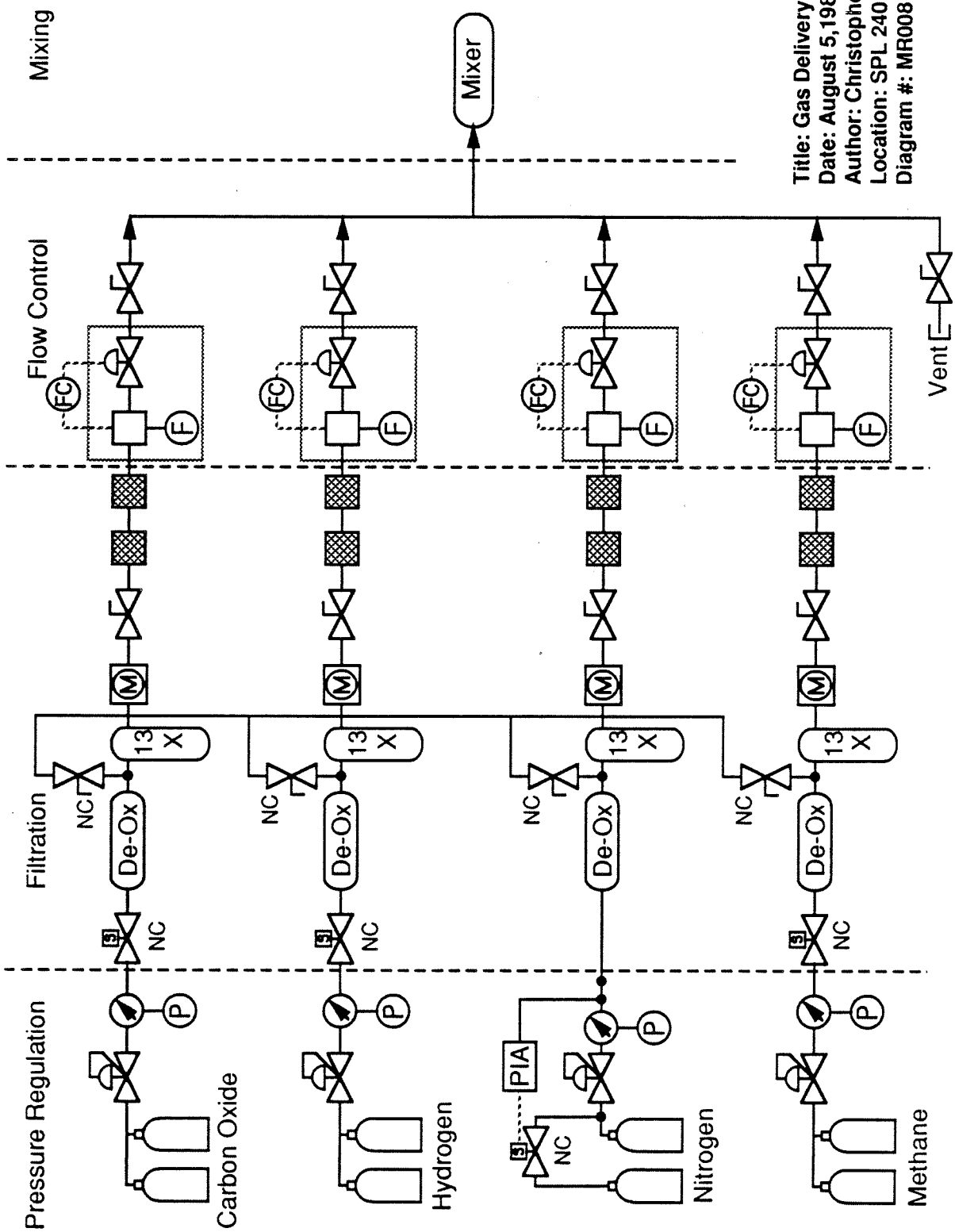

Figure 3.2: Flowsheet of gas delivery unit

Pressure Regulation

Four gases are supplied to the system: carbon dioxide, hydrogen, methane, and nitrogen. These feed gases come in pressurized gas cylinders with initial pressures between 2000–2500 psi. Each cylinder holds approximately 5400 standard liters of gas which lasts for approximately 6 hours at a nominal rate of 15 slpm. To provide for longer run times between cylinder changes, the nitrogen and hydrogen lines are equipped with gas manifolds. Furthermore, the nitrogen manifold has a special pressure switch which automatically opens a fresh cylinder when the nitrogen supply pressure is too low.

Normally, the supply pressure of each gas stream is regulated at 300 psi using a double stage pressure regulator. This regulated pressure should be roughly 50 psi greater than the anticipated inlet system pressure. The extra pressure is required for normal operation of the mass flow controllers. Since the maximum reactor operating pressure is 250 psi, the pressure regulators should not be set for more than 300 psi.

The end of each pressure regulator comes with a manual valve for positive flow shutoff. In addition, all lines, except for the nitrogen, are equipped with special solenoid valves rated for continuous operation. These valves are turned on at the operating panel only after an interlock has been energized. In the unlikely event of a loss of electrical power, these valves would shut off and remain off even after power is resumed. The nitrogen stream does not contain a solenoid valve because it is more desireable to continue its flow and remove any sensible heat still in the catalyst bed [116,117].

Gas Filtration

After pressure regulation, all supply gases pass through a number of filters to remove trace amounts of oxygen, oil, water, and other contaminants. It is extremely important to remove these contaminants from the supply gas for they can easily plug

the flow meters inside the mass flow controllers.

The first of these filters is a deoxygenation filter. This filter uses a copper catalyst to absorb oxygen onto its surface and, if possible, reduce it using the supply gas as a reducing agent. Oxygen should be removed from the feed stream to protect the methanation reactor from undesirable side reactions.

Following the deoxygenation trap is 13X molecular sieve cartridge filter. This filter removes trace amounts of tars, oils, heavy organics, and water as well as some catalytic poisons such as sulphur and selenium. These impurities bind to the surface of the molecular sieve and are discarded when the filter is changed.

A brass moisture indicator follows the molecular sieve. It contains several grams of a drying agent, silica gel, impregnated with a moisture indicating dye. This indicator turns pink when moisture is detected and serves primarily to monitor the condition of the two filters which precede it.

Finally, the supply gas passes through two particulate filters. The first filter uses a spongy borosilicate filter element to remove 99.95% of all particles with diameters greater than 0.3 microns. The second filter, which acts as a backup in case the borosilicate filter fails, uses a sintered stainless steel filter to trap particles within its pores.

Feed Gas Flow Controllers

A group of electronic mass flow controllers regulates the feed gas flow rates. Each controller is composed of three parts — a flow transducer, a flow control valve, and controller circuitry — integrated into a uniform package.

The flow transducer uses a flow splitter to send a small but constant fraction of the gas steam through a heated bypass tube. Platinum resistive thermometers located on either side of the heater measure the temperature increase in the gas. This temperature difference is proportional to the mass flow rate.

The flow control valve contains a vertically mounted proportional flow control valve attached to a steel valve stem. Surrounding the valve stem is a small solenoid coil. The strength of the magnetic field generated by this coil determines the valve stem position and hence orifice size. The force generated by this magnetic field is counterbalanced by a restraining spring which returns the valve to its fully shut position when no current is running through the solenoid coil.

The controller electronics unites the flow transducer with the control valve. It has two primary functions: flow transducer linearization and a PID control. The linearization circuit is calibrated by adjusting six internal potentiometers. When properly calibrated, the response of the transducer is within 1% of linearity. Experience has shown that it is best to check the calibration of each flow transducer at least once a year using a wet test meter. The PID controller is factory set and tuned so that the closed-loop response to a step change settles in approximately 10 seconds. If this is too long, the controller can be bypassed, using a built-in jumper, and the valve directly controlled using a computer.

Feed Gas Mixing

The outlets of each of the flow controllers is connected to a gas manifold which combines the four feed streams into one. From this manifold, the combined feed is mixed thoroughly with the recycle stream in a small 75 cc mixing chamber. Check valves located just upstream of the mixing chamber prevent backflow into either the recycle stream or the feed stream. If these check valves are removed, backflow can occur due to pressure variations caused by the reciprocating compressor. After it is thoroughly mixed, the gas stream enters the next processing unit, the gas heating unit.

3.2.2 Gas Heating Unit

The second processing unit is the gas heating unit, Figure 3.3. The purpose of this unit is to heat the feed gases to a desired temperature before they enter the reactor. The heating is accomplished using a number of different vehicles including a furnace, a feed-effluent heat exchanger, several heating tapes, and four cartridge heaters. The reactor inlet temperature is regulated not only by controlling the power used for heating but also by controlling the flow rate of gas through a bypass stream.

At the exit of the mixing chamber, the gas stream is split between the heating units and the bypass. In the heating side, the gas passes through a furnace and feed-effluent heat exchanger before reaching the block heater at the inlet of the reactor. In parallel with this stream is the bypass line which runs directly from the mixing chamber to the reactor inlet. Surrounding all interconnective tubing in this unit are a series of electrical tracing tapes.

The small thermal capacity of the gas can cause problems when being heated. Gas which is allowed to cool, even for a few seconds, can lose a substantial fraction of its enthalpy. Furthermore, due to the relatively large thermal capacity of the tubing, the gas temperature dynamics are controlled by the rate at which the interconnective tubing is heated. Until the tubing warms, the reactor inlet temperature will not increase much. For these reasons, it is very important to minimize the total length of all interconnective tubing and to properly insulate it.

Furnace

The first heating unit, the furnace, uses a 1800 watt furnace to radiate heat to the outside of a metal heat exchanger. The heat exchanger is composed of two 12 foot long concentric tubes which are wound into a helix with a 3 inch diameter and placed inside the furnace. The inner tube of the heat exchanger is a 1/4 inch brass tube which is chemically inert to the feed gases. The outer tube is a 1/2 inch

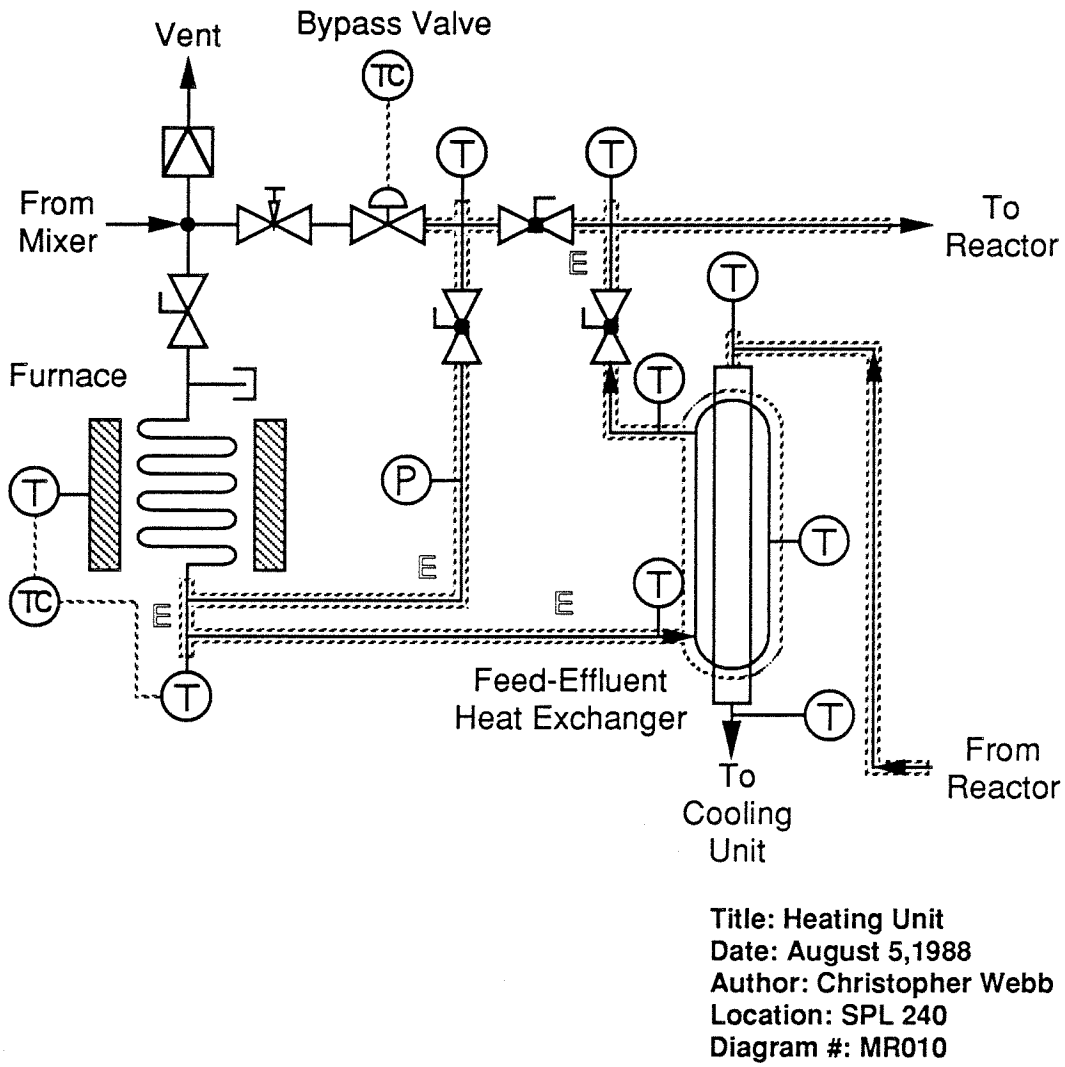

Figure 3.3: Flowsheet of gas heating unit

stainless steel tube used for its strength at high temperature. The tube bundle is sealed at the top of the exchanger, but opens at its exit. In this way, reactive gases flow through the brass tube as they are heated. The stress on the brass tube is negligible, however, since the pressure is the same both inside and outside of the brass tube.

The original design of the heat exchanger used a single 20 foot long stainless steel coil inside of the dual coil design. However, it was found that the stainless steel tended to catalytically decompose the carbon monoxide into carbon and carbon dioxide. The solid carbon then coated the sides of the heat exchanger restricting the flow of gas. This occurred until the exchanger was completely fouled.

The temperature of the furnace is maintained between 400–600°C using a PID controller to manipulate the current to the furnace. The setpoint to this controller is cascaded to a loop which regulates the exit gas temperature using a second PID controller. The setpoint to this second controller can be either set remotely using the computer or set locally using a built-in potentiometer. Both controllers have high temperature alarms which protect the equipment from overheating by shutting off the power to the furnace.

Feed-Effluent Heat Exchanger

After leaving the furnace, the gas stream enters the feed-effluent heat exchanger, FEHE (Figure 3.4). This exchanger uses the hot effluent gases coming from the reactor to heat the reactant gases going to the reactor. The heat exchanger is a double pipe heat exchanger built in a U shape. Each leg of the U is 25 inches long, and is separated from the other leg by a 3 inch interconnection. The inner tube of the heat exchanger has a 1/4 inch diameter while the outer tube has a 1/2 inch diameter. Hot gases coming from the reactor run inside the inner tube and transfer their energy to the cold feed which passes countercurrently in the annular space.

All fittings in the heat exchanger have been welded to eliminate leaks.

To reduce the heat loss to the environment, a number of precautions are taken. First, the outer tube is insulated with a braided ceramic insulation to reduce heat loss through natural convection. Second, the three clamps which structurally support the exchanger are milled from a ceramic material. Small electrical heaters are inserted inside the clamps to minimize the heat conduction through the clamp. A silicon controlled rectifier, SCR, based controller regulates the power to these heaters. Next, a 1/16 inch sheet of galvanized steel surrounds the whole tubing assembly. This sheeting creates a pocket of dead air which surrounds the heat exchanger and reduces the natural convection losses. The sheeting also facilitates in the handling of the heat exchanger. Finally, the outside of the galvanized steel is insulated with a 1 inch thick sheet of silicate insulation. Even with all of these precautions, the loss of heat to the environment is not negligible and has to be accounted for in the heat exchanger model, Section 4.1.

Heat Exchanger Bypass

In parallel with the furnace and FEHE is the heat exchanger bypass. The bypass uses a small metering valve under computer control to inject cold gas directly into the inlet of the reactor. This valve is the same type of control valve used in the flow controllers. Since it does not contain the internal PID electronics, however, the flow rate through the valve must be adjusted directly using a 5–12 volt signal supplied by the control computer. In most cases, a PID algorithm in the computer satisfactorily maintains the reactor inlet temperature at its desired setpoint. In case of an emergency, the reactor bed can be quickly cooled by fully opening this valve.

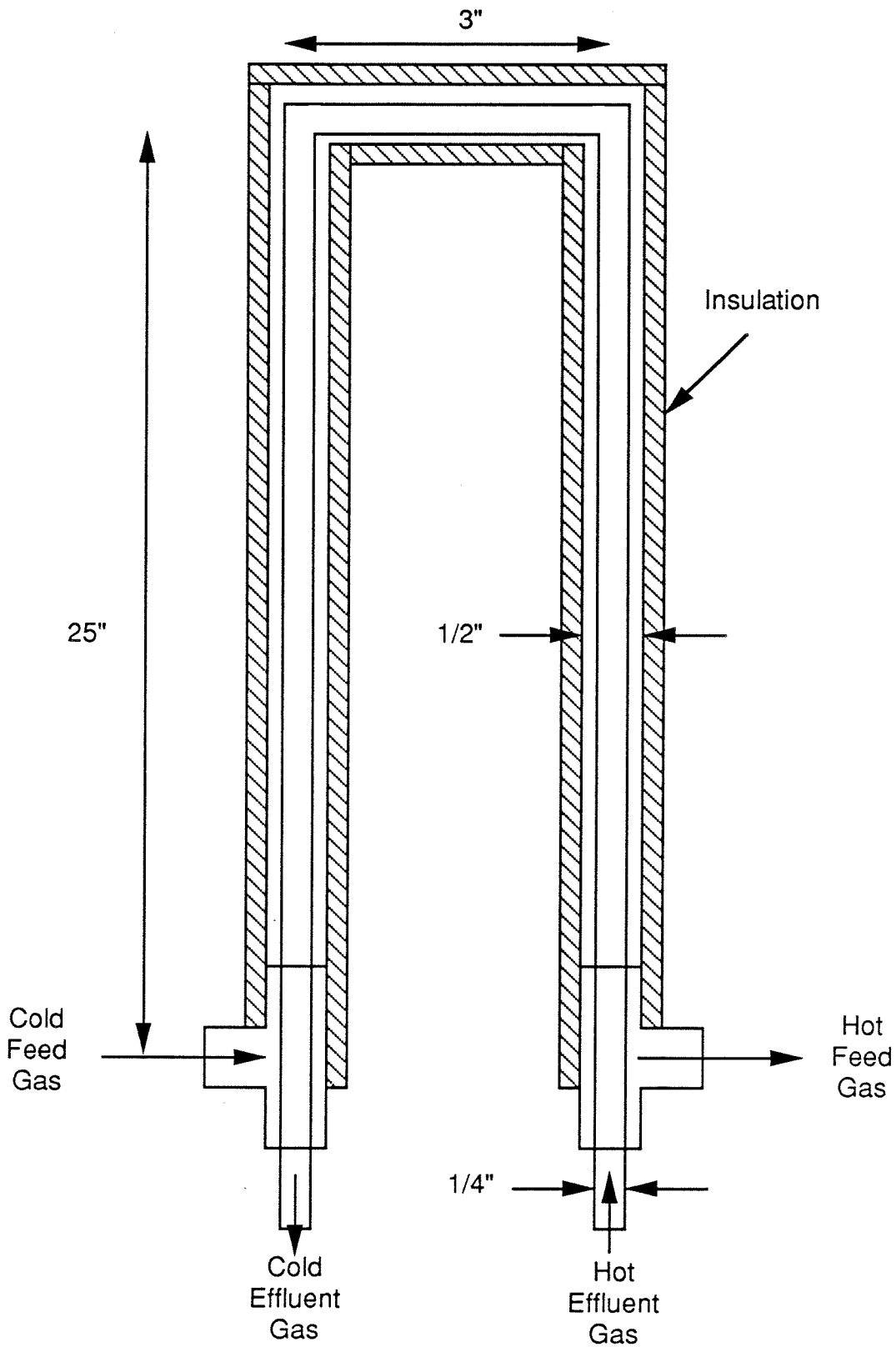

Figure 3.4: Schematic of feed-effluent heat exchanger

Heating Tape

Surrounding all interconnective tubing in this unit are a series of electrical heating tapes. These tapes compensate for the loss of heat to the environment through natural convection and also are used in lieu of the furnace to heat the feed gas to the proper inlet temperature. The heating tapes produce approximately 13 watts/inch^2 of electrical tape for a total of 1800 watts. SCR controllers supply this power to individual tapes or to groups of tapes depending on the experiment. This unit uses a fraction of time slicing technique to supply from 0 to 100% of full power.

The heating tape is composed of a set of Nichrome wires imbedded inside a Samox fiber mesh. The tapes are adhered to the walls of the stainless steel tubing using a high thermal conductivity - low electrical conductivity ceramic adhesive. Using this special ceramic adhesive reduces the possibility of shorting the heating tape to the metal tubing and also eliminates the potential for forming an electrical ground loop which would effect the thermocouple signals. Surrounding the heating tapes is a 1/2 inch layer of silicate insulation. This insulation helps to minimize heat losses from the system.

The upper temperature limit for all tapes is 760°C. Experience has shown that these tapes do indeed burn out if overheated for even short periods of time. Currently, circuitry is being added to the SCR controller to prevent this burn-out.

Block Heater

The final heating element is a block heater located at the entrance of the reactor. This heater consists of two 2 inch by 2 inch by 1/2 inch pieces of brass each imbedded with two 70 watt cartridge heaters. The two brass pieces are attached mechanically to both of the flat sides of the tube fitting which forms the inlet of the reactor. The resistive heaters can be controlled using either a SCR controller or a local PID temperature controller.

Because there are so many heaters in the gas heating unit their relative merits should be evaluated. The largest heaters, in terms of power, are the furnace and heating tapes. These subunits are used for heating the bulk of the gas and are efficient at large gas flow rates. However, at low gas flow rates, the furnace is ineffective because the gas coming from the furnace cools down before it reaches the reactor. On the other hand, the block heater, being close to the reactor inlet, is highly efficient though its small size makes it inefficacious at large flow rates. The heating tapes overcome both of these problems and is the preferred method of heating in most experiments.

3.2.3 Reactor

The third processing unit is the reactor, Figure 3.5. The purpose of the reactor is simply to react the feed components. This processing unit consists of a single reactor tube surrounded by a cooling jacket. The hot reactant gases coming from the heating stage, react with the catalyst inside the reactor tube and lose some of their energy to the cooling jacket before they exit to the following cooling unit.

The reactor is a fixed bed reactor with a constant wall temperature. This design has been chosen over other types of reactors because it is easy to build, model and operate and yet still presents challenging control problems. Furthermore, fixed bed reactors are common in industry and among the most important of unit operations. Being similar in design to some specialty chemical reactors, the constant wall temperature reactor is chosen over an adiabatic design. It would be worthwhile to check whether the reactor is adiabatic if the cooling jacket fluid is removed.

Reactor Tube

The reactor is composed of a 29 inch long by 1 inch in diameter stainless steel tube filled with a combination of catalyst and inert alumina. Both ends of this tube are

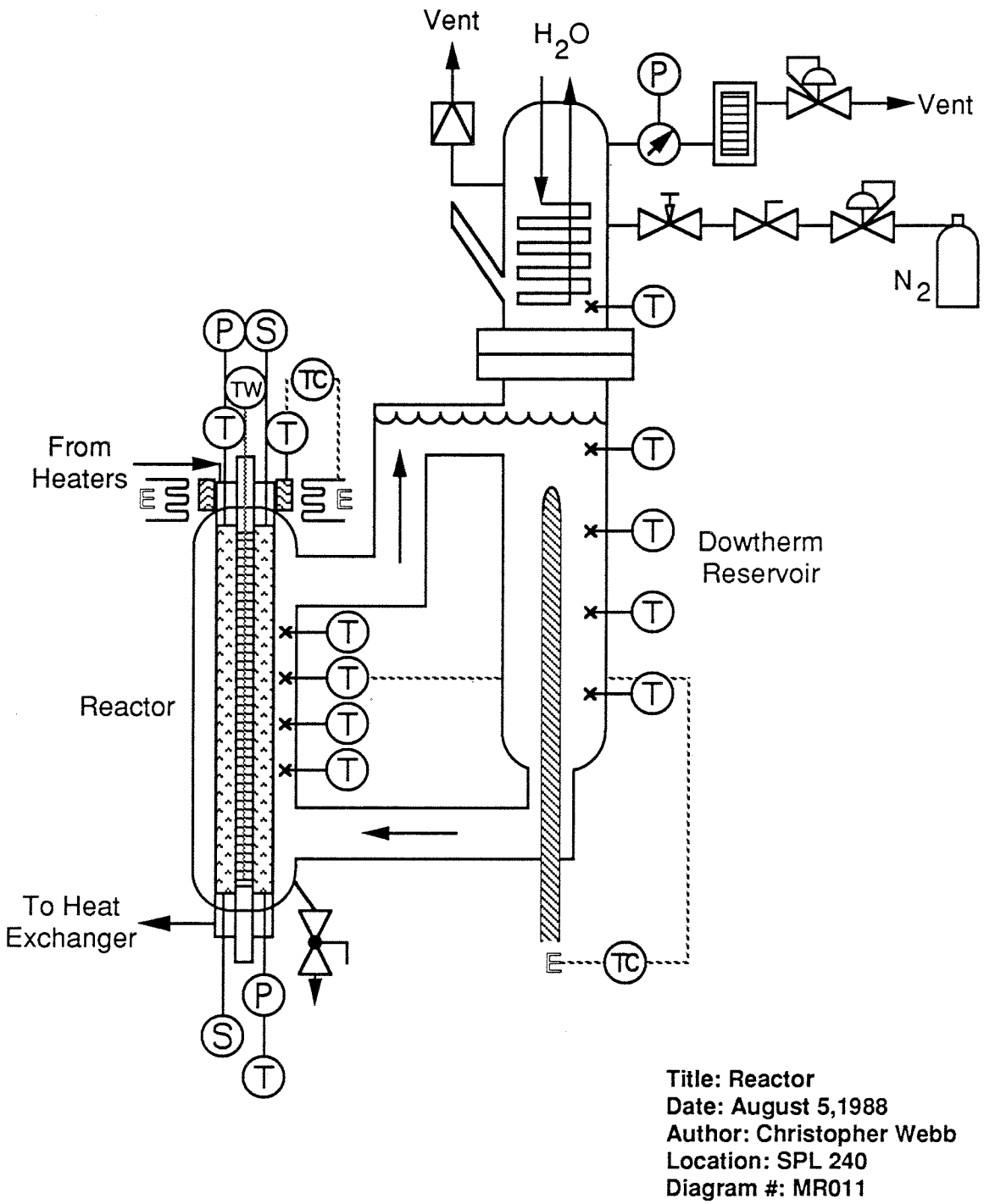

Figure 3.5: Flowsheet of the reactor unit

connected to 1 inch stainless steel cross tube fittings used as inlet and outlet ports, Figure 3.6. Crosses are preferred to tees for easy loading and unloading of catalyst. Gases enter and exit the reactor through the sides of these ports, perpendicular to the central axis of the reactor. Screens inside the exit port keep the catalyst from being blown out of the reactor.

The catalyst, United Catalyst's G-65RS methanation catalyst, is a nickel catalyst supported on a refractory material. The complete chemical makeup of this catalyst is shown in Table 3.4. The catalyst is mixed with an inert alumina before it is placed in the reactor. The alumina is dried at 100°C for 10 hours to remove all moisture and is quite porous and light. The current volumetric ratio is two parts inerts to one part catalyst. Diluting the catalyst spreads the reaction over a larger area and reduces the gradients inside the reactor.

This catalyst is designed to withstand large thermal stresses and should not sinter at temperatures below 1100°C. It has been ground in a ball mill and sifted using standard Tyler screens. Only the fraction between 14 ga. and 20 ga. corresponding to an equivalent catalyst diameter of 1 mm is used in the reactor. This means that the aspect ratios are approximately 25:1 in the radial direction and 290:1 in the axial direction. Despite the small catalyst diameter, pressure drops across the reactor are small.

The reactor can be divided into three zones: inlet, reaction, and outlet. In the inlet and outlet zones, the reactor tube is filled only with inert alumina, therefore, no reaction occurs in these zones. These zones are located at the inlet and outlet of the reactor where the reactor is inadequately cooled by the cooling jacket. The inlet zone consists of the top 2.5 inches of the reactor and the outlet zone is the bottom 2.5 inches. The reaction zone is the 24 inch section in the middle of the reactor which is properly surrounded by the cooling bath.

Running down the center of the reactor is a 1/8 inch by 41 inch long stainless

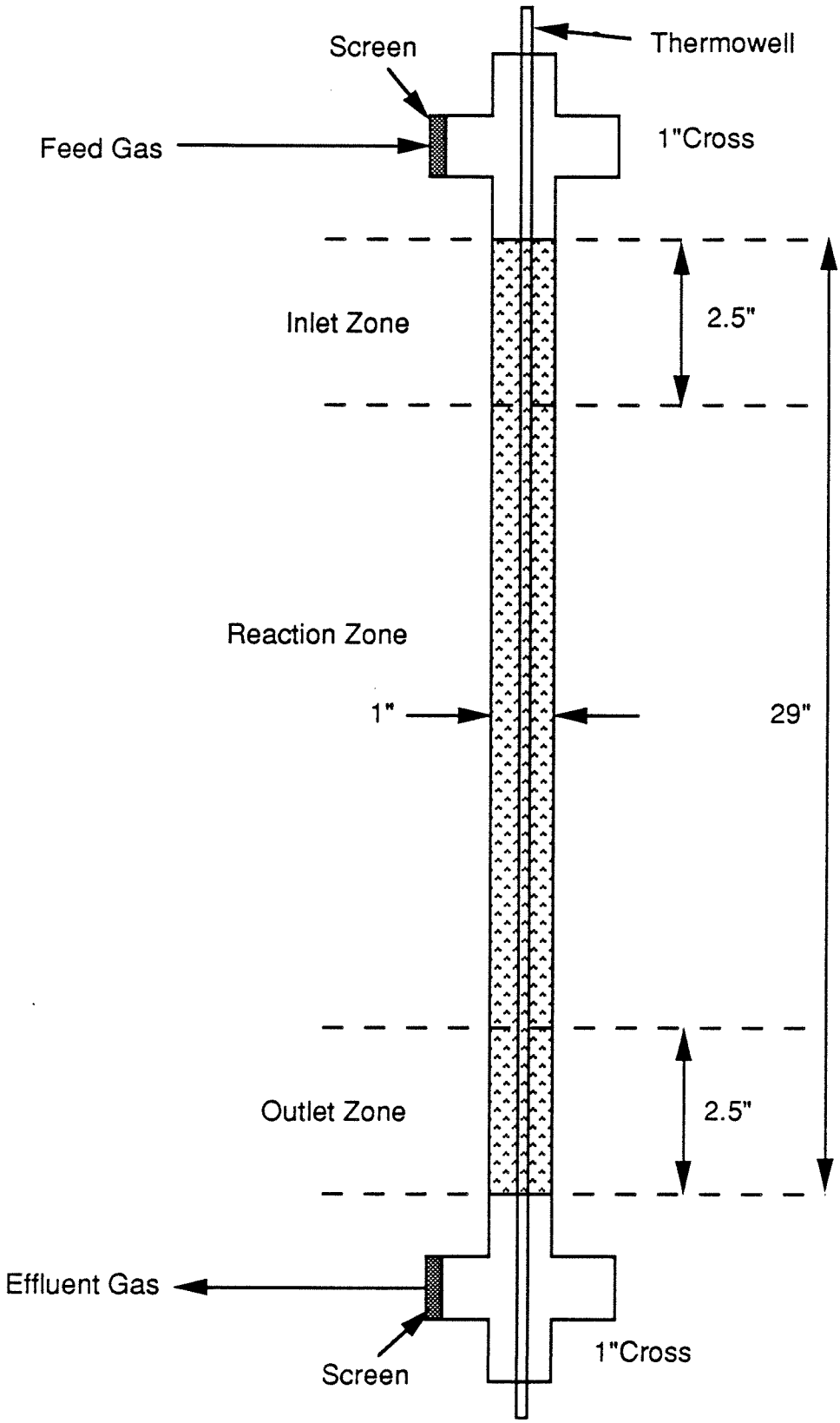

Figure 3.6: Schematic of the reactor tube

United Catalysts Inc.

Methanation Catalyst

Typical Chemical and Physical Properties

Catalyst Type, Form and Size

Catalyst Type	G-65
Form	Tablets
Size	¼" × ¼"

Effective: January 25, 1980
Supersedes: January 31, 1978

Chemical Composition

	Weight Percent
Ni*	24-27
Al_2O_3	55-65
CaO	4-8
SiO_2	<0.30
C (As Graphite)	3-5
S* (Maximum)	0.05
Na* (Maximum)	0.30

	Weight Percent
Fe_2O_3	<0.15
MgO	<0.10

LOI to Constant Weight at:

	Weight Percent
1000°F*	10.0 Max.

Physical Properties

A. Bulk Density, lbs./cu. ft. ..... 65 ± 5

B. Surface Area, m^2/g 35-65

The surface area is obtained by a modified BET method which consists of nitrogen adsorption by the sample. The sample is ground to a fine powder (60-100 mesh) and purged with nitrogen at 200°C to a constant weight.

C. Pore Volume, cc/g 0.15-0.25

The pore volume is obtained with a mercury porsimeter at 60,000 psig which corresponds to the total pore volume or pores greater than 29.2 Angstroms diameter.

D. Crush Strength, Minimum Average* ..... 90.0 lbs.
No More Than 5% Less Than ..... 40.0 lbs.

Apparatus — Hydraulic press with horizontal plates of which the bottom plate moves vertically. In series with the bottom plate is a pressure gauge which records the pressure exerted on the tablet.

Procedure — The tablet is placed on its side and the lower plate is raised to the tablet with zero pounds pressure on the gauge. The pressure is then increased on the bottom plate until the tablet crushes and the pressure at breakage is recorded.

The crush on a minimum of twenty-five tablets is obtained and the average is taken arithmetically.

To pretreat the sample, dry the catalyst at 400°F for three hours and allow to cool.

Crush Strength Range on Individual Tablets 40-150

*Properties normally measured by Quality Control.

Table 3.4: Physical and chemical properties of G-65RS catalyst

steel tube used as an axial thermowell. This thermowell allows the experimenter to measure the temperature of the reactor bed at any point along the center axis. Using tube fittings, the thermowell is anchored to the crosses which form the inlet and outlet ports. For easy disassembly, the ferrules used to seal the thermowell are nonpermanent reducing graphite-vespule ferrules normally used in chromatography.

In addition to the thermowell, the top and bottom ports each have four taps. Three taps are used as pressure or chromatography taps and have small frits inserted in the tubing line to prevent the transportation of catalyst dust. The fourth tap is welded on its reactor side and acts as a small thermowell for independent measurement of the inlet and exit temperatures.

Cooling Jacket

Surrounding the reactor tube is a cooling jacket filled with 4 liters of Dowtherm A heat transfer fluid. This fluid has a normal boiling point of 256°C, and circulates around the reactor driven by the boiling action of the fluid. A 1200 watt immersion heater initially brings the Dowtherm to its boiling point.

A water cooled heat exchanger inside the cooling jacket removes the latent heat from the Dowtherm vapor as it recondenses. The heat exchanger consists of a 10 foot coil of brass tubing through which tap water flows. Care must be exercised to keep the water flowing through the tubing at all times, or the cooling tube will overheat, and steam will be produced. At maximum operating conditions, this heat exchanger must remove about 3 kw of generated heat [117].

The pressure inside the cooling jacket is regulated using a back pressure regulator. Pressures greater than atmospheric pressure are obtained by pressurizing the cooling jacket with nitrogen gas. The flow rate of the nitrogen is controlled using a needle valve. By adjusting the pressure from 0 to 30 psi, the temperature of the boiling Dowtherm can be controlled from 256°C to 300°C.

At the top of the cooling jacket is an adjustable pressure relief valve currently set for 60 psi. In the event that there is a sudden increase in pressure, the relief valve opens and vents the gases inside the cooling jacket. This increase in bath pressure can occur if the brass cooling heat exchanger starts to leak tap water into hot Dowtherm fluid. Because this can lead to a potentially dangerous explosion, it is especially necessary to check the condition of the brass heat exchanger periodically. Furthermore, if the pressure inside the cooling jacket increases unexpectedly or if there is a sudden change in the flow rate of gas through the back pressure regulator, it will be necessary to check the heat exchanger for leaks and replace the unit if any are found.

3.2.4 Gas Cooling Unit

After the gas has passed through the reactor, the gas travels through the effluent side of the feed-effluent heat exchanger and enters the fourth processing unit, the gas cooling unit, Figure 3.7. The purpose of this unit is to separate any condensable gases (i.e., water) from the noncondensable gases. As pointed out earlier, it is imperative to remove any components which are liquids at room temperature because liquids can settle in the mass flow transducers where they bias the readings.

Water is removed from the process stream by cooling the gas to below room temperature and mechanically separating out any liquid components. The cooling is performed using three heat exchangers: an air cooled exchanger, a water cooled exchanger, and a refrigerated exchanger. The actual cooling process can be maintained using only the last two heat exchangers, but the first exchanger reduces the required heat duty on the later exchangers. The liquid entrained vapor stream then enters a knock-out tank which separates the liquid from the gas.

The first heat exchanger is an air cooled stainless steel heat exchanger. This exchanger is composed of a 55 inch piece of 1/4 inch stainless steel tubing through

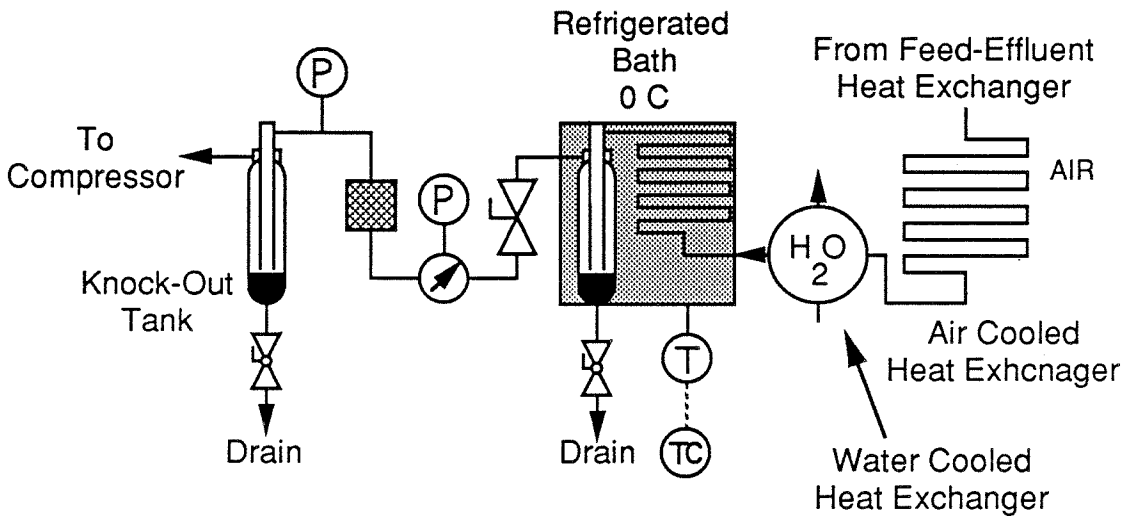

Title: Cooling Unit
Date: August 5,1988
Author: Christopher Webb
Location: SPL 240
Diagram #: MR010

Figure 3.7: Flowsheet of the gas cooling unit

which the hot gases flow. These gases lose their energy through the forced convection of air on the outside of the tube walls.

The second heat exchanger is a water cooled counter-current heat exchanger. This exchanger is a 69 inch double pipe heat exchanger with an aluminum inner tube through which the hot gases pass and a brass outer tube. This heat exchanger is very efficient at cooling the gas and typically cools the effluent stream to $< 20°C$.

The final heat exchanger consists of a 80 inch long piece of stainless steel tubing suspended inside a refrigerated ethylene glycol - water bath. This final heat exchanger cools the effluent gases to the desired temperature of 3°C for greater removal of water. A relay controller and portable refrigeration unit maintain this temperature inside the bath.

The cold vapor entrained gas stream then enters a knock-out tank, also located inside the refrigerated bath, which separates the liquid from the gas. The entrained gas stream runs from the final heat exchanger through a 1/4 inch tube into the bottom of a knock-out tank, a 1 liter sampling cylinder. Here the entrained water is separated from the gas due the sudden change in gas velocity. The condensate slowly accumulates at the bottom of the knock-out tank until it is drained using a purge valve. The vapor free gas proceeds to the top of the sampling cylinder where it exits the knock-out tank and proceeds to the recycle unit. Any trace quantities of liquid remaining in the gas re-evaporate as the gas warms to room temperature.

3.2.5 Mass Recycle Unit

After the gas leaves the cooling unit, it enters the last processing unit, the mass recycle unit, Figure 3.8, which recompresses the effluent gas and recycles it back through the system. This unit is also responsible for removing the product stream and filtering the recycle gas.

The effluent gas is first recompressed using a reciprocating compressor, then

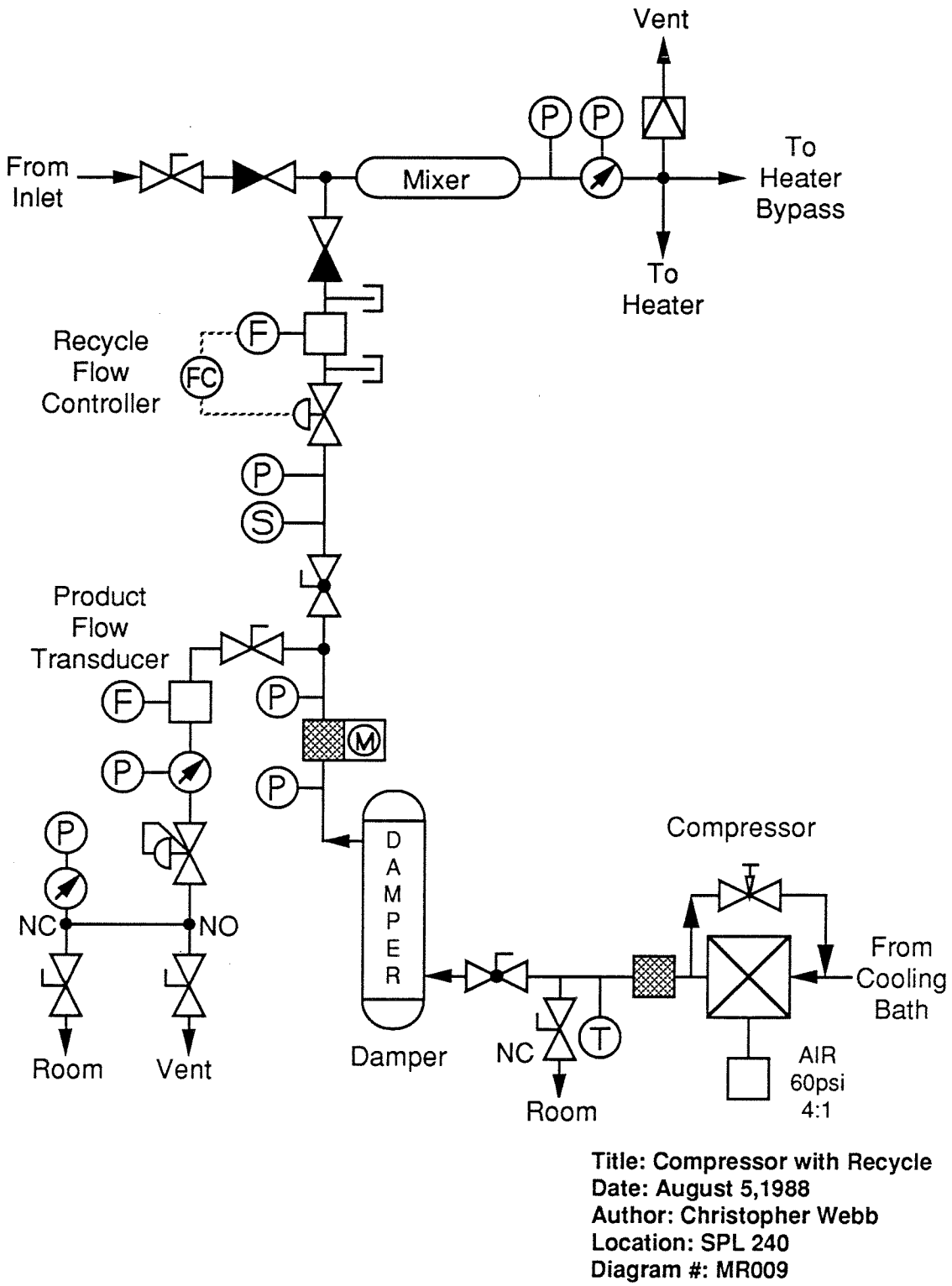

Figure 3.8: Flowsheet of the mass recycle unit

filtered and stored inside a large surge damper. From the damper, the gas either is recycled back to the gas heating unit or is removed and vented as the product stream. In single pass experiments, it is not necessary to recompress the effluent gas since there is no recycle flow.

Compressor

The recycle compressor is an air-driven double-acting single stage reciprocating compressor. The piston has a displacement volume of 0.316 liters, and cycles at a maximum rate of 140 strokes per minute. The compressor is mounted on rails secured to the floor which helps reduce vibrations imposed on the rest of the equipment. However, if in the future these vibrations become too severe, it will be necessary to replace this compressor with a more expensive centrifugal compressor.

Compressed air from the laboratory compressed air line drives the compressor. Typically, this air is at a pressure of approximately 60 psi. Since the compressor has 4:1 pressure ratio, the difference between the outlet and inlet pressure can be as high as 240 psi.

A manual bypass valve is installed across the compressor which allows gas to flow from the outlet of the compressor back to the inlet. This valve gives the operator the ability to adjust the pressure drop - flow rate operating curve for the compressor. Using a bypass valve to control the compressor throughput is better than adjusting the driver air flow rate since it gives finer flow rate control and places less stress on the compressor. Due to the compressor design, there is little control over the driver air flow rate.

Surge tanks are located on either side of the compressor and are required to smooth the pulsations produced by the compressor. The inlet surge tank has a volume of 1 liter and the outlet surge tank, the damper, 18.5 liters. These two tanks account for over 90% of the 21.0 liter total volume associated with the system.

Filter Traps

There are three filters located in the recycle section whose sole purpose is to protect the sensitive on-line instrumentation from particulate material and condensed water. One of these filters is located before the compressor and the other two just after the compressor. The filter before the compressor and the first filter after the compressor trap particles with diameters greater than 5 microns using a sintered metal element. The third filter contains a thick porous borosilicate glass filter element and removes any remaining particulate, water, or other foreign matter greater than 0.3 microns.

Recycle Stream

At the exit of the damper, the gas stream is split. One line removes to the product stream, while the other recycles the bulk of the gas back to the reactor through a recycle stream. The recycle line contains a mass flow controller which regulates the flow rate before it passes through the check valve and mixes with the fresh feed stream.

Like the mass flow controllers used to regulate the feed gas flow rate, the recycle flow controller consists of three parts: a flow meter, control valve and electronic controller. However, unlike the other flow controllers, the three parts are segregated and housed individually. The recycle flow meter has the same design as the other flow meters using a heated bypass tube to measure the mass flow rate. Likewise, the electronic controller uses a PID algorithm to control the flow rate and can be set either locally or from the computer. The only real difference is in the design of the control valve.

The recycle valve is a stainless steel rotary valve with a coefficient of flow, C_v, which is linear with position. This valve is rotated using an asynchronous motor. Positive voltages from the PID controller open the valve while negative voltages close

the valve; the valve remains at its current position if no voltage is supplied. It takes approximately 120 seconds to go from the fully opened to fully closed positions, and in the full closed position, pads located inside the valve are used to completely stop all gas flow. The upper bound on C_v is 0.1.

While C_v varies linearly with valve position, the flow rate through the valve does not. The gain of the valve, defined as the change in flow rate per change in position, is very large at low flow rates and monotonically decreases as the flow rate increases. Because the flow controller does not compensate for the change in gain, the closed-loop dynamic response to setpoint changes depends on the operating conditions. At the maximum flow rate of 180 slpm the response is very sluggish while at 30 slpm the controller is unstable. Opening the manual bypass valve across the compressor decreases the gain at low flow rates and, therefore, makes the controller stable although oscillatory. This action also limits the maximum recycle flow rate.

Product Stream

In parallel with the recycle stream is the product stream which currently vents the product gas. This stream uses an electronic flow meter for measuring the instantaneous product flow rate and a back pressure regulator for adjusting that flow rate. Addition of the back pressure regulator at this point helps to smooth out pressure variations caused by the compressor.

The back pressure regulator actually regulates the pressure inside the damper by dynamically manipulating the flow rate of the product stream. (At steady state, the product mass flow rate is equal to the feed mass flow rate.) The regulator has a pressure rating of up to 500 psi although during most experiments, the pressure is maintained between 200–225 psi. The orifice in the regulator has a diameter of 1/16 inch for a maximum C_v of 0.12.

3.3 Instrumentation

The purpose of this section is to describe the way process measurements are made, the instrumentation required to make them, and their relative importance. Four kinds of measurements are taken: temperature measurements, concentration measurements, flow rate measurements and pressure measurements.

Common to all measurements is a signal patch panel. All signals are sent from the reactor to the patch panel via an overhead conduit. From the patch panel they are routed either to the appropriate control computer or to intermediate monitoring equipment.

Most measurements and all controlled variables are connected to local monitoring boxes which can be used to operate the equipment without the aid of a computer. Each box contains a jack used either to send the measured variable to the process computer or to receive a control voltage from the computer and output it through the box. With this added layer of equipment the computer operator can select which variables to measure or control.

3.3.1 Temperature Measurements

All temperatures are measured with either ANSI type E or type K thermocouples. The type K thermocouples are attached to a local temperature controller whereas the type E thermocouples are read directly by the control computer. These thermocouples can be either grounded or ungrounded. A grounded thermocouple has its thermocouple junction grounded to the sheath which surrounds it; whereas the ungrounded thermocouple is insulted from this sheath. Grounded thermocouples have faster response times, but must be measured with special electronic equipment containing differential amplifiers. For this reason, most thermocouples are ungrounded.

The type K thermocouples connected to the temperature controllers have their

signals conditioned by the controller's electronics. These controllers output a 0–5 volt signal linearly corresponding with the temperature over the range of the controller. The PID controllers are exclusively applied to loops involving external heating: the furnace, the block heater and the Dowtherm jacket. For these loops, the control computer acts in a supervisor manner setting the setpoint to the controller.

The ungrounded type E thermocouples are read directly by the control computer using the available temperature ports. These ports are attached to an integrated circuit designed explicitly to measure thermocouples. Since the integrated circuit can measure only one port at a time, the temperature ports are multiplexed using a series of reed switches. These switches require 1/2 second to settle and ultimately limit the sampling rate of the computer.

The signals from the grounded thermocouples are sent to a series of differential amplifiers. These amplifiers condition the incoming signals and compensate for the cold junction. These signals are then read directly using the A/D converters in the process control computer. Since no relay switching is involved, very fast estimates of the temperatures are obtained. Of all the thermocouples, only the thermocouples located in the axial thermowell require the speed afforded by the grounded thermocouples.

The most important temperatures in the system are the reactor inlet and outlet gas temperatures, the thermowell temperatures, the reactor wall temperature, and the inlet and outlet temperatures in both the feed and effluent sides of the feed-effluent heat exchanger. The first three groups of temperatures monitor the dynamics of the reaction whereas the last group measures the efficiency of the heat exchanger.

There are two different ways in which the temperatures in the thermowell are measured. To obtain steady state temperature profiles, a long thermocouple is inserted into the axial thermowell until the tip of the thermocouple is at to the

bottom of the reaction zone. Then, this thermocouple is slowly lifted in discrete steps using a stepper motor. At each step, the control computer records and stores the temperature. When the thermocouple reaches the top of the reaction zone, the experiment is stopped and the thermocouple is reinserted back into the thermowell for the next experiment. The data are then off-loaded onto a Vax where the axial position of the thermocouple is correlated to the time. Since the speed of the stepper motor and the sampling rate are both set in the control computer, unassisted temperature profiles are easily obtained.

Using a single thermocouple is fine for obtaining steady state temperature profiles, but is unacceptable in control experiments since it is too slow. To obtain faster estimates, sixteen fixed thermocouples of various lengths (see Table 3.5) replace the single mobile thermocouple. These thermocouples are split into two groups of eight with each group being held in a brass retainer. These groups are inserted into the thermowell: one group through the top of the thermowell, and the other through the bottom. While the relative positions of the thermocouples are fixed by their lengths, the absolute positions vary and depend on the insertion depth.

3.3.2 Gas Chromatography

Gases are routed from the reactor to a Varian 3300 gas chromatograph, GC, which sits on a separate bench approximately 8 feet away. Between the reactor and the GC are two sets of solenoid valves which determine which gas will be analyzed and at what time, Figure 3.9. The first set of valves, consisting of three solenoid valves, selects which tap of the reactor is to be analyzed. Currently, the choices are restricted to the reactor inlet, reactor outlet, or the damper.

After the sample gas is selected with the first set of solenoid valves, it is regulated to 30 psi, cooled in the refrigerated bath to remove any water, and passed through a rotameter and a control valve before it reaches the second set of valves. This set is

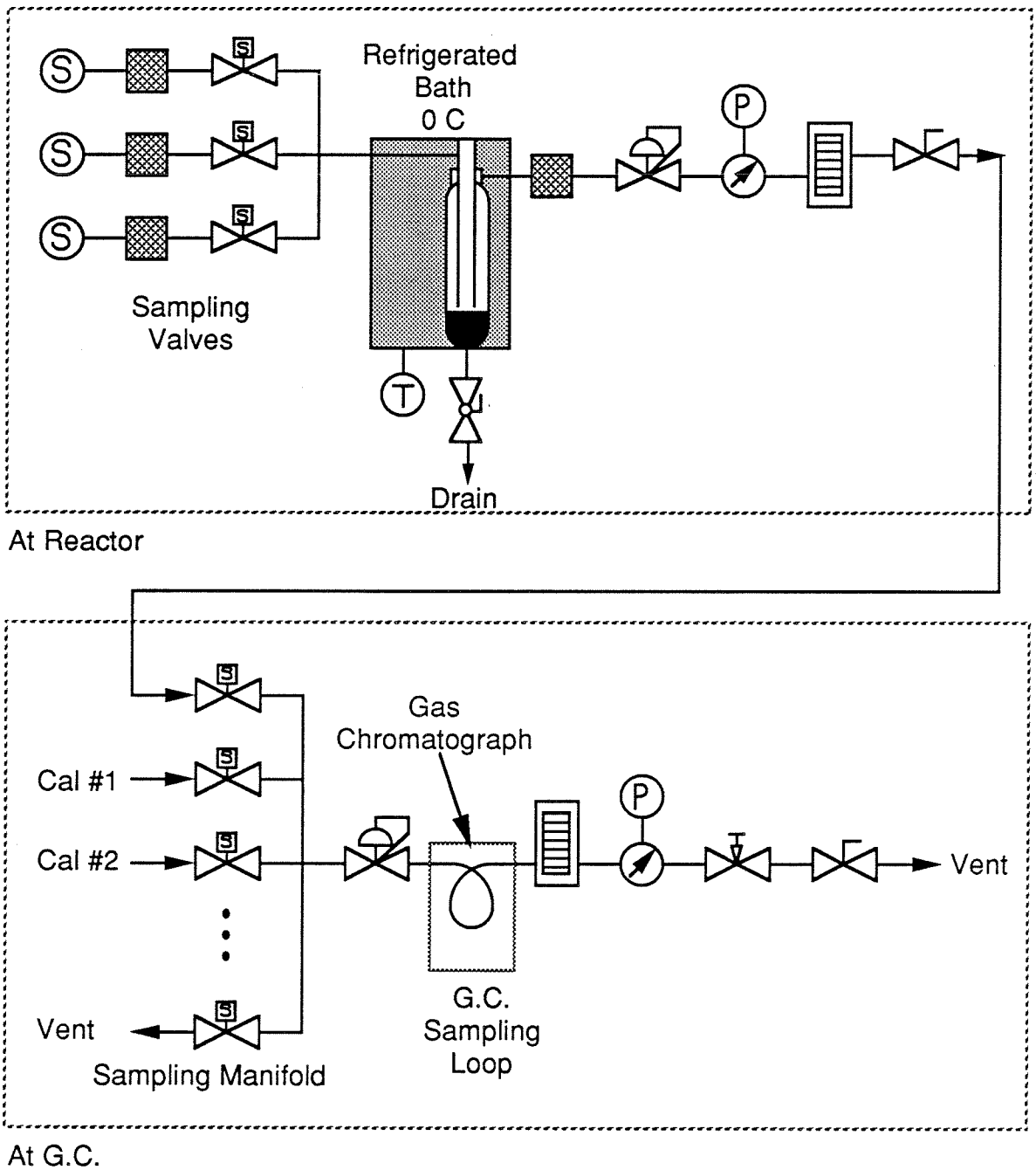

Figure 3.9: Flowsheet showing gas chromatography valving

at the GC itself and consists of a six valve sampling manifold used to select between the unknown reactor sample, four calibration gases, or a vent.

The purpose of the vent is to purge the reactor sample whenever the GC is not in the sampling mode. Although the transportation lag between the reactor and GC is small, the amount of gas stored behind the pressure regulator is not negligible. Without some type of purge, there is an extremely long time delay associated with the sampling process. The purge stream significantly reduces this delay by increasing the flow rate through the sampling lines. In a typical chromatography run, the vent is closed at the beginning of the GC run and, the pressure inside the GC sampling loop is allowed to build up. After a specified amount of time, the sampling valve is switched, starting the analysis of the gas, and the vent is opened, purging the sampling lines until the next sample is obtained.

After the second sampling manifold, the selected stream passes through a second pressure regulator, the GC gas sampling valve with a 1 ml gas sampling loop, a rotameter, and an outlet metering valve before being vented. The pressure and flow rate inside the sampling loop must be precisely controlled if accurate and repeatable estimates of the gas concentration are to be obtained.

Inside the gas chromatograph, the gas sample components are separated using an Alltech CTR-I column. This column is actually two concentric 6 foot long columns: an inner column filled with a polymeric packing, Porapak, and an outer column filled with an activated molecular sieve. The molecular sieve column is the workhorse column separating all gases with the exception of carbon dioxide. Carbon dioxide has a great affinity for the molecular sieve and, when monitored, produces a very broad peak [119] which is normally interpreted as a shift in the baseline of the chromatogram. The Porapak column elutes most light gases too quickly to separate them, but it does separate carbon dioxide from all the other light gases. Using the combination of both columns, the combined analysis time in roughly 9 minutes.

Example chromatograms and complete method details are found in [138].

3.3.3 Flow Measurements

There are six flow rates which are important for control: the four feed gas flow rates, the recycle flow rate, and the product flow rate (see Figure 3.10). All of these flow rates are controlled with electronic mass flow controller with the exception of the product stream which is regulated using a back pressure regulator. Each controller supplies a 0–5 volt output proportional to its measured flow rate and accepts a 0–5 volt input for its setpoint.

The controllers are interfaced to a six channel digital readout-power supply box which permits manual or computer control of the flow setpoints. A precision digital voltmeter inside the readout box displays the flow rate to within three significant digits. When computer control is needed, the computer sets the setpoint to the flow controller and thus act in a supervisory manner.

3.3.4 Pressure Measurements

All pressures are measured using electronic differential pressure transducers. The output of these transducers is sent to a readout box and is displayed using a precision digital voltmeter. This output is also routed to the control computer where it can be used in control experiments.

There are two pressure transducers in the system. One of the transducers measures the system pressure at one of six predefined locations, Figure 3.11. By varying the selection of the pressure tap, the operator can monitor the pressure drops across various processing units. The other transducer continuously measures the pressure drop across the reactor.

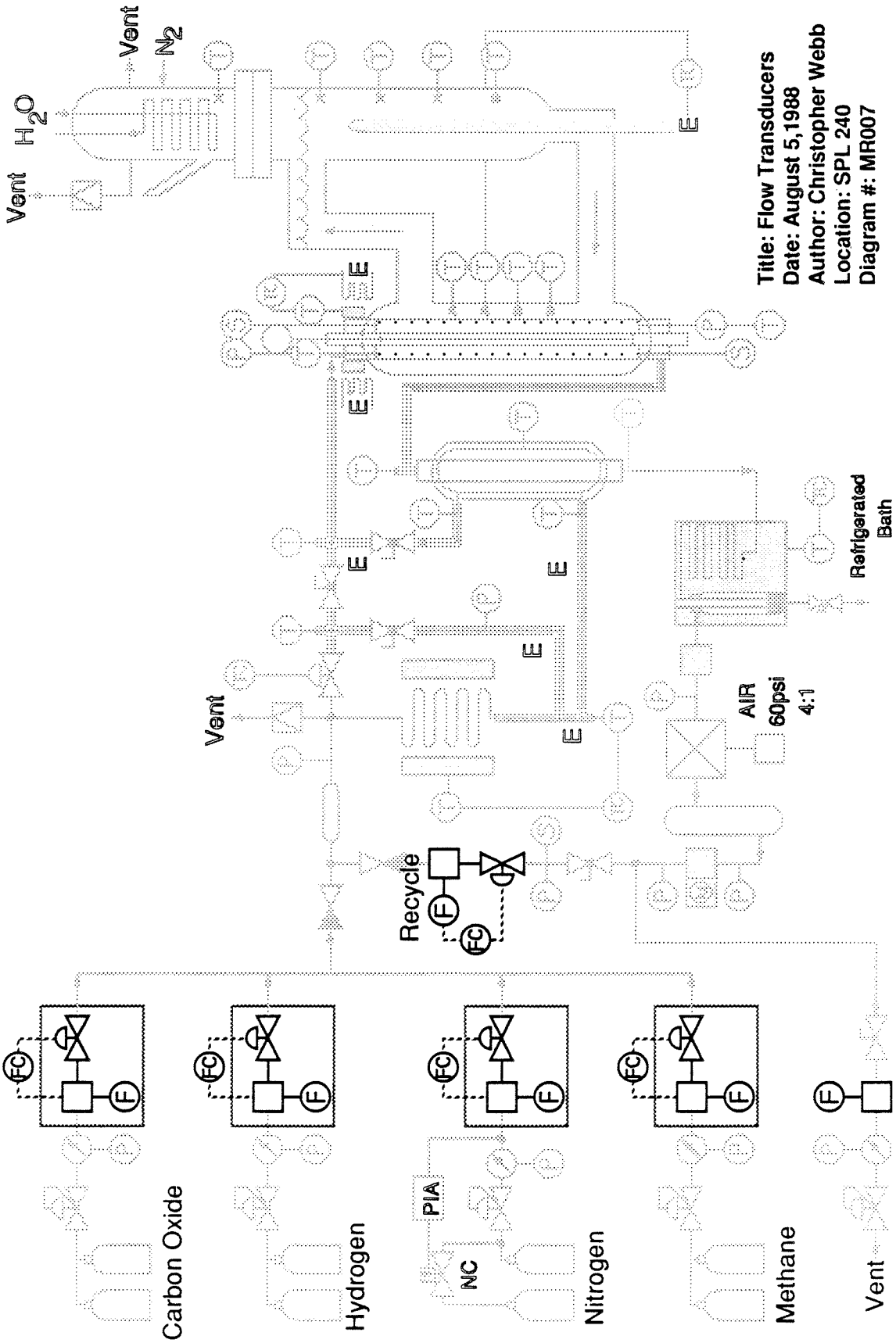

Figure 3.10: Location of flow measurements

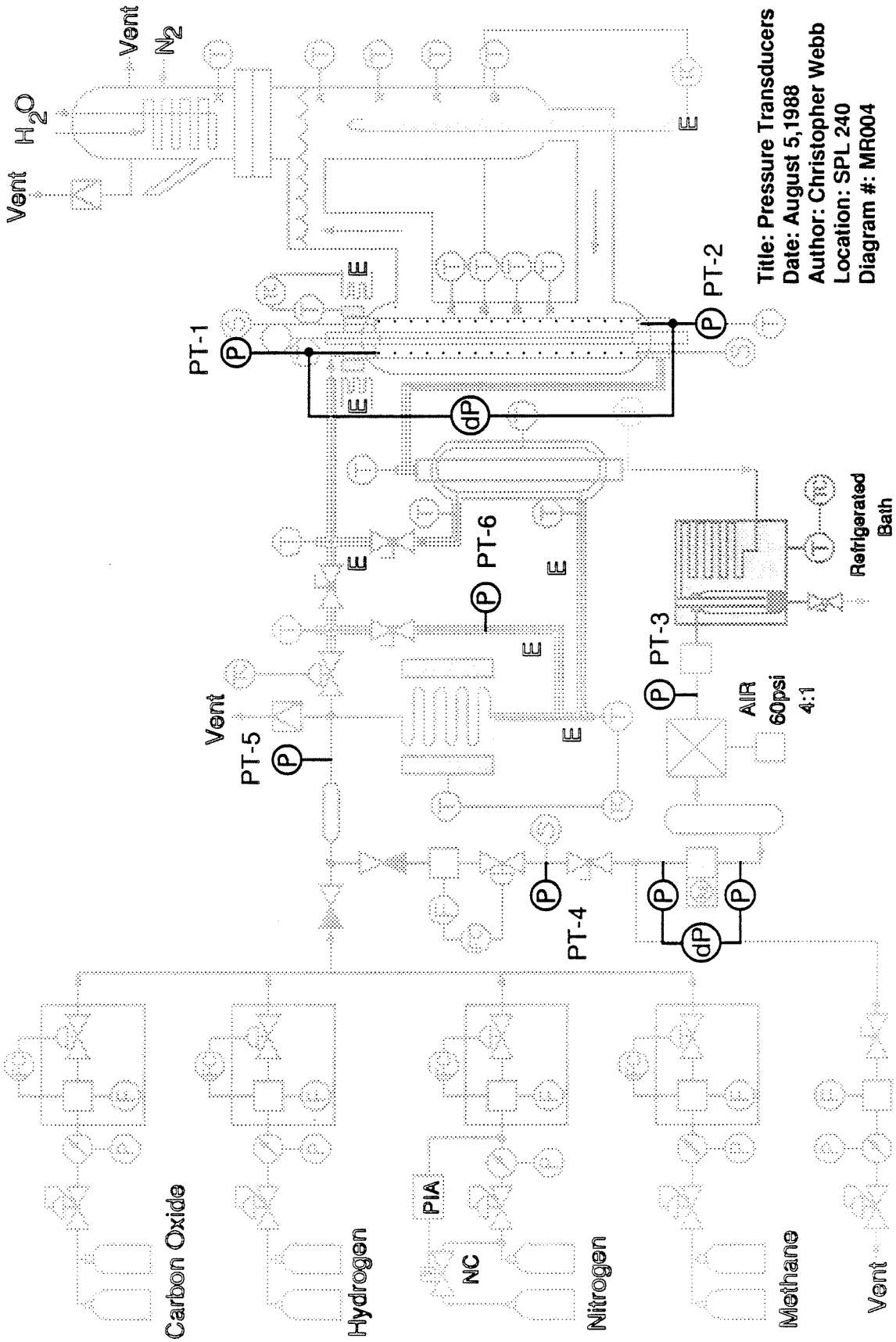

Figure 3.11: Location of pressure taps

3.4 Computer Systems and Software

This section describes the computers and software used in the experiments. The computer related tasks are divided among three machines: a chromatography computer, a control computer, and a data analysis computer. The chromatography computer is devoted exclusively to the acquisition and analysis of the gas chromatograms, the control computer performs the real time data acquisition and control, and the data analysis computer analyzes the experimental data after the experimental runs are completed.

3.4.1 Chromatography Computer

The chromatography computer is designed to acquire and analyze the gas chromatograms. The computer hardware consists of an IBM AT connected to a Keithley Instruments data acquisition unit. The AT is equipped with a 30 Mbyte hard disk, 3 Mbytes of extended memory, and I/O communication card. The AT communicates with a Keithley series 500 data acquisition unit by a special interface card. The Keithley unit has 4 analog inputs, 5 analog outputs, 16 digital inputs and 16 digital outputs, as well as an on-board clock.

The communications between the computer and the data acquisition unit are automatically controlled when running the chromatography analysis software package Maxima provided by Dynamic Solutions Corporation. This software maintains all aspects of the GC analysis with the exception of the selection of the unknown stream. This includes the proper timing of the vent stream, the acquisition of the chromatogram, the analysis of the chromatogram for concentrations, and the storage of the results for future reference. Currently, Dynamic Solutions is in the process of modifying the program to include a communications link for the transfer of results to the control computer.

3.4.2 Control Computer

The control computer executes all real time data acquisition and control for the reactor. The control computer consists of an IBM–9000 computer running the CSOS multi-tasking operating system. This computer communicates with the IBM–9040, an intelligent data acquisition unit, by way of an RS–232 serial line. The word intelligent implies that the data acquisition unit has its own microprocessor and operating program. The maximum sampling rate for the acquisition unit depends significantly on the number of sampled variables and the hardware configuration, but is currently on the order of one sample every 2 seconds.

Real time control of the chemical reactor requires several layers of software. At the bottom most layer, the control software needs to interface the computer with the processing equipment — sampling incoming measurements and sending various control signals. Often, these measurements and control outputs require some form of rescaling or conditioning before they are usable. This is the job of the second layer of software. Next, the program must monitor the system for unsafe conditions and alarm the operator if such conditions are found. Then the program should present the current measurements to the operator in either tabular or graphical form and allow the operator to modify the control signals. Finally, at the topmost layer, the control program must implement a sometimes complicated control algorithm.

In addition to the structure, there are other requirements for the control program. The software must be able to handle processing equipment with inherently different sampling rates. The software should allow the control computer to talk to different computers and exchange data. Finally, the software should be flexible and allow for the incorporation of new control algorithms or different signal conditioning.

Luckily, all of these requirements are met in the Real Time Control Program, RTCP [80]. In addition to the structural layering, RTCP also offers:

Physical variable mapping All inputs and outputs are converted to physical

quantities before being displayed to the operator. This may include nonlinear mappings.

Variable checking The program checks the consistency of a number of operator inputs and flags the operator if an error is noticed.

Multi-loop time sharing Up to three different control loops, with different timings, can be set up. The program prioritizes the loops to determine timing inconsistencies.

Run-time communication The operator can update a number of control parameters during an experimental run.

Three types of control Three types of control are programmed into the software: decentralized PID, finite dimensional linear time invariant control as stored in state space file, and user specified control written in a subroutine.

Identification Signals Several control input sequences can be used for system identification. These include sinusoids, ramps, steps, pulses, and, most importantly, user specified inputs where the inputs are read from a file. This allows for the implementation of uncorrelated random signals, such as a pseudo random binary signals, useful for multi-variate system identification.

3.4.3 Data Analysis Computer

After the experimental data are obtained, it is transferred to the data analysis computer, a MicroVax II, where it is analyzed. The MicroVax offers a number of analytic tools for parameter estimation, system identification, error analysis, and controller design. For this project, the most important software tool is the Control System Design, CONSYD, package [53]. In addition, the MicroVax acts as a gateway to other computer systems and control programs including MATLAB and HoneyX.

After the experimental data are analyzed and a linear controller synthesized, the state space model representing this controller is downloaded to the control computer where it can be incorporated immediately into RTCP.

3.5 System Variables

This section examines the many system variables: controlled, manipulated, and disturbance. The control objectives are discussed generally, and from this discussion, the most likely candidates for the controlled and manipulated variables are chosen. All other input variables may be used to simulate disturbances. For convenience, Table 3.6 lists these key manipulated and controlled variable in advance.

3.5.1 Controlled Variables

There are two key controlled variables in fixed bed reactor control: temperature and concentration. It is important to keep the concentration at the outlet of the reactor at its operating specification while maintaining the temperatures inside the reactor within some operating window. This operating window is often defined to avoid catalyst sintering, to eliminate undesirable side reactions, and to insure the safety of the system. This is a very general statement covering all sorts of operating goals including control of the inlet, outlet, or hot spot temperatures, control of the position of the hot spot, control of the exit concentration, and control of the selectivity of one reaction over another.

Often, concentrations cannot be measured fast enough to be used in on-line control. In this case, the exit concentration must be inferred from other operating parameters. Typically, this is done using either inferential control or state estimation on the temperatures inside the axial thermowell.

Finally, if the flow rate through the system is not fixed, as with this reactor, then one can also consider the instantaneous product flow rates or the total flow

Thermocouple #	Length (in)	Distance from Reactor Inlet (in)
1	21.75	0
2	22.5	0.75
3	23.25	1.5
4	24.0	2.25
5	24.75	2.25
6	25.5	3.75
7	26.25	4.5
8	27.0	5.25
9	27.75	6.0
10	30.0	6.75
11	28.5	8.25
12	27.75	9.0
13	26.25	10.5
14	24.75	12.0
15	22.5	14.25
16	21.75	15.0

Table 3.5: Size and position of thermowell thermocouples

Category	Controlled Variables		Manipulated and Disturbance Variables	
Concentrations	c_{out}	Outlet Concentration(s)	c_{in}	Inlet Concentration(s)
	X_{out}	Conversion		
Flow Rates	F_t	Total Flow Rate	F_t	Total Flow rate
			F_b	Heat Exchanger Bypass Flow Rate
			F_r	Recycle Flow Rate
Temperature	T_x	Internal Bed Temperatures	T_{in}	Inlet Temperature
	T_{out}	Outlet Temperature	T_w	Wall Temperature
	T_{hs}	Hot Spot Temperature	Q	Power Supplied to Heaters
	L_{hs}	Hot Spot Location		

Table 3.6: Candidates for manipulated and controlled variables

rate through the reactor as a controlled variable.

3.5.2 Manipulated and Disturbance Variables

Two logical candidates for the manipulated variables are the amount of heat input to the feed stream and the flow rate of the gas through the system. The heat input to the feed stream comes from a number of sources including the heating tapes, furnace, and block heaters. Also affecting the amount of heat input is the flow rate through the bypass valve.

Of these variables, the heating tape has the largest operating range and acts the fastest and is, therefore, the key manipulated variable. The other three variables tend to be operated in conjunction with the heating tape for specialized operating conditions: the block heater for flow rates below 2 slpm, the furnace for flow rates above 80 slpm and the bypass for very fast cooling of the reactor. More often, these variables simulate disturbances in the heat occurring either before or after the feed-effluent heat exchanger.

The inlet flow rate is controlled using the feed flow controllers and the recycle flow controller. The feed flow controllers determine both the inlet flow rate and the inlet concentration. Typical experiments involve controlling one or more feed controllers keeping the other controllers constant. This allows the operator the ability to partially control the inlet stream.

If experiments are desired in which the inlet stream cannot be manipulated, as if it were coming from another piece of equipment, then the key control variable is the recycle flow rate. The recycle stream controls flow rates from 1 to 150 slpm. Compared to the typical inlet flow rate of 15 slpm, the recycle ratio has a much larger operating range. Typical disturbances in these schemes include inlet flow rate or concentration changes due to a change in the flow rate of the uncontrolled inlet stream.

The gas that flows through the recycle valve comes from the pressure damper located at the exit of the compressor. Due to the large damper volume, the time constant associated with gas mixing inside the damper is fairly large, 25 minutes for an operating pressure of 250 psi and an feed flow rate of 20 slpm, and cannot be neglected. Furthermore, this time constant changes as the feed flow rate changes.

In addition to the disturbances in inlet flow rate, concentration or temperature, changes in two other variables are often considered disturbances: changes in the reactor wall temperature and changes in the system pressure. The reactor wall temperature is regulated by the flow of boiling Dowtherm around the reactor tube. If the pressure inside the cooling jacket changes, so does the boiling point of the Dowtherm. This change in the reactor wall temperature modifies the rate at which heat conducts through the reactor wall and sets up new profiles inside the reactor. Potentially, these new profiles have significantly different shapes. Likewise, the system pressure enters into the reaction rate equation, and changes in the system pressure cause different steady state profiles.

Chapter 4

Mathematical Modelling

Introduction

In this chapter, mathematical models for the feed-effluent heat exchanger and the fixed bed reactor are presented. While these models are vastly different in their complexity and purpose, the objectives behind the modelling are the same:

- to explain phenomena which cannot be described by simple design calculations
- to predict the output of the system for a new set of operating conditions
- to understand the physics behind the process and the relationships between various model parameters

The two sections which describe the mathematical models are organized in a similar fashion. First, the aim of the model is revealed, and the characteristics which are to be included in the model are explained. From these criteria, a list of simplifying assumptions is drawn, and using these assumptions, the model is generated from mass and energy balances. Next, the numerical implementation of the model is addressed. Finally, the parameters used in the model are estimated from steady state experiments, and the accuracy of the model is tested by comparing the predicted results with the experimental data.

4.1 Feed-Effluent Heat Exchanger Model

In this section, a simple model predicting the steady state operating temperatures for the feed-effluent heat exchanger is developed. This model incorporates the effects of heat loss to the environment and the simultaneous heat gain by the heaters inside the heat exchanger. This model is not a dynamic model, but aids in the development of such a model. The heat transfer coefficients estimated from static experiments can be used in both static and dynamic models. Examples of dynamic models for heat exchangers have been given elsewhere [109].

4.1.1 Model Characteristics

The primary reason for developing the model is to estimate the rate of heat transfer between the feed stream and the effluent stream under conditions where there is significant heat loss to the environment. Initial experiments on the feed-effluent heat exchanger failed to maintain the energy balance inside the heat exchanger indicating a substantial heat loss to the environment. Simple design calculations using log-mean temperature differences are invalid, and a more accurate model incorporating the heat loss must be developed. The addition of a number of heaters inside the heat exchanger (refer to Section 3.2.2) to reduce the heat loss only complicates the situation. The developed model should incorporate the effects of these heaters as simply as possible.

Figure 4.1 shows the interactions allowed in this model. As the hot effluent gas flows through the inner tube, it transfers its energy to the cold feed gas which passes countercurrently in the annular space. In turn, this cold gas loses some of its energy to the environment through the outer tubing wall.

Several assumptions are made with this model. Plug flows are assumed in both gas streams, and the heat transfer between the hot and cold streams is described by an overall heat transfer coefficient. Likewise, the heat flux to the environment is assumed to be proportional to the difference between the cold gas temperature and the ambient temperature (Newton's law of cooling). Other assumptions include:

- no axial conduction in the gas
- radially uniform gas temperatures
- no axial conduction in the tubing wall
- ambient temperature independent of position and fixed at 25°C
- heat lost to environment function of the power supplied to internal heaters

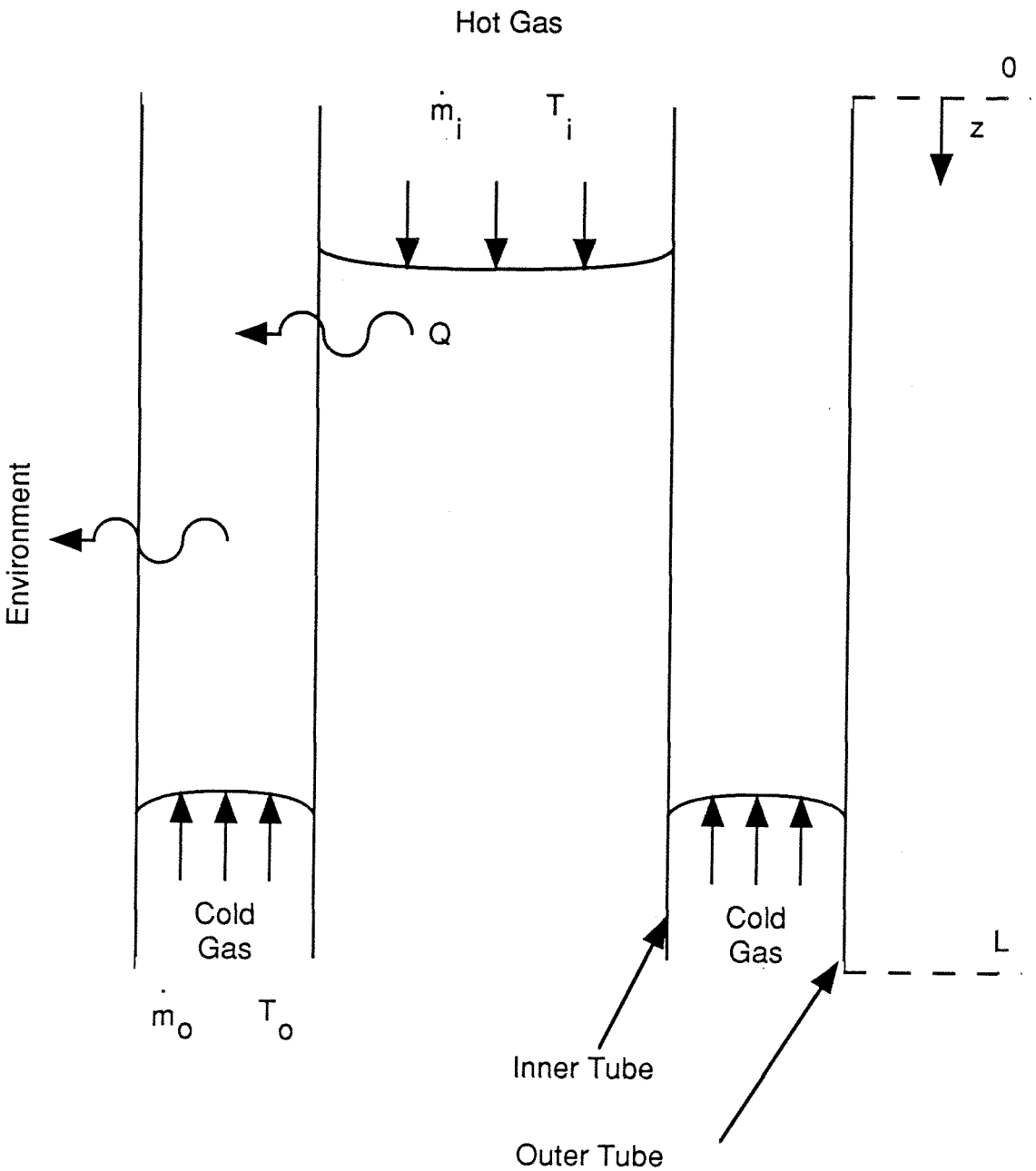

Figure 4.1: Cross section of FEHE showing modelled heat transfer effects

4.1.2 Mathematical Model

Using the previous assumptions, a one dimensional steady state model is developed employing energy balances in both the hot and cold streams. This model is

$$0 = -\dot{m}_i C_p \frac{dT_i}{dz} + (2\pi R_i)U(T_o - T_i) \tag{4.1}$$

$$0 = \dot{m}_o C_p \frac{dT_o}{dz} + (2\pi R_i)U(T_i - T_o) + (2\pi R_o)V(T_a - T_o) \tag{4.2}$$

where T_i, T_o, T_a are the temperatures of the inner stream, outer stream and ambient, respectively. This pair of linear ordinary differential equations, ODEs, can be solved analytically. The solution, assuming equal flow rate in both stream, is

$$\begin{aligned} T_i &= T_a + C_2 \exp\left(\frac{(2\pi R_i)z}{\dot{m}C_p}\left[\frac{V + \sqrt{V^2 + 4UV}}{2}\right]\right) \\ &\quad + C_3 \exp\left(\frac{(2\pi R_o)z}{\dot{m}C_p}\left[\frac{V - \sqrt{V^2 + 4UV}}{2}\right]\right) \end{aligned} \tag{4.3}$$

$$\begin{aligned} T_o &= T_a + C_2\left[\frac{2U + V + \sqrt{V^2 + 4UV}}{2U}\right]\exp\left(\frac{(2\pi R_i)z}{\dot{m}C_p}\left(\frac{V + \sqrt{V^2 + 4UV}}{2}\right)\right) \\ &\quad + C_3\left[\frac{2U + V - \sqrt{V^2 + 4UV}}{2U}\right]\exp\left(\frac{(2\pi R_o)z}{\dot{m}C_p}\left[\frac{V - \sqrt{V^2 + 4UV}}{2}\right]\right) \end{aligned} \tag{4.4}$$

where C_2 and C_3 are determined from the initial conditions.

$$\begin{aligned} C_2 &= \frac{U}{\sqrt{V^2 + 4UV}} \times \\ &\quad \left(T_o|_{z=0} + T_a\left[\frac{V - \sqrt{V^2 + 4UV}}{2U}\right] - T_i|_{z=0}\left[\frac{2U + V - \sqrt{V^2 + 4UV}}{2U}\right]\right) \end{aligned} \tag{4.5}$$

$$C_3 = \frac{U}{\sqrt{V^2 + 4UV}} \times \tag{4.6}$$

$$\left(-T_o|_{z=0} + T_a\left[\frac{-V-\sqrt{V^2+4UV}}{2U}\right] + T_i|_{z=0}\left[\frac{2U+V+\sqrt{V^2+4UV}}{2U}\right]\right)$$

This model is only useful for describing the static heat transfer in the exchanger. A dynamic model can be developed from this steady state model by adding the appropriate time derivatives to the left side of Equations 4.1–4.2. However, this is not recommended since the largest heat capacity is in the tubing walls and not the gas. Accurate dynamic models need to have a separate energy balance for the heat exchanger wall.

4.1.3 Parameter Estimation

Steady State Experiments

The data used to compute the heat exchanger coefficients are obtained from a series of steady state experiments. These experiments consist of operating the heat exchanger at different inlet temperatures, flow rates, and heating powers and recording the steady state exit temperatures. Typically, a new steady state is reached 20 minutes after a change has occurred in one of the input variables.

The operating ranges for the input variables are selected to closely match the conditions found during normal operation. These operating ranges are listed in Table 4.1. Since no reaction occurs inside the reactor during the experiments, the inlet effluent temperature is confined to the cooling jacket temperature of 256°C. Smaller values of flow rate were attempted but the environmental heat loss was too large to obtain meaningful results.

Numerical Results

Equations 4.3–4.7 form a set of nonlinear algebraic functions of the independent parameters U,V. Using a simple nonlinear algebraic equation solver, based on Newton's method, the two heat transfer coefficients are deduced from the inlet and exit

temperatures of the inner and outer streams. In this scheme, the two temperatures at z=0 are used to compute the coefficients C_2 and C_3, while the other two temperatures define the values of U,V. In the few cases where the Jacobian matrix is nearly singular, this technique fails to converge to the correct answer, and the results must be discarded.

Figure 4.2 shows the overall heat transfer coefficient, U, as a function of flow rate. Error bounds are drawn through each data point in this figure. These bounds are computed assuming a 1 degree error in any one of the four thermocouples. Even after accounting for the numerical resolution, there is still a considerable spread associated with the data.

There are two lines drawn on this figure. The solid line represents the best fit of the data to a power law relationship; the dashed line represents the heat transfer coefficient predicted using standard design calculations. As expected, U decreases as the flow rate decreases although not as fast as predicted by the design calculation. As hoped, the difference between the two curves is within engineering precision.

Figure 4.3, shows the heat loss coefficient, V, as a function of flow rate for various heating powers. Like Figure 4.2, this figure has significant spread associated with the data. Lines representing the best fit of the data are shown for the three operating powers. As the power to the internal heaters increases, V decreases. In fact, at full power and large flow rates, the calculated heat loss coefficient is below zero. Under these circumstances, the cold stream is heated beyond that necessary to overcome the cooling of the environment. No theoretical curves are shown in this figure because the mechanisms for heat loss are complicated, and the heat loss coefficient difficult to predict.

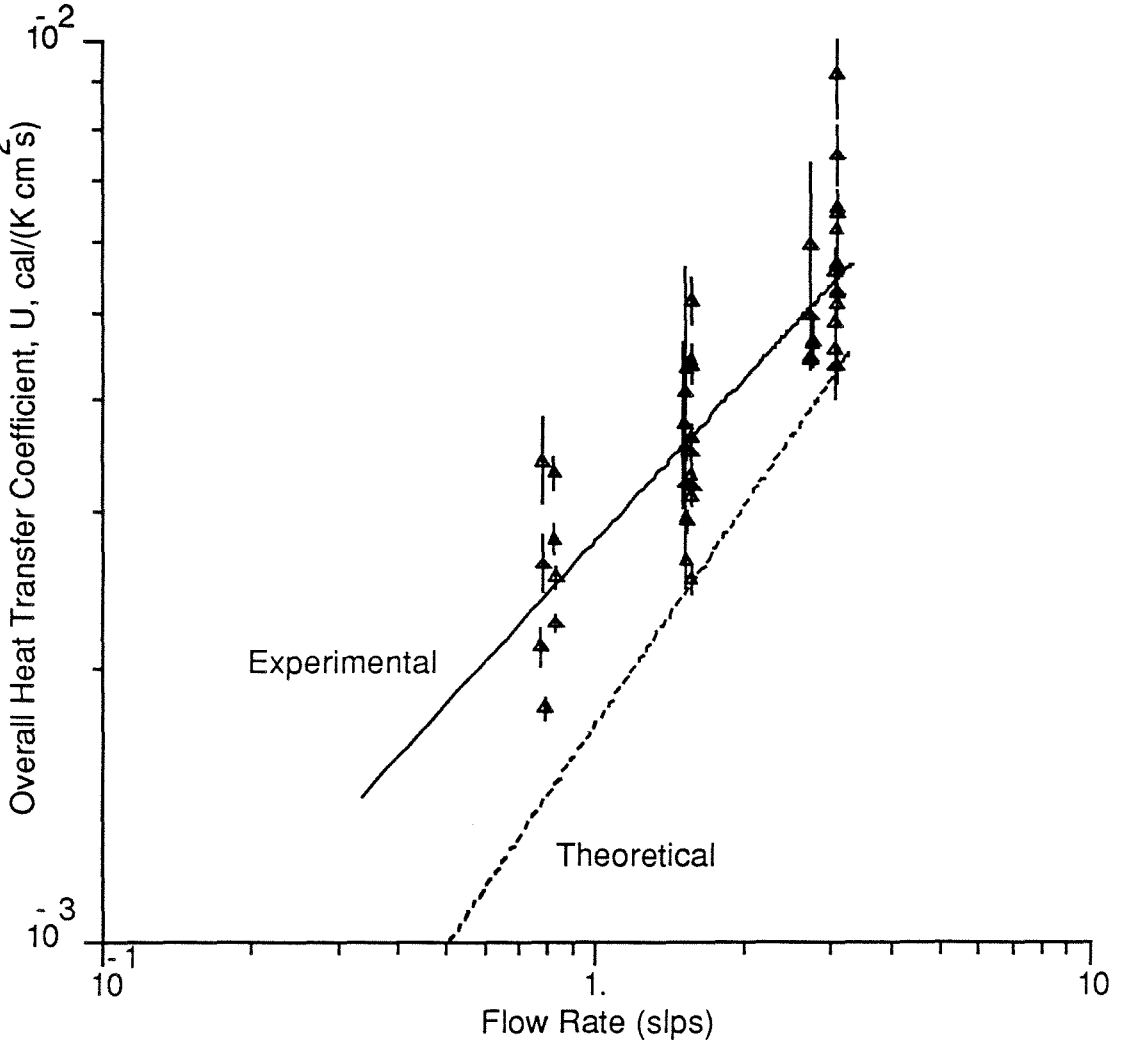

Figure 4.2: Overall heat transfer coefficient for various flow rates

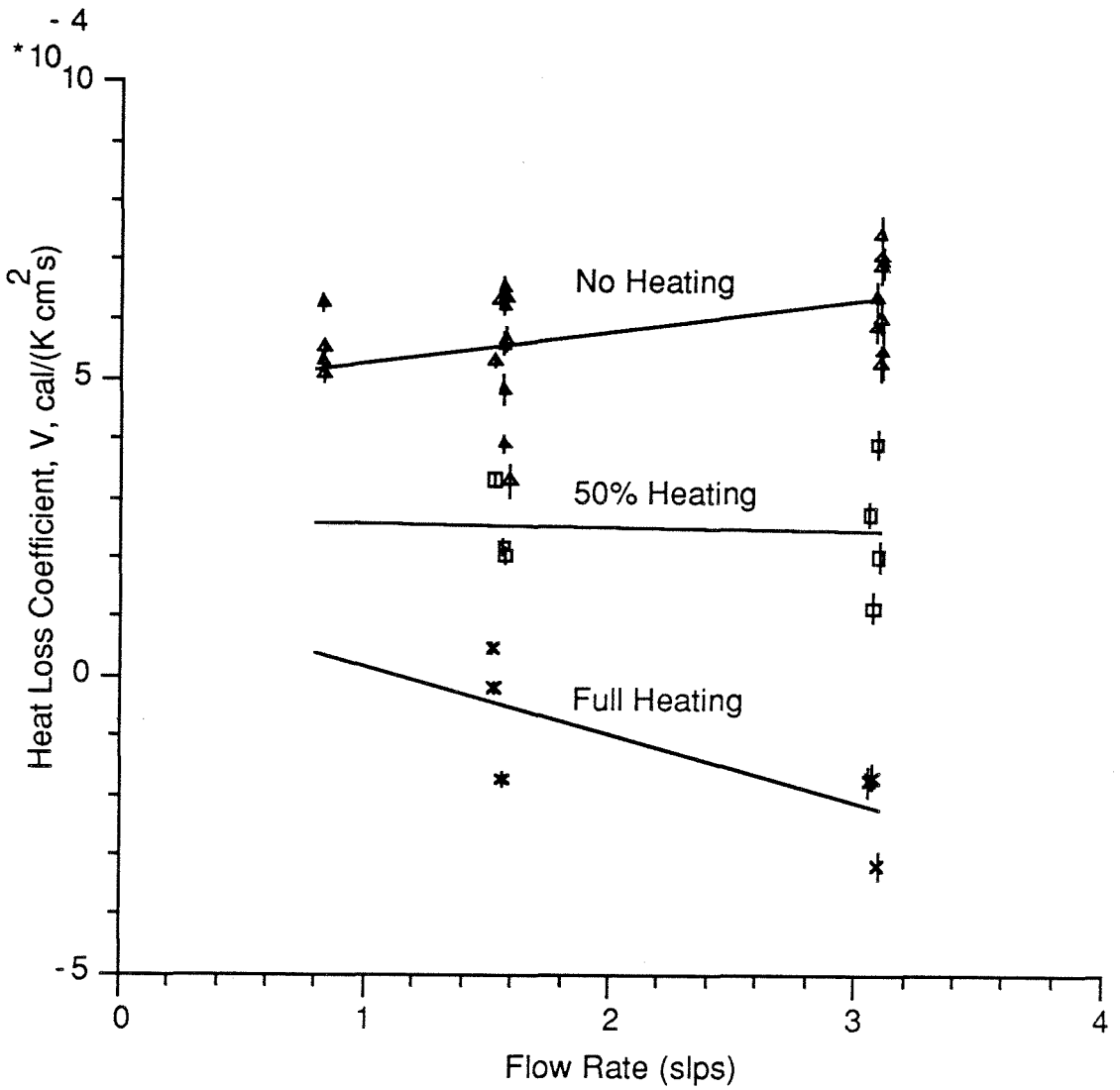

Figure 4.3: Heat loss coefficient as a function of flow rate and power input

4.2 Fixed Bed Reactor Model

In this section, a dynamic first principles mathematical model of the reactor is developed. The purpose of this model is four fold:

1. to predict the steady state temperature and concentration profiles given an arbitrary set of operating parameters

2. to characterize the dynamic relationship between the output variables, concentrations and temperatures, and the manipulated variables, inlet flow rate, concentration, and temperature, in the face of disturbances

3. to determine the sensitivity of the system dynamics to changes in the modelling parameters

4. to design a robust control system based on the dynamics of the model

Due to the complexity of this last step, the robust controllers presented in Chapters 5 and 6 are based on simpler black-box models. The use of this mathematical model for robust control design is left for future research.

The reactor model incorporates the physical interactions associated with mass and energy transport with the chemical relationships found in heterogeneous catalysis. Since nonlinear equations often better describe these relationships than linear equations, it is expected that the nonlinear first principles model will be valid over a wider operating range than a simple linear time invariant model. The effort spent in developing this model is warranted if valuable insight into the dynamic interrelationships of a fixed bed reactor is obtained. This insight is useful when reconfiguring the experimental equipment or when examining new control problems.

4.2.1 Model Characteristics

This section addresses the important physical characteristics found in exothermic fixed bed chemical reactors and in particular the pilot plant system discussed in Chapter 3 and shown schematically in Figure 3.1. These characteristics are then translated into a series of modelling criteria which will be used in the next section to develop a complete mathematical model. Since the pilot plant reactor has been discussed in detail previously, only the main features pertinent to the mathematical model will be summarized in the following.

Figure 4.4 shows an expanded cross section of the reactor bed. The reactor consists of a 1.15 cm radius stainless steel tube filled with 1.0 mm nickel catalyst particles intermixed with inert alumina. As the reactant gases pass through this bed, they contact the nickel catalyst where they react to form the product gases and release a substantial amount of heat. This heat is absorbed by a boiling Dowtherm liquid circulating countercurrently in an outer cooling jacket. Since the liquid is assumed to be boiling at all times, the reactor wall temperature is independent of length and assumed equal the liquid's boiling point.

Along the central axis of the reactor runs a 0.159 cm radius thermowell containing 16 thermocouples of various lengths. These thermocouples can be placed anywhere in the thermowell although they must be moved as a group since they are bundled together. A dedicated on-line gas chromatograph provides periodic concentration measurements of both the inlet and outlet streams; current implementation does not allow continuous concentration measurement.

A number of fast settling mass flow controllers regulate the inlet gas concentration and flow rate, and a series of electrical heaters control the reactor inlet temperature. The temperature of the fluid in the cooling jacket, and, therefore, the reactor wall temperature, can be varied slowly, but only over a limited range, by changing the pressure inside the jacket.

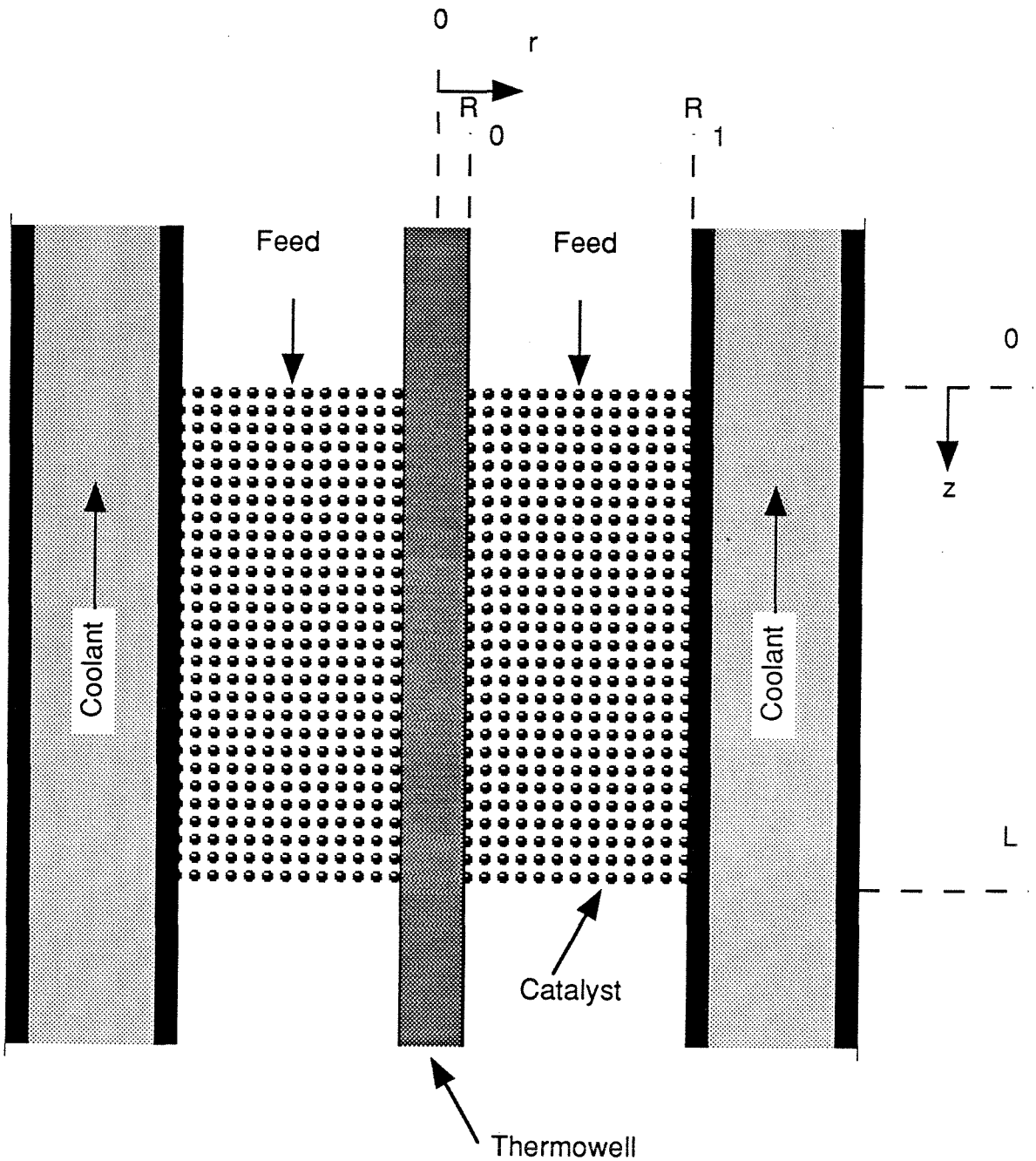

Figure 4.4: Reactor tube cross section

Concentration and temperature control of exothermic fixed bed reactors has traditionally been a difficult task. Some of the characteristics of a fixed bed reactor which make it difficult to control include:

- the spatial dependency of the reactor response
- the strong coupling of the thermal and reaction processes
- the inherent nonlinearity of the rate of reaction
- the time varying change in the reactor dynamics due to catalyst deactivation
- the unavailability of continuous on-line concentration measurements

These characteristics lead to many fascinating and often adverse behaviors including hot spots [61,63], inverse or "wrong way" response [122,123], time delays [115], steady state multiplicity [88], instabilities [144], and regions of large parametric sensitivity [86]. While some of these behaviors place limitations on the achievable closed-loop performance [92], the others limit the operating range of the linearized model used in the controller design. This model is often highly uncertain and can only be used near the operating point. While nonlinear control theory, and especially nonlinear robust control theory [23] may overcome some of these limitations, it is still an area of active research with few applicable results.

To represent the above, the following attributes are incorporated in the mathematical model:

Spatial Dependency The model is a distributed parameter model incorporating spatial derivatives in both the axial and radial directions. This model is described in terms of partial differential equations instead of more amenable ordinary differential equations. For controller design and simulation, it will be necessary to approximate these PDEs by a series of ODEs.

Coupling of Thermal and Reaction Processes The rate of reaction appears in both the mass and energy transport equations and is a function of the local concentration and temperature. Since the reaction is exothermic, temperatures inside the bed increase as the reaction proceeds. These increased temperatures accelerate the rate of reaction increasing the bed temperatures even further. At steady state, there is a balance between the heat generated by the reaction and the cooling of the Dowtherm jacket resulting in a highly nonlinear concentration and temperature profiles.

Nonlinear Reaction Rate The reaction rate term should be modelled as accurately as possible using the available kinetic information. In the case of CO_2 methanation, the reaction rate is a nonlinear function of both concentration and temperature being modelled by a Langmuir-Hinshelwood rate expression with a modified Arrenhius temperature dependence (see Section 3.1.3). No attempt should be made to linearize this term.

Time Varying Catalyst Activity As pointed out in Section 3.1, there are a number of mechanisms for catalyst deactivation. This deactivation can be modelled by a time dependent factor in the reaction rate equation. Initial experiments on the catalyst point to a very slow deactivation and therefore, this term has been neglected in this study. The term remains in the model, though, for future studies.

Discrete Concentration Measurements The gas concentration measurements come from an on-line process gas chromatograph. This unit has a sampling time of 20 minutes which is typically on the order of the dominant system time constant. While the mathematical model should produce a continuous estimate of this concentration, any simulation employing direct feedback on the concentration measurement should be limited to a sampling rate of once

every 20 minutes.

Steady State Multiplicity Because of the complex interactions inside a reactor, reactor models often admit multiple steady states. These steady states can be an outcome of internal catalyst gradients [141] or localized heating in the reactor [140,50]. The number of multiplicities often increases when adding energy recycle [124,125] or mass recycle [85,105]. While it is difficult to cover all of this phenomena in a single model, with the exception of Assumption 2 below, no attempt has been made to restrict the number or kind of steady states. Furthermore, the reactor model should easily interact with models of other processing units, such as the feed-effluent heat exchanger and the recycle stream, to form a more comprehensive, and in general complex, system model.

In addition to these attributes, a number of other notable features include:

Heterogeneous Model The reactor bed is assumed to be composed of two separate phases, a gas phase and a solid phase, which interact through heat and mass transfer coefficients. Each phase is assumed to behave as a "continuum insofar as changes occur smoothly and continuously within each phase" [65].

Variable Gas Properties The model accounts for the temperature, pressure, and concentration dependencies of the gas density, average molecular weight, heat capacity and heat of reaction. Furthermore, the gas pressure varies in the axial direction to account for the pressure drop across the bed.

Axial Thermowell Due to the large axial conduction in the central thermowell, the dynamics of the thermowell are included in a separate energy balance equation.

Uneven Catalyst Loading The reactor bed may have an uneven catalyst loading. The reactor bed is unevenly loaded if the concentration of active catalyst in

the bed is a function of position. Even if the bed is uniformly loaded at the start of the experiment, poisoning of the catalyst at the inlet of the reactor can cause the loading to change with time. To account for this non-uniform catalyst loading, the rate expression is multiplied by a position dependent loading factor, Ξ.

4.2.2 Mathematical Model

Using the above criteria as guidelines, a detailed first principles model of the reactor has been derived. This model is based extensively on the reactor model developed by Mandler [86] which in turn is based on the model of Khanna [65,66]. In fact, the model presented below is identical to the Mandler's model with exception of the inclusion of a catalyst loading factor and the redefinition of the mass flux. While the mathematical models are nearly identical, their numerical implementation is completely different. These differences will be discussed in detail in the Section 4.2.3.

When developing the model, a number of different modelling assumptions are made. A complete discussion of the validity of these assumptions has been performed elsewhere [65,86] and will not be attempted here. These assumptions include:

1. The methanation reaction is the only reaction occurring in the system.

2. The reaction rate is based on the local gas phase concentrations. This implies that all mass and energy transfer effects within a catalyst particle and between particles must be lumped into a global rate expression.

3. The reactor bed contains a uniformly active catalyst except for a small region at the beginning of the reactor where the catalyst is assumed to be completely poisoned.

4. The gas velocity has no radial component, and is radially uniform across the bed (i.e., no channeling).

5. The total mass flux is independent of length and equal to the inlet mass flow rate divided by the cross sectional area of the bed.

6. All gases are ideal gases, and their properties are known functions of temperature, pressure and concentration.

7. The reactor wall temperature is equal to the Dowtherm cooling jacket temperature and is independent of axial distance. In turn, the cooling jacket temperature is an independent parameter which is allowed to vary with time.

8. Radiative heat transfer is ignored.

9. All heat transfer coefficients are constant and therefore independent of the flow rate.

Using these assumptions, unsteady-state mass and energy balances have been developed.

Energy balance for the solids phase:

$$(1-\epsilon)\rho_s C_{p_s}\frac{\partial T_s}{\partial t} = k_s\frac{\partial^2 T_s}{\partial z^2} + \frac{k_s}{r}\frac{\partial}{\partial r}\left[r\frac{\partial T_s}{\partial r}\right] - (h_{sg}a_{sg})(T_s - T_g) + (-\Delta H_M)\tilde{R}_M \quad (4.7)$$

$$\begin{aligned} r &= R_0 & k_s\tfrac{\partial T_s}{\partial r} &= h_{st}(T_s - T_t) \\ r &= R_1 & -k_s\tfrac{\partial T_s}{\partial r} &= h_{sw}(T_s - T_w) \\ z &= 0 & k_s\tfrac{\partial T_s}{\partial z} &= h_{sg}(T_s - T_g) \\ z &= L & -k_s\tfrac{\partial T_s}{\partial z} &= h_{sg}(T_s - T_g) \end{aligned}$$

Energy balance for the gas phase:

$$\epsilon\rho_g C_{p_g}\frac{\partial T_g}{\partial t} = -GC_{p_g}\frac{\partial T_g}{\partial z} + k_g\frac{\partial^2 T_g}{\partial z^2} + \frac{k_g}{r}\frac{\partial}{\partial r}\left[r\frac{\partial T_g}{\partial r}\right] - (h_{sg}a_{sg})(T_g - T_s) \quad (4.8)$$

$$
\begin{aligned}
r &= R_0 & k_g \tfrac{\partial T_g}{\partial r} &= h_{gt}(T_g - T_t) \\
r &= R_1 & -k_g \tfrac{\partial T_g}{\partial r} &= h_{gw}(T_g - T_w) \\
z &= 0 & k_g \tfrac{\partial T_g}{\partial z} &= h_{sg}(T_g - T_s) - GC_{p_g}(T_{in} - T_g) \\
z &= L & -k_g \tfrac{\partial T_g}{\partial z} &= h_{sg}(T_g - T_s)
\end{aligned}
$$

Energy balance for the thermowell:

$$\rho_t C_{p_t} \frac{\partial T_t}{\partial t} = k_t \frac{\partial^2 T_t}{\partial z^2} + (h_{st} a_t)\left(T_s|_{r=R_0} - T_t\right) + (h_{gt} a_t)\left(T_g|_{r=R_0} - T_t\right) \tag{4.9}$$

$$
\begin{aligned}
z &= 0 & T_t &= T_{in} \\
z &= L & \tfrac{\partial T_t}{\partial z} &= 0
\end{aligned}
$$

Species balance for the CO_2:

$$\epsilon \rho_g \frac{\partial \hat{x}}{\partial t} = -G \frac{\partial \hat{x}}{\partial z} + \frac{D_r \epsilon}{r} \frac{\partial}{\partial r}\left[r \rho_g \frac{\partial \hat{x}}{\partial r} + \frac{2\rho_g \hat{x} r}{1 - 2\delta} \frac{\partial \delta}{\partial r} \right] - \tilde{R}_M \hat{M}_g \tag{4.10}$$

$$
\begin{aligned}
r &= R_0, R_1 & D_r \tfrac{\partial \hat{x}}{\partial r} &= 0 \\
z &= 0 & \hat{x} &= x_{in}
\end{aligned}
$$

Additional relationships:

$$\tilde{R}_M = \left[R_M(1-\nu)\Xi\right] \rho_s \psi (1 - \epsilon) \tag{4.11}$$

$$R_M = \frac{k_0 e^{-\frac{E_{a_0}}{RT}} P_{CO_2}}{\left[1 + k_1 e^{\frac{E_{a_1}}{RT}} P_{CO_2}\right]} \tag{4.12}$$

$$\nu = \frac{P_{CH_4} P_{H_2O}^2}{K_p P_{CO_2} P_{H_2}^4} \tag{4.13}$$

$$\delta = \frac{x_{in} - x}{1 - 2x} \tag{4.14}$$

$$\hat{x} = x(1 - 2\delta) \tag{4.15}$$

$$\rho_g = \frac{M_g P}{RT_g} = \frac{\hat{M}_g \hat{P}}{RT_g} \tag{4.16}$$

$$\hat{M}_g = M_g(1 - 2\delta) \tag{4.17}$$

$$\hat{P} = P(1 - 2\delta)^{-1} \tag{4.18}$$

The pseudo-pressure, $\hat{P}$, defined by the previous equation is a mathematical convenience designed specifically to account for changes in the total number of moles of gas with reaction [65]. While correlations such as the Blake-Kozeny, Burke-Plummer or the Ergun equations [6,31] can be used to describe the pressure drop across a packed bed and, therefore, the pseudo-pressure, in this study, the pseudo-pressure is assumed to be a linear function of axial position.

$$\hat{P} = \left[\frac{\hat{P}|_{z=L} - \hat{P}|_{z=0}}{L}\right] z + \hat{P}|_{z=0} \tag{4.19}$$

4.2.3 Numerical Analysis

This first principles model consists of four coupled nonlinear partial differential equations (Equations 4.7–4.10) mixed with a series of nonlinear algebraic equations (Equations 4.11–4.18). Solving this set of equations can be a formidable task for any numerical algorithm.

Mandler [86] solves these equations using a three step procedure. First, the dimensional equations are non-dimensionalized to determine the relevant dimensionless groups, and values of these dimensionless groups are computed. Second, the non-dimensional partial differential equations, PDEs, are transformed to a set of ordinary differential equations, ODEs, using orthogonal collocation [132,28,91,131]. This is done first in the radial direction, using one interior collocation point, then in the axial direction. Finally, the set of ODEs is solved using a nonlinear differential-algebraic equation solver.

This model predicts temperature and concentration profiles which are considerably milder than those found in the experimental reactor. Initial experiments established the formation of a temperature maximum or hot spot inside the reactor. This hot spot is typical of a region with a sudden change in both concentration and temperature. When the model is updated to reflect more accurate parameter estimates, the collocation scheme fails to converge to a steady state.

This convergence problem is uniquely related to orthogonal collocation's inability to handle sharp gradients. In collocation, the operating profiles are described by high order polynomials. When these polynomials must describe a profile which is nearly discontinuous, they introduce oscillations in the estimated profiles. In the specific case of the concentration profile, the predicted concentrations downstream from the hot spot oscillate around zero concentration and sometimes assume negative values. Unfortunately, the reaction rate expression cannot handle negative concentrations, and the solution scheme fails. This is one of the known shortcomings of collocation.

One solution to the problem is to use orthogonal collocation on finite elements, OCFE [15]. This scheme consists of dividing the operating space into several smaller regions, called finite elements, and applying orthogonal collocation to each of these elements. Since the collocation technique needs to describe the operating profiles only over the space of the element, lower order polynomial approximations are administered. The boundaries of the elements are then matched by forcing the combined profiles to be continuous and differentiable.

This technique suffers from two drawbacks. First, adding elements proportionally increases the number of ODEs to be solved and, therefore, increases the simulation time. Second, the size of every finite element must be specified *a priori* at the start of each simulation. This is often difficult to do since the finite elements should be concentrated in the region where the profiles have steep gradients, yet the steady state gradients are not known until after the simulation is run. Often, the simulation

needs to be run twice: the first time to determine where the gradients are steepest and the second time to determine the shape of the profiles. In dynamic simulations, this problem is further complicated by the movement of the fronts with changes in the operating conditions.

To overcome this second problem, a variation on OCFE termed orthogonal collocation on finite elements with moving boundaries [57,29,37] has been proposed. Like OCFE, the operating space is divided into a number of smaller elements and orthogonal collocation is applied to each element. However, unlike OCFE, the size of the finite elements adapts to dynamic changes in the gradient steepness. This technique has been used successfully by [35,5] to study chemical reactor dynamics.

An alternative to the collocation schemes, and the method used in this work, is the finite difference technique [72]. Like the finite element schemes, finite difference first discretizes the operating space into a number of smaller regions; however, the temperatures and concentrations in each region are assumed to be uniform. Difference equations then replace the spatial derivatives, and the initial PDEs are transformed to a set of ODEs in time.

Finite difference has the advantage of being simple to formulate and easy to implement, but suffers from the need to have a relatively large number of mesh points to obtain adequate resolution of the profiles. Unfortunately, increasing the number of mesh points tends to significantly slow the computer. Simulations have shown that the amount of time needed to converge to the steady state answer depends quadratically on the number of mesh points. Therefore, to obtain reasonably fast simulations, the number of mesh points must be limited.

In order to keep a high resolution in the axial direction and yet still have fast simulations, the radial discretization is dropped, and the operating profiles are assumed to be radially uniform. This assumption holds, at least at steady state, when the dominant resistance to heat flow is between the cooling jacket wall and

the reactor bed and not conduction through the catalyst. By dropping the radial derivatives and incorporating the radial boundary conditions inside the model, the reactor model is rewritten as:

Energy balance for the solids phase:

$$\begin{aligned}(1-\epsilon)\rho_s C_{p_s}\frac{\partial T_s}{\partial t} &= k_s\frac{\partial^2 T_s}{\partial z^2} - (h_{sw}a_w)(T_s - T_w) - (h_{st}a_t)(T_s - T_t) \\ &\quad -(h_{sg}a_{sg})(T_s - T_g) + (-\Delta H_M)\tilde{R}_M \end{aligned} \tag{4.20}$$

$$\begin{aligned} z &= 0 \qquad & k_s\tfrac{\partial T_s}{\partial z} &= h_{sg}(T_s - T_g) \\ z &= L \qquad & -k_s\tfrac{\partial T_s}{\partial z} &= h_{sg}(T_s - T_g) \end{aligned}$$

Energy balance for the gas phase:

$$\begin{aligned}\epsilon\rho_g C_{p_g}\frac{\partial T_g}{\partial t} &= -GC_{p_g}\frac{\partial T_g}{\partial z} + k_g\frac{\partial^2 T_g}{\partial z^2} - (h_{gw}a_w)(T_g - T_w) \\ &\quad -(h_{gt}a_t)(T_g - T_t) - (h_{sg}a_{sg})(T_g - T_s) \end{aligned} \tag{4.21}$$

$$\begin{aligned} z &= 0 \qquad & k_g\tfrac{\partial T_g}{\partial z} &= h_{sg}(T_g - T_s) - GC_{p_g}(T_{in} - T_g) \\ z &= L \qquad & -k_g\tfrac{\partial T_g}{\partial z} &= h_{sg}(T_g - T_s) \end{aligned}$$

Energy balance for the thermowell:

$$\rho_t C_{p_t}\frac{\partial T_t}{\partial t} = k_t\frac{\partial^2 T_t}{\partial z^2} - \mathcal{P}(h_{st}a_t)\,(T_t - T_s) - \mathcal{P}(h_{gt}a_t)\,(T_t - T_g) \tag{4.22}$$

$$\mathcal{P} = \frac{\pi R_1^2 - \pi R_0^2}{\pi R_0^2}$$

$$\begin{aligned} z &= 0 \qquad & T_t &= T_{in} \\ z &= L \qquad & \tfrac{\partial T_t}{\partial z} &= 0 \end{aligned}$$

Species balance for the CO_2:

$$\epsilon\rho_g\frac{\partial \hat{x}}{\partial t} = -G\frac{\partial \hat{x}}{\partial z} - \tilde{R}_M\hat{M}_g \tag{4.23}$$

$$z = 0 \qquad \hat{x} = x_{in}$$

By replacing the axial derivatives with difference operators, these equations can be approximated by a set of ordinary nonlinear differential equations. In the original implementation of the finite difference scheme, a second central difference approximation, μ^2, replaced the second order partial derivatives, and a first central difference, μ_{2h}, replaced the first order partial derivatives.

$$\mu y(z_i) = \frac{y(z_{i+1/2}) - y(z_{i-1/2})}{h} \tag{4.24}$$

$$\mu^2 y(z_i) = \mu(\mu y(z_i)) = \frac{y(z_{i+1}) - 2y(z_i) + y(z_{i-1})}{h^2} \tag{4.25}$$

$$\mu_{2h} y(z_i) = \frac{y(z_{i+1}) - y(z_{i-1})}{2h} \tag{4.26}$$

$$h = z_{i+1} - z_i = z_i - z_{i-1} \text{ is the mesh size}$$

This was a logical choice for the difference operators since the truncation error in both operators is of $\mathcal{O}(h^2)$. Unfortunately, using a first central difference approximation leads to an unwanted spurious oscillation in the gas temperature profile at large gas flow rates. This oscillation is due in part to the first central difference not being a function of the local value (i.e., μ_{2h} does not depend on $y(z_i)$). To overcome this oscillation, the current scheme uses a first backward difference approximation, ∇, for the first order partial derivatives.

$$\nabla y(z_i) = \frac{y(z_i) - y(z_{i-1})}{h} \tag{4.27}$$

To keep the number of mesh points small and yet to concentrate these points near the steep gradients, spatially variable difference approximations supplant the

standard finite difference approximations.

$$\tilde{\mu}^2 y(z_i) = 2\left(\frac{y(z_{i+1}) - y(z_i)}{(z_{i+1} - z_i)(z_{i+1} - z_{i-1})} - \frac{y(z_i) - y(z_{i-1})}{(z_i - z_{i-1})(z_{i+1} - z_{i-1})}\right) \quad (4.28)$$

$$\tilde{\nabla} y(z_i) = \frac{y(z_i) - y(z_{i-1})}{z_i - z_{i-1}} \quad (4.29)$$

With these approximations, a fine mesh is used in the region of the hot spot and a much courser mesh at the edges of the reactor where the gradients are not as steep. Like the finite element schemes, the position of the mesh points must be specified *a priori* at the start of the simulation. Special software has been added to the simulator which automatically computes the gradients of the current steady state profile and reconcentrates mesh points in the region of the hot spot for use in the next simulation.

Each mesh point has four unknown quantities associated with it: gas, catalyst, thermowell temperatures and the CO_2 concentration. Assuming there are $N + 2$ total mesh points, then there are $4(N + 2)$ unknowns of which $4N + 1$ are solved from the differential equations. Of the seven remaining unknowns, five are solved from the implicit algebraic boundary conditions and two from explicit boundary conditions.

This set of equations is solved using the differential-algebraic equation solver, DASSL [99]. DASSL uses the backward differentiation formulas of orders one through five to solve a system of equations in the form

$$\mathcal{G}(t, y, y') = 0 \quad (4.30)$$

for y and y'. In its solution of these equations, DASSL forces $\mathcal{G}$ to be within a user specified error tolerance before proceeding to the next time. One advantage of DASSL over other differential equations solvers is that algebraic equations and

differential equations can be solved simultaneously. Algebraic equations are treated as a special case of Equation 4.30 with $y' = 0$.

Because there is no disadvantage in retaining the concentration time derivative, the CO_2 concentration is not assumed to be quasi-stationary. A number of authors [121,43,113] make this quasi-stationary assumption since the concentration wave is several orders of magnitude faster than the temperature wave. Little difference is expected between the two models except for the short time after a change in the inlet concentration when the concentration wave is proceeding through the reactor.

As part of its solution procedure, DASSL computes the Jacobian matrix of $\mathcal{G}$. In the current finite difference scheme, the temperatures and concentrations at any axial location are only a function of the values at the current mesh point and its nearest neighbors. This significantly reduces the spatial coupling of the equations and makes the Jacobian matrix banded. Having a banded Jacobian aids in the calculation of the solution by reducing the required storage space and by increasing the efficiency of the algorithm. Typical simulation times are reduced by an order of magnitude over the non-banded case and are comparable with those found with collocation. For example, a finite difference reactor simulation with 100 internal mesh points can be solved using only 10% more time than the 12 point collocation model of Mandler.

4.2.4 Parameter Estimation and Model Validation

In this section, the experiments used to measure the reactor parameters and validate the mathematical model are discussed. Table 4.2 lists all the parameters employed in the reactor model and their current estimate. The values for most of these parameters come from one of three sources: direct measurement of the geometry, pre-selection during the design of the reactor, or manufacturer and pub-

lished literature. Only those parameters pertaining to heat transfer have to be estimated from steady state experiments. Once all parameters have been estimated, the mathematical model must be validated by comparing the results of steady state and dynamic simulations to the profiles obtained in the reactor.

Kinetics Validation

The parameter estimation and model validation step has been divided into three stages: kinetic parameter validation, non-reactive experimentation and reactive experimentation. The first stage involves the estimation of the kinetic parameters associated with the methanation reaction. This reaction is discussed in detail in Section 3.1. In the previous work of Vatcha [129] and Strand [117], serious questions arose as to the correct functional form and kinetic constants associated with the rate equation. Since the rate expression is of vital importance to the model, accurate identification of the global rate expression is necessary. The word global implies that all interparticle and intraparticle gradients are accounted for in a single rate expression based on the local gas concentration and temperature.

Strand [117] built a small differential recycle reactor [97] to measure the CO methanation reaction rate. This reactor operates under isothermal and gradientless conditions, and is safer and simpler to operate than the pilot plant allowing for more accurate evaluation the reaction rate. Chiang [17] used this reactor to estimate the reaction rate coefficients of several Langmuir-Hinshelwood functional forms. The reaction rate coefficients for each functional form were fit to the steady state data using standard nonlinear regression techniques, and the expression which best fit the data was chosen as the rate expression. The resultant rate expression, Equation 3.1, is comparable both in form and value to those obtained by other researchers [140, 126].

Because the predicted CO methanation rate is nearly identical to the results

Operating Parameter	Range	Units
Inlet Feed Temperature	20–200	°C
Inlet Effluent Temperature	256	°C
Flow Rate	45–180	slpm
Heating Power	0,50,100	% of full power

Table 4.1: Operating conditions for heat exchanger parameter estimation

Parameter	Symbol	Value	Units
Solids Parameters			
Void Fraction†	ϵ	0.61	cm^3/cm^3
Density§	ρ_s	0.734	g/cm^3
Heat Capacity§	C_{p_s}	0.27	cal/g K
Effective Thermal Conductivity*	k_s	0.0022	cal/sec cm K
Heat Transfer Coef. Solids-Wall*	h_{sw}	5.5E-4	cal/sec cm^2 K
Heat Transfer Coef. Solids-Thermowell*	h_{st}	5.5E-4	cal/sec cm^2 K
Heat Transfer Coef. Solids-Gas*	h_{sg}	1.0E-4	cal/sec cm^2 K
Gas Parameters			
Density§	ρ_g	¶	g/cm^3
Heat Capacity§	C_{p_g}	¶	cal/g K
Effective Thermal Conductivity*	k_g	1.0E-4	cal/sec cm K
Heat Transfer Coef. Gas-Wall*	h_{gw}	5.5E-4	cal/sec cm^2 K
Heat Transfer Coef. Gas-Thermowell*	h_{gt}	5.5E-4	cal/sec cm^2 K
Inlet Molecular Weight§	MW_i	¶	g/mol
Thermowell Parameters			
Density§	ρ_t	8.02	cal/cm^3
Heat Capacity§	C_{p_t}	0.12	cal/g K
Thermal Conductivity§	k_t	0.039	cal/sec cm K

Table 4.2: Reactor parameters

Parameter	Symbol	Value	Units
Reaction Parameters [§] [‖]			
Rate of Reaction	R_M	‖	mol CO_2 / g_{cat} sec
Heat of Reaction	ΔH_r	$\Delta H_r = (\Delta H_a)T_g + \Delta H_b$	cal/mol
	ΔH_a	-8.79	cal/mol K
	ΔH_b	-37400	cal/mol
Equilibrium Constant	$\ln(K_p)$	$\ln(K_p) = K_{p_a} + K_{p_b}/T_g$	
	K_{p_a}	-24.8	
	K_{p_b}	21600	K
Catalyst Dilution Factor[‡]	ψ	0.369	g_{cat} / g_{solid}
Dead Zone Length[*]	χ	6.0	cm
Others			
Reactor Length[‡]	L	60	cm
Thermowell Radius[‡]	R_0	0.159	cm
Reactor Radius[‡]	R_1	1.15	cm
Wall Surface Area per Unit Reactor Volume[†]	A_w	1.78	cm^{-1}
Thermowell Surface Area per Unit Reactor Volume[†]	A_t	0.247	cm^{-1}
Catalyst Surface Area per Unit Reactor Volume[*]	A_{cat}	90	cm^{-1}
Inlet Pressure	$P\|_{z=0}$	14	atm
Outlet Pressure	$P\|_{z=L}$	13	atm

[†] found by direct measurement
[§] found in literature
[*] determined experimentally
[¶] varies with inlet gas concentration
[‖] refer to Table 3.3
[‡] selected *a priori*

Table 4.2: Reactor parameters continued

obtained by other researchers, the reaction rate expression for the methanation of CO_2 is taken directly from the literature [140]. Any variation in the activation energy or pre-exponential factor can be indirectly evaluated using the reactive experiments on the pilot plant.

Two modifications are made to this reaction rate expression. First, the rate expression is multiplied by the expression $(1 - \nu)$, where

$$\nu = \frac{P_{CH_4} P_{H_2O}^2}{K_p P_{CO_2} P_{H_2}^4} \tag{4.31}$$

Vatcha [129] advocates the use of this expression to prevent the reaction from proceeding beyond equilibrium. Second, the rate expression is multiplied by the function $\Xi(z)$ to account for deactivated or improperly loaded catalyst at the beginning of the reactor. This function has the form

$$\Xi(z) = \begin{cases} 0 & \text{for } z < \chi \\ 1 & \text{otherwise} \end{cases} \tag{4.32}$$

where χ is determined from experiments.

Non-Reactive Experimentation

In the second stage, non-reactive experiments are used to estimate the heat transfer coefficients of the reactor model. These coefficients are estimated from experiments carried out directly on the pilot plant and not on the smaller kinetics reactor. By carrying out the experiments under non-reactive conditions, the heat transfer effects are better isolated since the heat and the mass transfer problems are decoupled.

Under these circumstances, the mathematical model describing the reactor is significantly simpler and easier to solve. Since there are no concentration gradi-

ents, the concentration equation is dropped, and the remaining partial differential equations reduce to a set of three nearly linear coupled equations. (The equations are linear if the gas heat capacity and density are assumed to be constant.) The unknown parameters describing this non-reactive model are a small subset of the original parameter set.

In the non-reactive experiments, pure nitrogen flows through the reactor and is cooled (or possibly heated) by the walls of the Dowtherm jacket. The steady state axial temperature profiles are measured for various inlet temperatures and flow rates, and the rate of heat transfer in the reactor is determined from these profiles.

Under the non-reactive conditions, the reactor acts as a vehicle through which the heat from the incoming gas is transferred to the boiling Dowtherm. There are two mechanisms by which this energy is transported, through the solids and through the gas, and either mechanism can dominate depending on the relative magnitude of the heat transfer parameters: k_s, $h_{sw} = h_{st}$, k_g, and $h_{gw} = h_{gt}$. In addition, the interphase heat transfer coefficient, h_{sg}, connects these mechanisms by allowing heat to be transferred between the solids and the gas. If h_{gw} is small and yet h_{sw} and h_{sg} are large, the hot feed gas still cools quickly. Since the gas and solid phase temperatures cannot be directly measured, a certain amount of ambiguity is expected in the results.

The numerical analysis of these experiments proceeds in two steps. First, the heat transfer parameters are estimated using correlations given in the literature [21, 89,98]. Mandler [86] calculated these parameters for his simulation studies, and his estimates serve as initial estimates in the current simulations. Second, each of the parameters is individually varied and the parametric sensitivity of the temperature profiles determined. The coefficients with the largest sensitivity are updated to minimize the error with the data while the other coefficients are held constant. This

analysis is somewhat qualitative with the emphasis placed on obtaining the proper order of magnitude for each parameter rather than a specific value.

The heat transfer coefficients with the wall, h_{sw} and h_{gw}, have the largest effect on the simulated temperature profiles. They have roughly equal effect, and are by far the most sensitive parameters. The next most sensitive parameters are the interphase coefficients, h_{sg} and A_{cat}. By increasing either of these parameters, the temperature difference between the gas and solid phases decreases, and the model is more homogeneous. It is difficult to isolate the effects of the these two parameters since h_{sg} appears without A_{cat} only in the boundary conditions of the gas and solids temperatures which cannot be directly measured. The final two parameters, the effective thermal conductivities, k_s and k_g, have little effect on the non-reactive temperature profiles. It is anticipated that they will have a greater importance in the reactive experiments where a hot spot is formed.

Reactive Experimentation

In the final stage, experiments involving CO_2 methanation are used to validate the mathematical model and to re-estimate the most sensitive parameters. It is important to estimate carefully those parameters for which the model is most sensitive since these parameters may change slightly between the reactive and non-reactive cases. In these reactive experiments, the steady state axial temperature profiles and exit gas concentration are recorded for various inlet concentrations, flow rates and temperatures and then compared to the results of the simulations. No recycle is used in these experiments since this tends to complicate the estimation problem.

To obtain the best possible estimation of the parameters, it is important to operate the system where the parametric sensitivity is large. This often implies having steep temperature or concentration gradients. Because of this, it is decided to operate the reactor under conditions where it will form a hot spot. Under these

conditions, the CO_2 conversion is complete and measurements of the exit gas concentration prove only to confirm this fact. Any changes in the kinetics manifest themselves in changes in the size, shape or position of the hot spot.

Two different kinds of reactive experiments are run. In the first experiments, the inlet temperature, CO_2 flow rate and H_2 flow rate are held constant, while the N_2 flow rate is allowed to vary. In these experiments, the inlet temperature is fixed at 230°C and four different N_2 flow rates are employed: 2, 4, 8, and 16 slpm. Two sets of reactant flow rate have been examined with each set having a 5:1 ratio of H_2 to CO_2. The first set has a total reactant flow rate of 1 slpm and the second 3 slpm. The steady state temperature profiles for each set are shown in Figures 4.5 and 4.6 respectively.

The distinguishing feature in all of the profiles is the presence of the temperature maximum or hot spot. The location and height of this hot spot are unique functions of the N_2 flow rate (for all other operating conditions fixed). As the N_2 flow rate increases, the height of the hot spot decreases, the width of the hot spot increases, and the position of the hot spot is shifted toward the exit of the reactor. All of these changes can be explained by the increased convection inside the reactor. This increase in gas convection tends to spread the heat generated by the reaction over a wider area by transporting energy away from the hot spot toward the exit of the reactor. If the N_2 flow rate is large enough, the gas convection will force the hot spot out of the reactor. As the reactant flow rates increase, the size of the hot spot peak increases, but the general behavior with respect to N_2 flow rate remains the same.

At the hot spot, the reaction proceeds quickly, and large amounts of energy are released, but this energy is rapidly conveyed to the cooling jacket as the system cools down. It is the cooling of the jacket which forces the temperatures after the hot spot to decrease. The jacket can also work in the reverse to heat incoming gases

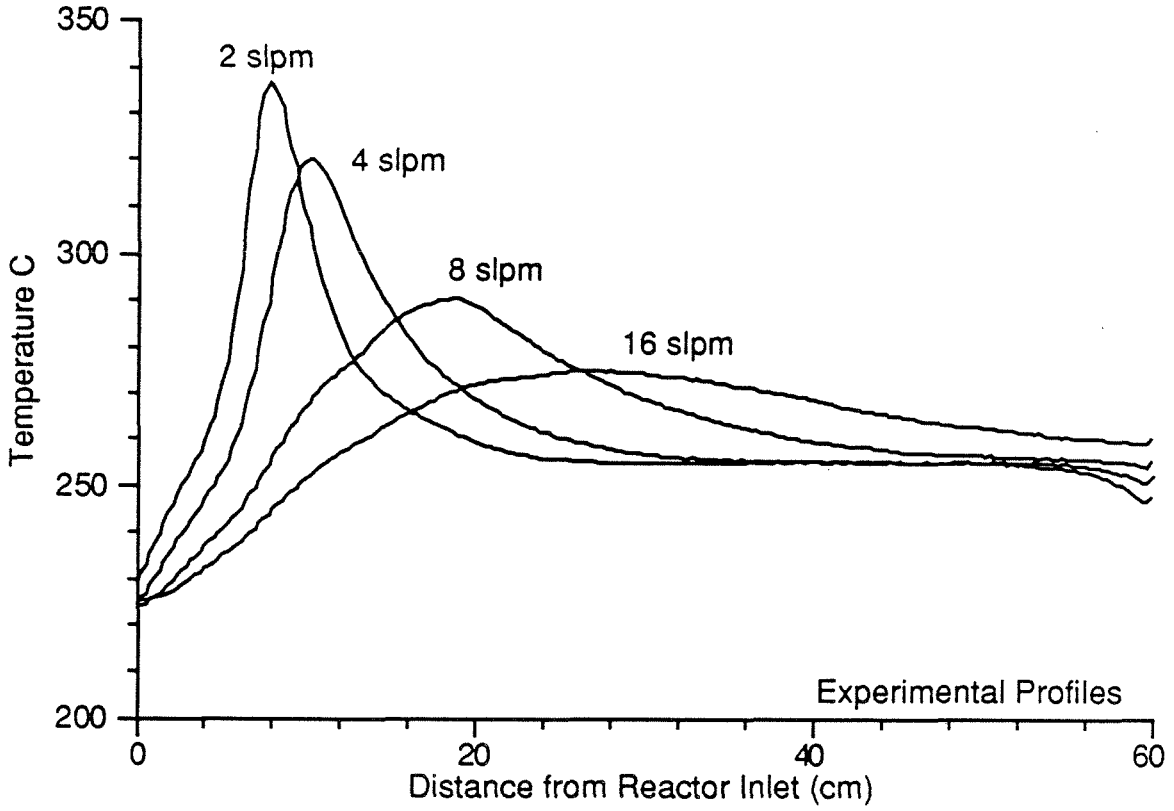

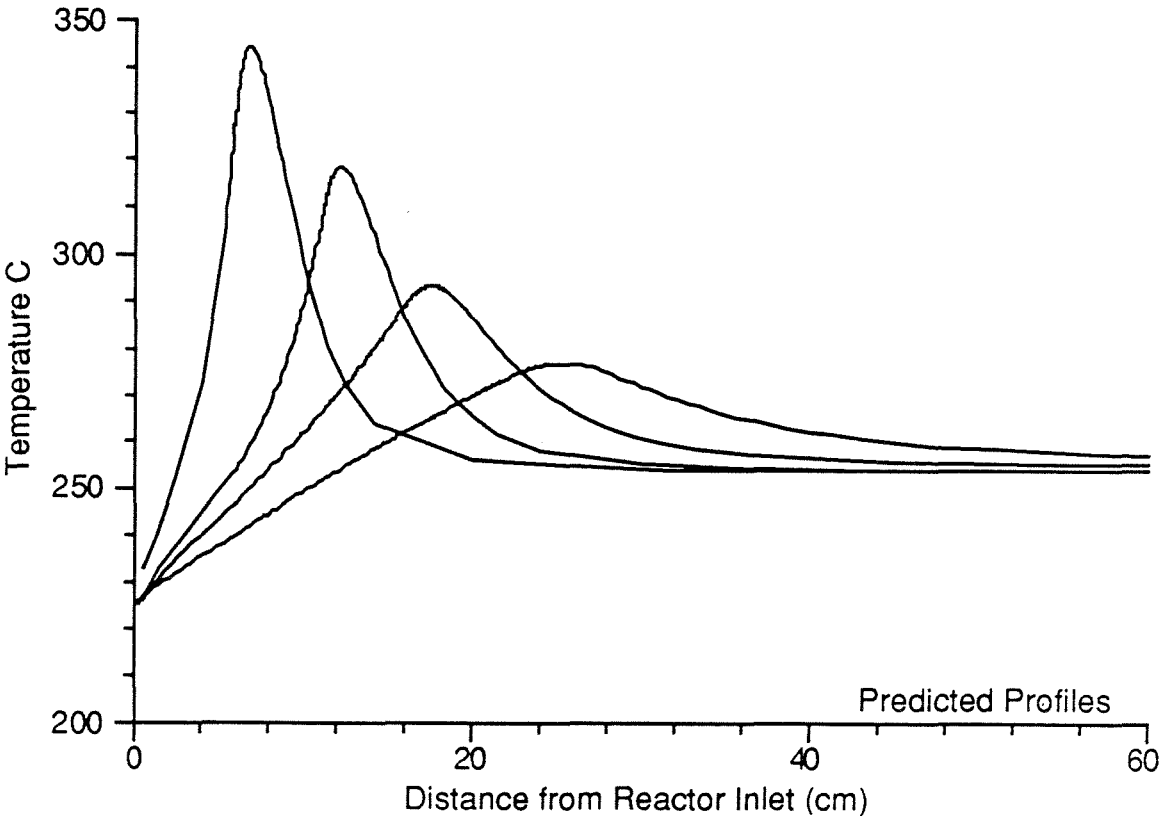

Figure 4.5: Steady state temperature profiles for 1 slpm total reactant flow

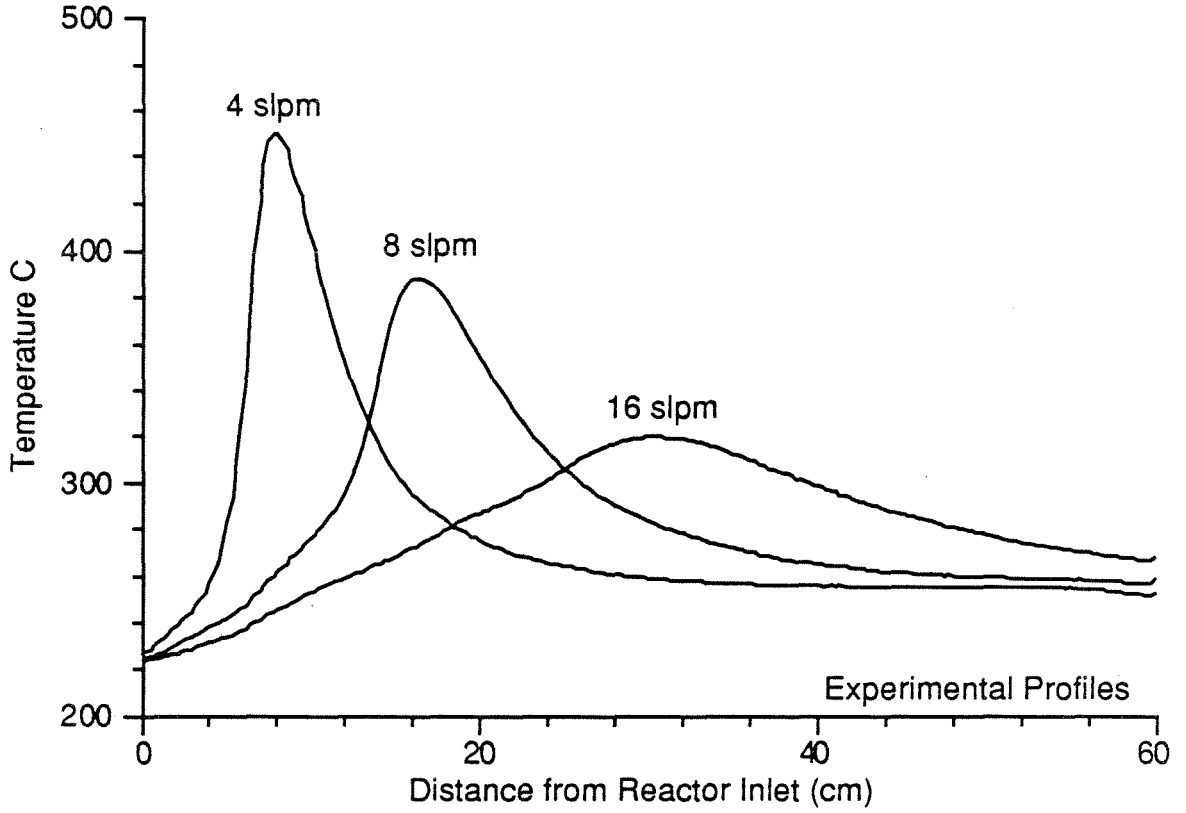

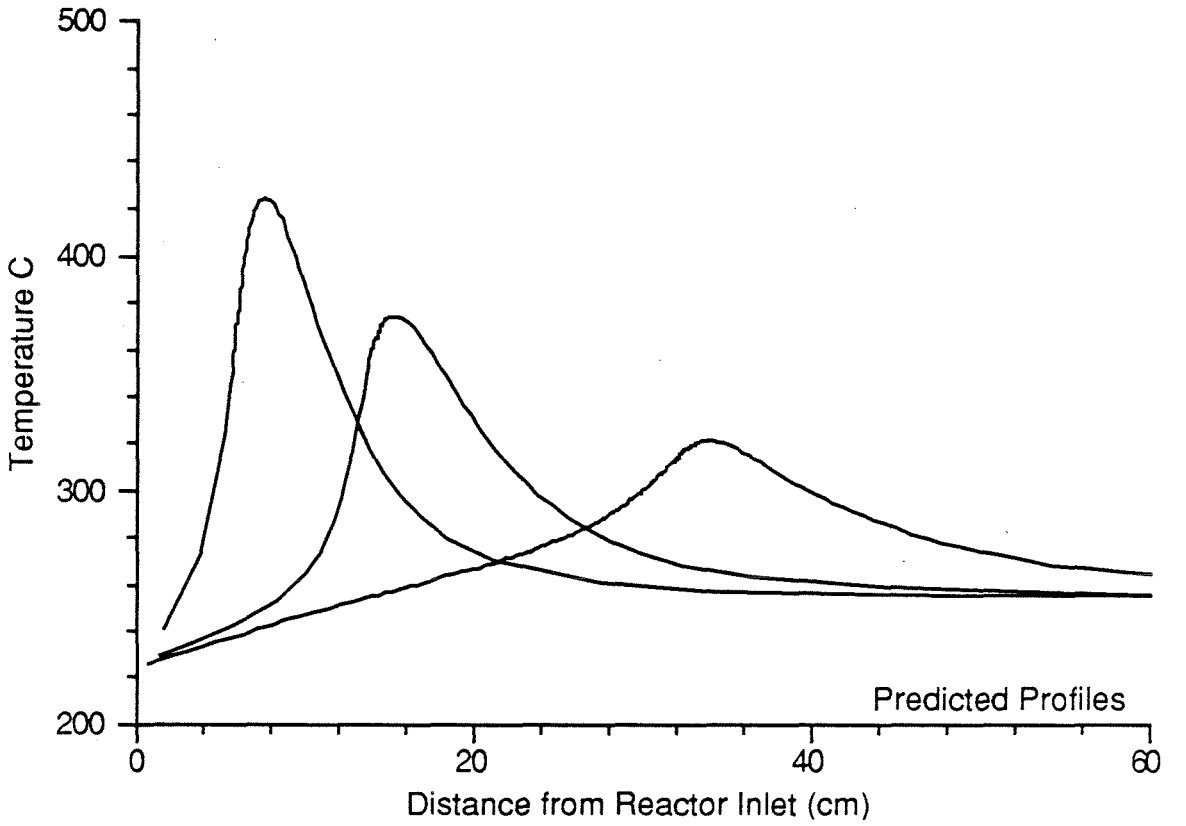

Figure 4.6: Steady state temperature profiles for 3 slpm total reactant flow

which are below the wall temperature to the point where they will react. Because the cooling jacket effectively modulates the system temperatures, no steady state multiplicity has been identified in this reactor although unsuccessful attempts were made to force the steady state to a lower operating conversion by admitting reactive gases at room temperature.

In the second set of experiments, the inlet concentration and total flow rate are held constant, while the inlet temperature varies. Figure 4.7 shows the temperature profiles for inlet temperatures of 170, 235, and 275°C and a total flow rate of 10 slpm.

As expected, increasing the inlet temperature accelerates the rate of conversion resulting in hot spots which are closer to the reactor inlet. At inlet temperatures above the wall temperature, though, a curious thing happens: the gas initially *cools* as it moves through the reactor. From these observations, it is presumed that there exists a small section at the inlet of the reactor, which we shall call the dead zone, in which no reaction occurs. Such a zone may be explained by improper loading of the catalyst or catalyst poisoning. The mathematical model incorporates this zone using the simple modification to the rate equation found in Equations 4.11 and 4.32. The dead zone length, χ, is estimated from the experimental data.

The estimation of the dead zone length and other model parameters, k_0, E_{a_0}, h_{sw}, k_s, k_g, proceeds as follows. An operating window is chosen for each of the uncertain parameters, and a series of parameter sets is created based on the combination of high, low, and nominal values for each of the uncertain parameters. Using each parameter set, the steady state temperature and concentration profiles are computed for each of the ten experimental operating conditions listed above. This computation is performed using the dynamic model and simulating long enough for the time derivatives to vanish. Then, each simulated steady state thermowell temperature profile is compared to its respective experimental profile for size, shape and position

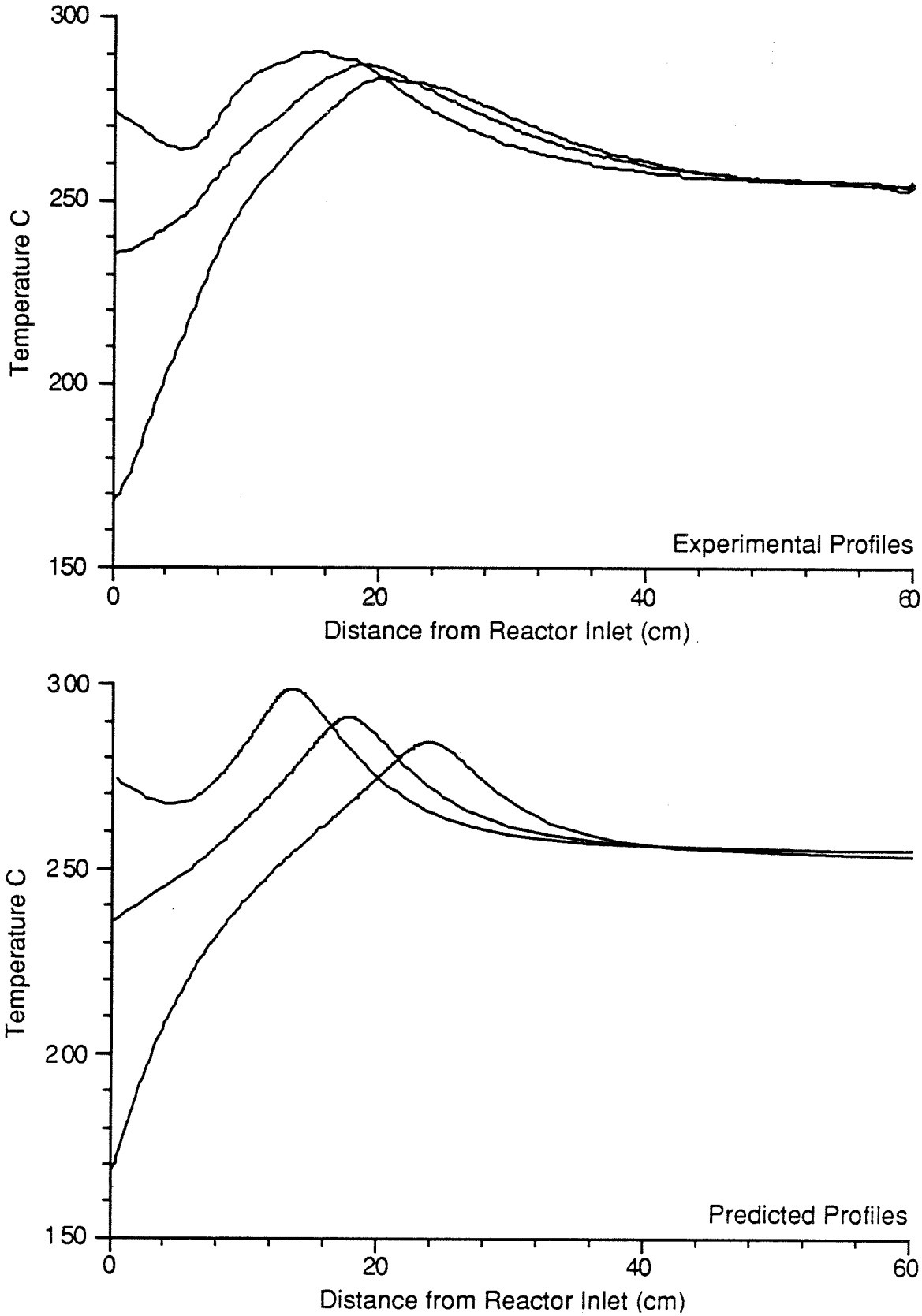

Figure 4.7: Steady state temperature profiles for different inlet temperatures

of the hot spot. This information is recorded, and the process is repeated with the next set of parameters.

After all parameter sets have been evaluated, the parameter set which best describes the experimental data is chosen as the operating set. It should be stressed that no single set of parameters is optimal in the description of every experiment. The data set chosen tends to best describe the profiles over a wide range of operating conditions. The predicted thermowell temperature profiles, for selected operating conditions, are shown in Figures 4.5–4.7 along with the experimental profiles for comparison. As can be seen from these figures, the predicted temperature profiles qualitatively represent the experimental data although the agreement is not perfect. This mismatch is due in part to assumptions made when developing this model — especially with the elimination of the radial derivatives.

The simulated steady state temperature and concentration profiles for typical operating conditions are shown in Figure 4.8. The three temperature profiles are all characterized by the presence of a hot spot, but the hot spots in the gas and catalyst phases are significantly higher than the thermowell hot spot. This difference is due to the larger axial conduction in the thermowell and reinforces the need for a separate thermowell energy balance equation. The concentration profile is characterized by a sudden change at the hot spot similar to a step discontinuity. This is not too surprising considering the height of the hot spot. While the shapes of the profiles vary with operating conditions, the above characteristics are found in all simulations.

When simulating the reactor, several implementation questions arose:

- Will the model converge to a unique steady state?
- How does the mesh size affect the steady state profiles?
- What is the sensitivity of the solution to various parameters?

Each of these question will be addressed in turn.

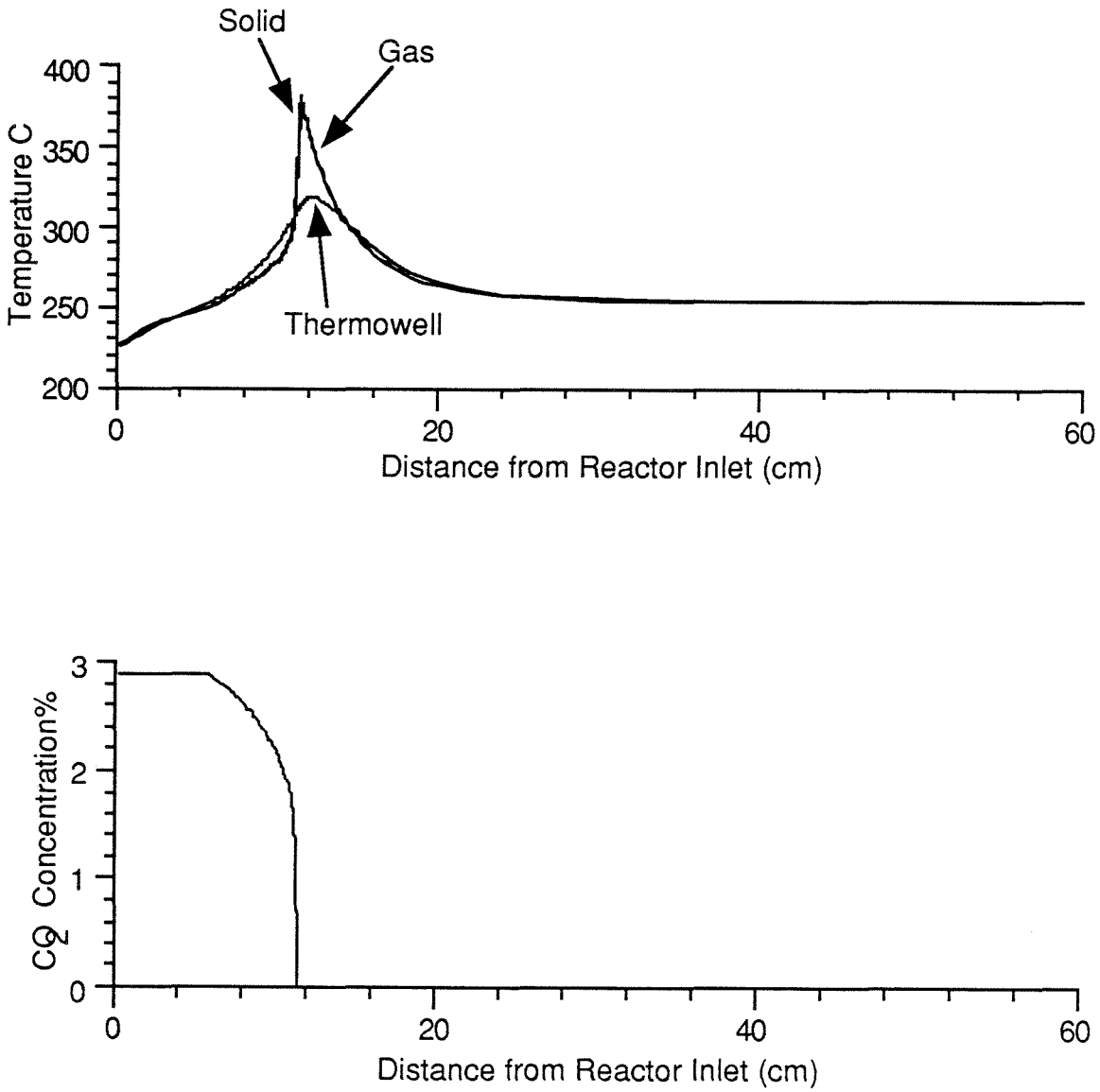

Figure 4.8: Simulated steady state temperature and concentration profiles for a total reactant flow rate of 1 slpm and an inerts flow rate of 4 slpm.

The question of convergence is resolved by extensive testing of the simulator. Generally, there are no convergence problems with this simulator although in few instances, the simulation fails to converge to an answer because the Jacobian becomes singular. However, it is difficult to prove that these solutions are unique. It is conjectured that the model, like the reactor, has only one steady state for each of the tested operating conditions. This conjecture is based on the fact that the initial starting guess for every simulation consists of flat temperature and concentration profiles where all temperatures are equal to the wall temperature and all concentrations are equal to the inlet concentration. These conditions are generally more conducive to mild conversions where the system fails to produce enough energy to form a hot spot. Since hot spots are observed in all simulations it is believed that the milder steady state does not exist at the current operating conditions.

To resolve the second question, the steady state profiles are computed several times with the mesh spacing changed after each calculation. Initially, a uniform spacing is assumed, and the steady state determined. From this result, the mesh spacing is revised to concentrate mesh points around the hot spot where the gradients are the steepest. This process is repeated until the hot spot position and shape do not change. This can require four or more iterations depending on the size and position of the hot spot.

The last question is an important question without a complete answer. A heuristic analysis of the model, based on the results of the parameter estimation, points to k_0 and h_{sw} as being the most sensitive model parameters. A more sophisticated quantitative analysis can be performed using sensitivity analysis techniques available in the literature [14].

Conclusions

In conclusion, mathematical models for the feed-effluent heat exchanger and the methanation reactor have been presented. Both of these models grew out of a need to explain phenomena which could not be quantified using standard chemical engineering design calculations. The complexity of the model depends on the needs of the designer. In the case of the feed-effluent heat exchanger, the model simply explains the steady state relationship between heat transfer in the heat exchanger and heat loss to the environment; in the case of the reactor, the model explains the complex dynamical relationships for two dimensional heat and mass transport in the presence of an exothermic chemical reaction.

Each model was developed in the same way. First, the aim of the model was established, and the characteristics to be included in the model were given. Then, the model was generated from mass and energy balances using a series of simplifying assumptions. Finally, the model parameters were determined from steady state experiments and the accuracy of the model was checked.

While the resultant models sufficiently represent the experimental data, a more accurate estimation of modelling parameters can be realized using a couple of modifications to the solution procedure. First, dynamic information can be used in the place of steady state data. As explained by Mandler, "One dynamic run is expected to yield the same amount of information that only many steady state experiments would give, in a very small fraction of the time that the latter would require" [86]. Unfortunately, the increased amount of information also increases the complexity of the estimation scheme. Second, the experimental conditions can be expanded to cover a wider variety of operating conditions. In the case of the reactor, this is tantamount to operating the reactor under conditions where there is partial conversion. This information is especially valuable when the conversion is large enough to be accurately measured using the gas chromatograph but still not complete.

Chapter 5

Robust Identification Experiments

Abstract

A new methodology for computing frequency domain uncertainty bounds for single-input single-output systems is presented. This new methodology uses spectral analysis to identify a series of non-parametric frequency domain models and a "regions-mapping" technique to bound these models in the complex plane. The methodology is compared to existing non-parametric techniques and shown to be superior for identifying the uncertainty bound associated with a nonlinear system. This methodology is then applied to the identification of a fixed bed reactor. A robust controller with a single adjustable parameter is designed for the reactor using Internal Model Control (IMC) theory. The computed uncertainty bounds are experimentally validated using the IMC controller.

5.1 Introduction

One of the more recent advances in process control theory has been the development of robust control theory (as summarized in [92]). This theory addresses the problem of designing the best single controller which will simultaneously stabilize a family of plants. This set of plants may arise when modelling uncertainty is explicitly considered in the system identification problem. Typically, one considers as the family of plants all linear and time-invariant (LTI) systems with frequency responses which are "close" to a nominal model. This nominal model should provide a good approximation of the system's behavior at least for controller design. Mathematically, the family of plants under consideration is parameterized by

$$P(\omega) \in \tilde{P}(\omega)(I + \ell_m(\omega)\Delta) \tag{5.1}$$

where $P(\omega)$ is the "true" plant, $\tilde{P}(\omega)$ is a nominal LTI model, ℓ_m is the multiplicative frequency dependent uncertainty bound, and Δ is any complex number with $|\Delta| < 1$.

While not strictly applicable to nonlinear or time varying systems, linear robust control theory is often applied to systems with slowly varying or position dependent parameters. It is assumed that a controller which simultaneously stabilizes the plant for all possible parameter combinations will stabilize the true system. While it is sometimes possible to derive ℓ_m for these systems from the physics of the system, more often, the uncertainty bound is estimated empirically from observations of the system response.

While much work has gone into developing robust control theory, relatively little work has gone into experimentally estimating uncertainty bounds for control purposes. This chapter addresses this problem and demonstrates a technique for constructing the family of models from input-output data.

Currently, most uncertainty bounds are derived from bounds placed on the parameters of a parametric model [100,96,74]. Typically, a linear parametric model is proposed to describe the nominal response of the system. The parameters used in the model are allowed to vary over specified ranges around their nominal values to account for deviations in the response of the true system from the nominal response. These parametric bounds can be determined either from experimentation or from physical arguments. When obtained experimentally, the system is generally excited at a number of different operating conditions and the dynamic response at these operating conditions is compared to the nominal response. The parameters in the model are then allowed to vary in order to capture the different dynamics.

While certain techniques exist for analyzing this problem assuming real parameter perturbations, a common simplification is to convert these bounds to bounds on the Nyquist plot of the nominal plant. A conservative simplification often made is to bound the complicated geometric shape formed from the parametric uncertainty bounds at each frequency by a circle (Equation 5.1). Generally, the center of this circle does not correspond to the Nyquist plot of the nominal parametric model.

While the parametric methods mentioned above are effective, the bounds obtained depend on the specific form of the system model. It is often more desirable to have a black-box method which will directly compute a dynamical model when given a set of input-output data and automatically give a bound on the uncertainty associated with this model. Recently, two non-parametric frequency domain techniques have been proposed which do just that [83,104].

This chapter examines these frequency domain methods and proposes a new method for computing the uncertainty bound of single-input single-output systems. This new method uses spectral analysis, a black-box identification method, to identify a series of non-parametric frequency domain models from noisy input-output time records at a finite number of equally spaced frequencies. The method then relies on a "regions-mapping" method [75,76] to bound the individual frequency response models in the complex plane. From this bounded region, a non-parametric model and uncertainty bound are determined.

The chapter is organized as follows. In Section 5.2, spectral analysis theory for the identification of a non-parametric frequency domain model is reviewed. Using spectral analysis, three uncertainty bounds are then developed — two based on the residual spectrum and a third on a regions-mapping approach. In Section 5.3, the spectral estimates are compared to Fourier estimates. It is shown that the uncertainty bound is actually composed of two parts: one part which measures the deviation of the model from the so-called "empirical transfer function estimate" [82] and a second part which accounts for noise. In Section 5.4, the nature of the input signal used in an identification experiment is discussed. Two aspects of this signal are detailed: its frequency content and its shape. A simple technique is described for determining the frequency range over which the open-loop identification should be performed. This technique which uses a relay controller can, under certain circumstances, yield insight into the uncertainty bound. In Section 5.5, the previously

developed identification techniques are tested on a simple linear system in series with a nonlinear gain element. From this experiment, it is shown that the uncertainty bounds based on the residual spectrum can lead to misleading results when applied to a nonlinear system. The regions-mapping approach overcomes some of the problems associated with the other methods and yields an uncertainty bound which is nearly identical to the true bound.

In the second half of the chapter, a case study is presented which uses the approach developed in the previous sections. In Section 5.6, the control problem, the control of a hot spot in a fixed bed chemical reactor, is introduced. In this section, the flow rate through the reactor is chosen as the manipulated variable. In Sections 5.7 and 5.8, the results of the identification experiments — closed-loop relay identification, Section 5.7, and open-loop identification, Section 5.8 are discussed. Finally, in Section 5.9, a robust controller is designed and used to experimentally validate the accuracy of the uncertainty bound.

5.2 Spectral Analysis

In this section, the spectral analysis theory for the identification of a non-parametric frequency domain model is reviewed. It is shown how the residual spectrum obtained from spectral analysis can be combined with statistical theory to develop two different frequency dependent uncertainty bounds. These bounds differ only in their statistical assumptions. Then, a new uncertainty bound is developed based on a regions-mapping approach. The dynamic experiments used to obtain this new bound are similar to the experiments mentioned in the introduction for parametric modelling. Since spectral analysis theory is well established, the description which follows is only an overview of the theory as it applies to uncertainty estimation. The interested reader is referred to [11,56,82,36] for more details on the theory including the mathematical proofs.

The system under consideration is shown in Figure 5.1 and is described by the equation:

$$y(t) = \int_{-\infty}^{t} g(t-\tau)u(\tau)d\tau + v(t) \tag{5.2}$$

and its Fourier transform

$$Y(\omega) = G(\omega)U(\omega) + V(\omega) \tag{5.3}$$

where

$$Y(\omega) \triangleq \int_{-\infty}^{\infty} y(t)e^{-i\omega t}dt \tag{5.4}$$

This system is assumed to be stable, casual, linear, and time invariant. For simplicity, the signals entering the system are assumed to be bounded-magnitude bounded-power signals which may be either deterministic or stochastic. Generally, u is a deterministic signal whereas v contains both deterministic and stochastic components. In the analysis to follow, the expectation operator is implicitly applied to all calculations involving stochastic signals.

If $U, V,$ and Y are all known then G can be deduced directly from Equation 5.3. Unfortunately, V is usually not known and must be estimated from the identification procedure. Although V is unknown, its effect on the outlet time series must be removed before the system can be identified. One way to remove the effects of V is to rely on correlation analysis.

In correlation analysis, both sides of Equation 5.2 are multiplied by $u(t-T)$ and integrated over all time to yield

$$\int_{-\infty}^{\infty} y(t)u(t-T)dt = \int_{-\infty}^{\infty} \left(\int_{-\infty}^{t} g(t-\tau)u(\tau)\,d\tau \right) u(t-T)\,dt + \int_{-\infty}^{\infty} v(t)u(t-T)\,dt \tag{5.5}$$

If v is uncorrelated with u, then $\int_{-\infty}^{\infty} v(t)u(t-T)dt \triangleq 0$ and Equation 5.5 reduces

to

$$R_{yu}(T) = \int_{-\infty}^{T} g(T-\tau)R_{uu}(\tau)d\tau \tag{5.6}$$

where

$$R_{yu}(T) \triangleq \int_{-\infty}^{\infty} y(t)u(t-T)dt \tag{5.7}$$

$$R_{uu}(T) \triangleq \int_{-\infty}^{\infty} u(t)u(t-T)dt \tag{5.8}$$

The functions R_{uu} and R_{yu} are called the autocovariance and cross covariance functions[1], respectively. If the input is correlated with the disturbance signal then computing the covariance functions effectively divides the disturbance signal into its correlated and uncorrelated parts. The correlated part then biases the estimate of g. For instance, if $v(t) = \int_{-\infty}^{t} \Delta(t-\tau)u(\tau)d\tau + e(t)$ where e is a white noise signal (see Figure 5.2), then the estimated impulse response function is $g + \Delta$ and not just g.

The frequency domain equivalent to correlation analysis is spectral analysis. Taking the Fourier transforms of Equations 5.6–5.8 yields

$$\Phi_{yu}(\omega) = G(\omega)\Phi_{uu}(\omega) \tag{5.9}$$

where

$$\Phi_{uu}(\omega) \triangleq \int_{-\infty}^{\infty} R_{uu}(t)e^{-i\omega t}dt = U(\omega)\bar{U}(\omega) \tag{5.10}$$

$$\Phi_{yu}(\omega) \triangleq \int_{-\infty}^{\infty} R_{yu}(t)e^{-i\omega t}dt = Y(\omega)\bar{U}(\omega) \tag{5.11}$$

The overbar denotes the complex conjugate. Like the covariance functions, the functions Φ_{uu} and Φ_{yu} are referred to as the autospectrum and cross spectrum, respectively. These equations play a central role in the identification of the plant,

[1]Strictly speaking, the covariance functions are only defined for stationary stochastic processes with mean value zero. The terminology used here is based on the terminology found in Ljung [82].

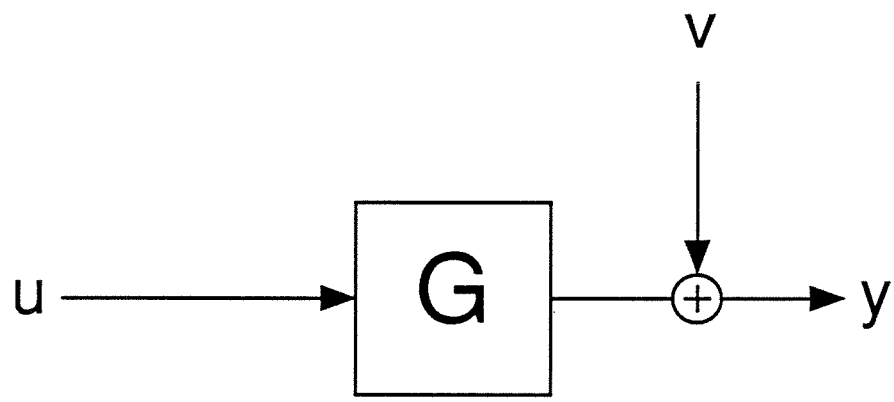

Figure 5.1: Block diagram of system with output noise

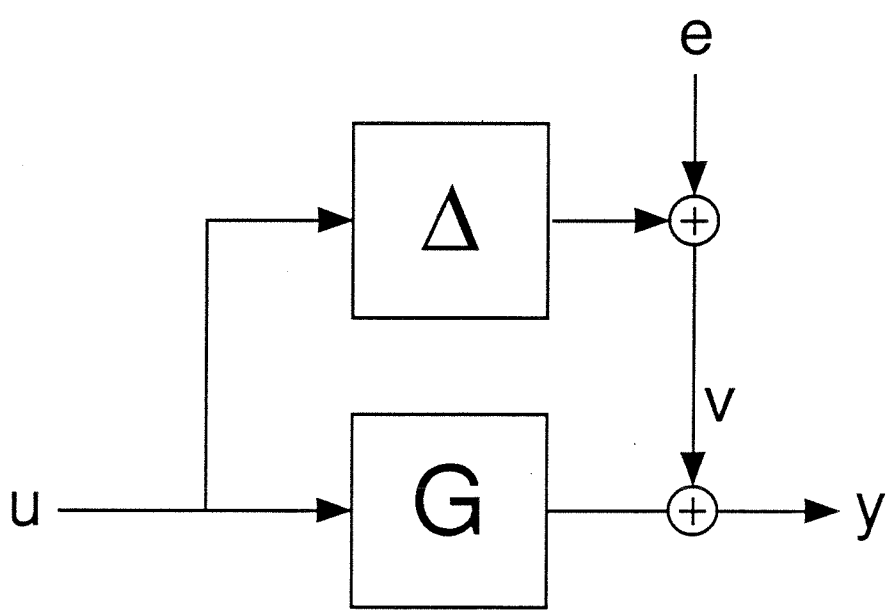

Figure 5.2: Block diagram of system with output noise and uncertainty

for

$$G(\omega) = \frac{\Phi_{yu}(\omega)}{\Phi_{uu}(\omega)} \tag{5.12}$$

when $\Phi_{uu}(\omega) \neq 0$. The residual spectrum, Φ_{vv}, is obtained by multiplying both sides of Equation 5.3 by $\bar{Y}(\omega)$

$$\Phi_{vv}(\omega) = \Phi_{yy}(\omega) - |G(\omega)|^2 \Phi_{uu}(\omega) \tag{5.13}$$

$$= \Phi_{yy}(\omega) - \frac{\Phi_{yu}(\omega)\Phi_{uy}(\omega)}{\Phi_{uu}(\omega)} \tag{5.14}$$

Unfortunately, when spectral analysis is applied to finite length discrete time series, certain convergence problems arise. Given the series,

$$u_N = \{u(T_s), u(2T_s), \ldots, u(NT_s)\}$$

$$y_N = \{y(T_s), y(2T_s), \ldots, y(NT_s)\}$$

(where T_s is the sampling period), and their discrete Fourier transforms U_N and Y_N then a simple estimate of the transfer function at the points $\omega_k = \frac{2\pi k}{NT_s}$, $k = 0, \frac{N}{2} - 1$ is

$$\hat{G}(\omega_k) = \frac{Y_N(\omega_k)}{U_N(\omega_k)} \tag{5.15}$$

Using trigonometric interpolation for frequencies intermediate to the points ω_k, Ljung [82] defines a continuous function, $\hat{G}(\omega)$, which passes through the points $\hat{G}(\omega_k)$ and calls it the empirical transfer function estimate, ETFE. For the given set of input-output data, $\hat{G}$ perfectly describes the data. By this it is meant that the output time series can be reconstructed from the input time series and $\hat{G}$ without any error. However, due to its large sensitivity to noise, the ETFE can still be a poor estimate of the true transfer function. For most practical experiments the variance associated with this estimate is controlled by the noise to signal ratio and does not decrease as the length of the experiment increases [82,81]. To overcome

these problems, $\hat{G}$ is smoothed.

There are several ways in which this smoothing can be performed (see for example [64,36]) of which two will be examined: Blackman-Tukey ("indirect") smoothing [20,56,7] and Cooley-Tukey ("direct") smoothing [4,69,42]. In the Blackman-Tukey method, the spectrum (either cross or auto) at frequency ω_o is estimated using a weighted averaging of the unsmoothed spectrum around the frequency ω_o. This method takes advantage of the fact that the spectral estimates, $\hat{\Phi}_{yu}$ and $\hat{\Phi}_{uu}$, are uncorrelated in frequency. The weighting function used in the smoothing, termed the spectral window, is generally large around ω_o and decreases as $|\omega - \omega_o|$ increases. Because the spectrum is the Fourier transform of the covariance function, smoothing can also be done in the time domain where the time domain analog of the spectral window is the lag window.

Using this smoothing procedure, the smoothed estimates of the transfer function and residual spectrum are

$$\hat{G}^s(\omega_k) = \frac{\hat{\Phi}^s_{yu}(\omega_k)}{\hat{\Phi}^s_{uu}(\omega_k)} \tag{5.16}$$

$$\hat{\Phi}^s_{vv}(\omega_k) = \hat{\Phi}^s_{yy}(\omega_k) - \frac{\hat{\Phi}^s_{yu}(\omega_k)\hat{\Phi}^s_{uy}(\omega_k)}{\hat{\Phi}^s_{uu}(\omega_k)} \tag{5.17}$$

where $\hat{\Phi}^s_{yu}$ and $\hat{\Phi}^s_{uu}$ are the smoothed estimates of the cross spectrum and autospectrum. These estimates are computed from

$$\hat{\Phi}^s_{yu}(\omega_k) = \frac{1}{N}\sum_{l=0}^{N-1} R_{yu}(l)w(l)e^{-i(\frac{2\pi kl}{N})} \tag{5.18}$$

$$\hat{\Phi}^s_{uu}(\omega_k) = \frac{1}{N}\sum_{l=0}^{N-1} R_{uu}(l)w(l)e^{-i(\frac{2\pi kl}{N})} \tag{5.19}$$

where $w(l)$ is the lag window and $R(l)$ is the discrete covariance estimate.

As the size of the spectral window increases, and, hence, more smoothing occurs, the variance of $\hat{G}^s$ decreases. If the spectral window is large, then the unsmoothed

spectra at many different frequencies are weighted together to estimate $\hat{\Phi}^s(\omega_o)$. This smoothed estimate involves frequency estimates that are far away from ω_o with true values that may differ considerably from the true spectrum at ω_o. This causes biasing of the estimate. With this smoothing there is a trade-off between variance and bias — large spectral windows are needed for reduced variance while small windows are needed for reduced bias. In practice, a closing procedure is applied to the data whereby different size filters are used to smooth the data. The estimate which appears to be the best compromise between variance and bias is chosen as the smoothed estimate.

In the Cooley-Tukey method, instead of averaging over frequency, smoothing is performed using a group averaging of several spectral estimates. The original times series are subdivided into several smaller equal length pieces. The spectrum is then estimated for each piece, and the resulting spectra are averaged together to form the smoothed spectral estimate. Finally, the frequency response estimate is computed using Equation 5.16.

Three common variations on this technique are found in the literature [69,82]. First, a data tapering filter, similar to $w(l)$, can be used to smooth the individual spectra. Second, instead of averaging the spectra and then computing the transfer function, the individual transfer function estimates for each section can be averaged together. Finally, instead of having totally disjoint data sets, the data sets can be allowed to overlap. This variation leads to a smoothing procedure known as the Faded Overlap method.

While these two techniques may seem rather different, Carter and Nuttall [16] present a generalized framework for spectral estimation in which the Blackman-Tukey method and the Cooley-Tukey method are special cases. These authors propose a five part smoothing procedure for spectral estimation and, using this procedure, give an expression which relates the description of the data tapering filter to

that of an equivalent lag window. However, one important advantage still remains with the Faded Overlap method — namely its ability to follow the variations in the transfer function with time (and therefore operating conditions).

Using the different smoothing techniques, uncertainty bounds for the frequency response can be derived. These bounds relate the fact that noise in the system corrupts the estimate of the transfer function, and a quantitative bound on how much corruption has occurred is necessary. While noise itself cannot make a linear system under feedback control go unstable, the inaccurate identification of the model can. Three different uncertainty bounds are derived. These bounds differ in the type of smoothing performed and the statistical assumptions used in their derivation.

5.2.1 Uncertainty Bound Based on Distribution Theory

Using the distribution theory associated with linear least squares estimation, Jenkins and Watts [56] convert the estimate of the residual spectrum into a bound on uncertainty. Specifically, these authors show that

$$\Pr\left\{\frac{\nu-2}{2}\frac{\hat{\Phi}^s_{uu}(\omega_k)|G(\omega_k)-\hat{G}^s(\omega_k)|^2}{\hat{\Phi}^s_{vv}(\omega_k)} \le f_{2,\nu-2}(1-\alpha)\right\} = 1-\alpha \tag{5.20}$$

from which a confidence interval is derived

$$\ell_a^2(\omega_k) \triangleq |G(\omega_k)-\hat{G}^s(\omega_k)|^2 \le \frac{2}{\nu-2} f_{2,\nu-2}(1-\alpha)\left[\frac{\hat{\Phi}^s_{vv}(\omega_k)}{\hat{\Phi}^s_{uu}(\omega_k)}\right] \tag{5.21}$$

In these equations, $\Pr\{x \le y\}$ is the probability that x is less than or equal to y, $f_{2,\nu-2}(1-\alpha)$ is the cutoff point associated with Fisher's F distribution of 2 and $\nu-2$ degrees of freedom, and ν is the number of degrees of freedom associated with the spectral window. ν is a function not only of the spectral window size but also of its shape.

The F distribution is a sampling distribution which arises when computing the

ratio of two independent χ^2 distributed random variables. Because it often measures the ratio of two variance estimates, the F distribution is sometimes referred to as the Variance-Ratio distribution. Tables of the f_{ν_1,ν_2} are available in most mathematical reference books including [1]. From these tables it is apparent that in the limit as $\alpha \to 0$, $f_{2,\nu-2} \to \infty$. Therefore, in order to be 100% confident that all uncertainty is bounded, the uncertain bound is infinitely large. For most applications, it suffices to choose $\alpha = 0.05$.

A plausibility argument for using this bound in the design of a robust controller can be made by looking at the noise free linear system,

$$Y(\omega) = G(\omega)U(\omega) \tag{5.22}$$

Let G^+ be any transfer function estimate of G. Subtracting G^+U from both sides of equation 5.22 yields

$$V(\omega) \triangleq Y(\omega) - G^+(\omega)U(\omega) = (G(\omega) - G^+(\omega))U(\omega) \tag{5.23}$$

Multiplying by the complex conjugate

$$V(\omega)\bar{V}(\omega) = |G(\omega) - G^+(\omega)|^2 U(\omega)\bar{U}(\omega) \tag{5.24}$$

or

$$|G(\omega) - G^+(\omega)|^2 = \frac{\Phi_{vv}(\omega)}{\Phi_{uu}(\omega)} \tag{5.25}$$

The similarity between equations 5.21 and 5.25 becomes clear when $\frac{2}{\nu-2} f_{2,\nu-2}(1-\alpha)$ is set to 1. This factor predicts the fraction of the residual spectrum which is due to model inaccuracy instead of noise. In the examples to follow, the factor $f_{2,\nu-2}(1-\alpha)$ is set equal to $\frac{\nu-2}{2}$. Since ν is relatively large in these examples, the probability is relatively large (>.95).

5.2.2 Uncertainty Bound Based on Probability Distribution Functions

A different uncertainty bound is obtained using a method presented by Loh, Corrêa, and Postlethwaite [83]. Using Cooley-Tukey smoothing, these authors obtain an asymptotically unbiased and consistent estimate of the spectrum. They then rely on the statistical theory of Wishart distributions [40] to develop a set of probability distribution functions, PDFs, for the estimated squared coherency, $\frac{|\hat{\Phi}_{yu}|^2}{\hat{\Phi}_{uu}\hat{\Phi}_{yy}}$; normalized transfer function gain; and phase. The coherency, $\sqrt{\frac{|\hat{\Phi}_{yu}|^2}{\hat{\Phi}_{uu}\hat{\Phi}_{yy}}}$, can be viewed as the frequency dependent correlation coefficient between the input, u, and the output, y. These PDFs are implicit functions of the true squared coherency and phase. Once the PDFs are known, confidence intervals for both magnitude and phase can be derived in a straightforward manner although when expressing the uncertainty as Equation 5.1 only the magnitude bound is required.

Because the developed probability distribution functions are rather complicated functions containing infinite sums of gamma functions, the cumulative probabilities are presented in graphical format. The confidence intervals are read directly from these graphs and depend on the amount of confidence one desires in the solution. Like the Jenkins and Watts bound, an uncertainty bound with probability of 1 (100% certain) is infinitely large. For this study, a 95% confidence level is assumed, and the uncertainty at this level fit to a power law relation for explicit evaluation.

This procedure can be applied to the identification of the individual elements of a MIMO system. However, the element by element representation of the uncertainty in this manner does not account for correlations between elements and is therefore generally conservative. This is especially important for systems with large condition numbers [92].

5.2.3 *Uncertainty Bound Based on Regions-Mapping Approach*

A new technique for estimating the transfer function and its associated uncertainty bound can be derived from regions-mapping concepts. The first step of this technique consists of dividing the operating window, the admissible range over which y and u are allowed to vary, into a number of subsections. For each subsection, a local identification experiment is performed, and the resultant time series are analyzed using spectral analysis (Equation 5.16). In this way, a set of local non-parametric frequency domain models is generated.

At each frequency, these models represent a series of points on a Nyquist diagram. The second step of the technique is to find the smallest circle in the complex plane that bounds this set of points. This step can be formulated as the min-max problem:

$$\min_{\hat{G}^{rm}(\omega)\in\mathcal{C}} \left(\max_{\hat{G}_i^s\in\mathcal{G}} |\hat{G}_i^s(\omega_k) - \hat{G}^{rm}(\omega_k)| \right) \quad \forall \omega_k \tag{5.26}$$

$$\mathcal{G} = \{\text{local smoothed transfer function estimates}\} \tag{5.27}$$

At each frequency, the transfer function estimate, $\hat{G}^{rm}(\omega_k)$, and the uncertainty bound, $\ell_a(\omega_k) = \max_{\hat{G}_i^s\in\mathcal{G}} |\hat{G}_i^s(\omega_k) - \hat{G}^{rm}(\omega_k)|$, are the center and the radius of the smallest circle which encompasses the set of plants $\mathcal{G}$. An algorithm which solves equation 5.26 can be found in [76].

There are many similarities, and one important difference, between this technique and the Faded Overlap method of spectral smoothing. In both cases, the input-output time series are divided into several smaller sections, a data tapering filter is used to smooth the data, and the transfer function for each section is determined. However, in the Faded Overlap method, the resultant transfer functions are averaged together to form a smoothed transfer function estimate whereas with the regions-mapping approach, the local transfer functions are merely bounded and the transfer function estimate is taken as the center of the bound. While the regions-

mapping uncertainty bound is not directly based on the residual spectrum, it is still a function of the amount of smoothing since the local models, $\hat{G}_i^s$, are functions of the filter. If the uncertainty associated with the local models is relatively large, the uncertainty bounds for the individual estimates can be included in the global optimization (Equation 5.26).

As the number of local experiments increases, the likelihood of identifying the true bound, $|G - \hat{G}^{rm}|$, increases. However, since the computed bound is a solution to a min-max problem, not all $\hat{G}_i^s$ affect this bound. In practice, it is only necessary to identify the system at those points where the uncertainty bound will increase. While such *a priori* knowledge is not available in general, physical insight into the particular uncertainty present can be very useful for reducing the number of experiments. For instance, if the endpoints of the operating range are known to bound the frequency response, it is only necessary to identify the model at its endpoints.

A big advantage of this scheme over the residual based methods is the straightforward way in which it incorporates changes in the linear model (due to changes in the operating conditions) directly into the uncertainty description. These other methods must first relate changes in the model to an equivalent residual spectrum before these changes can be handled in the uncertainty description. As demonstrated in Section 5.5 these methods are not always effective at doing this. Furthermore, since the residual lumps together both measurement noise and model uncertainty, there is a certain vagueness with what exactly constitutes "noise" in the system.

This same philosophy of operating the system at several different operating points is also found in some of the parametric methods listed in the introduction. However, unlike these other methods, the form for the parametric model which approximates the frequency response is not determined until after a bound on the uncertainty is found. This has the advantage of minimizing the size of ℓ_a associated

with the model.

5.3 Fourier Analysis

In this section, the uncertainty bounds developed in the previous section are compared to bounds obtained from Fourier analysis. Consider again the system shown in Figure 5.2 for which the input-output time series, u_n and y_n have been collected. Assume that $\tilde{G}$, an estimate of G, is available and that the magnitudes of both E and Δ are bounded.

$$|E(\omega_k)| \leq B_E(\omega_k) \tag{5.28}$$

$$|\Delta(\omega_k)| \leq \ell_a(\omega_k) \tag{5.29}$$

Then, one can ask the question, "What is the minimum bound on Δ necessary to describe the observed data?"

This question can be mathematically posed as the minimization problem

$$\min_{E(\omega_k)} \ell_a(\omega_k) \tag{5.30}$$

subject to

$$Y_N(\omega_k) = \tilde{G}(\omega_k)U_N(\omega_k) + \Delta(\omega_k)U_N(\omega_k) + E(\omega_k) \tag{5.31}$$

$$|E(\omega_k)| \leq B_E(\omega_k) \tag{5.32}$$

$$|\Delta(\omega_k)| \leq \ell_a(\omega_k) \tag{5.33}$$

for which the solution is given by

$$\ell_a(\omega_k) = \begin{cases} \frac{|Y_N(\omega_k) - \tilde{G}(\omega_k)U_N(\omega_k)| - B_E(\omega_k)}{|U_N(\omega_k)|} & \text{if } |Y_N(\omega_k) - \tilde{G}(\omega_k)U_N(\omega_k)| > B_E(\omega_k) \\ 0 & \text{otherwise} \end{cases} \tag{5.34}$$

Using ℓ_a as the uncertainty bound for the robust controller design, however, may prove to be too optimistic, for the noise signal is assumed to perfectly line up with the residual and cancel its effects. On the other hand, an overly conservative bound on the uncertainty can be derived assuming that instead of cancelling the residual, the noise adds to it. In this case,

$$\ell_{a_{cons}}(\omega_k) = \frac{|Y_N(\omega_k) - \tilde{G}(\omega_k)U_N(\omega_k)| + B_E(\omega_k)}{|U_N(\omega_k)|} \tag{5.35}$$

When using Equation 5.34 (or 5.35), we are free to select the system model. In one extreme, $\tilde{G}$ can be taken to be the ETFE in which case $\ell_a(\omega_k) \triangleq 0$ independent of B_E since by definition $Y_N(\omega_k) - \hat{G}(\omega_k)U_N(\omega_k) = 0$. However, the ETFE has already been shown to be a highly variable estimate of the true frequency response. In the other extreme, $\tilde{G}$ may be a specific model. In this case, the model identification step has been completely avoided, and uncertainty may arise strictly due to a poor model choice. Somewhere between these two extremes are the models derived from spectral analysis.

The estimated uncertainty bound is actually composed of two parts: one which measures the deviation of the model from the ETFE, $\frac{|Y_N(\omega_k) - \hat{G}(\omega_k)U_N(\omega_k)|}{|U_N(\omega_k)|} = |\hat{G} - \tilde{G}|$, and the other which measures the noise effects, $\frac{B_E(\omega_k)}{|U_N(\omega_k)|}$. When Equation 5.34 is compared to Equation 5.25, it is seen that the spectral techniques do not explicitly divide the residual between noise and uncertainty, but rather rely on statistics to implicitly make this factorization.

This uncertainty analysis is actually a special case of a more general model

validation analysis presented by Smith [112]. This author addresses the problem of whether an assumed linear MIMO model with multiple uncertainties and noises can explain the observed input-output data obtained from an experimental process. Other uncertainty bounds based on frequency response analysis are found in [48,146].

5.4 Input Design

This section addresses the design of the input signal used in the identification of an experimental system. Two important characteristics of the input signal are discussed: its frequency content and its shape.

5.4.1 Frequency Content

The first step in any experimental identification is to determine the frequency range over which the plant is to be identified. The input signal used to identify this system should concentrate its power over this frequency range. For control purposes, the frequencies of greatest importance are those around the crossover frequency of the system. While the crossover frequency can be determined from a number of different identification experiments, a closed-loop identification experiment using a relay controller predicts the crossover frequency directly and, potentially, yields insight into the magnitude of the uncertainty bound.

A relay controller is a simple on-off controller for which the output of the controller is set to an upper limit, $+d$, if the input to the controller is greater than zero and to a lower limit, $-d$, if the input is less than zero. Using describing function methods [130,2], it can be shown that the describing function for this controller is given by

$$N(a) = 4d/\pi a \tag{5.36}$$

where $N(a)$ is the describing function, d is the amplitude of the controller output

signal, and a is the amplitude of the input signal.

When this controller is placed in closed-loop with a linear plant, the system requires

$$1 + G(\omega)N(a) = 0 \tag{5.37}$$

Since $N(a)$ is independent of ω, equation 5.37 reduces to

$$1 + G_r(\omega)N(a) = 0 \tag{5.38}$$

$$G_i(\omega) = 0 \tag{5.39}$$

where G_r and G_i are the real and imaginary parts of the transfer function, respectively. The lowest frequency for which Equation 5.39 holds is the crossover frequency, ω_C. Hence, the output of the plant in closed-loop tends to oscillate at its crossover frequency and has a gain given by $1/N(a)$.

$$|G(\omega_C)| = \frac{\pi a}{4d} \tag{5.40}$$

While formulas for the exact frequency of oscillation exist [2,3], the frequency of oscillation predicted by Equation 5.37 is sufficiently accurate for most engineering applications.

A simple variation on this controller is to precede the relay with a lead compensator [111]. By adding phase lead to the plant, the crossover frequency of the plant with the lead compensator can be gradually increased.

Eventually, a point is reached where too much lead has been added, and the output of the plant ceases to be periodic. There are two possible causes for this behavior. First, at higher frequencies the nonlinearities associated with the plant may dominate the response. For robust control design, this nonlinear response can be regarded as the output of a set of linear plants with complete phase uncertainty.

Second, as the crossover frequency increases, the output of the plant becomes small. If the magnitude of the noise remains the same, eventually a point is reached where the relay is switching because of the noise and not the signal. We shall call the highest frequency for which the system under relay control is still periodic the *breakdown frequency.*

As shown above, either noise or uncertainty is large at the breakdown frequency. From robust control theory it is known that because of stability and performance requirements, the closed-loop bandwidth is limited by the amount of uncertainty and noise in the system [92]. This limitation forces the closed-loop bandwidth to be smaller than the breakdown frequency. For this reason, it is only necessary to identify the plant up to the breakdown frequency.

5.4.2 Shape

To reduce the amount of time needed in the identification experiment, it is desirable to have an input signal which simultaneously excites many different frequencies. One such signal is a pseudo random binary signal, PRBS [38]. This signal is a two level signal which uses a variable switching rate to excite multiple frequencies. When properly designed, the power spectral density of the PRBS is flat over the frequency range of interest and, therefore, approximates white noise in this range. However, since the amplitude of the signal is constant, the input can be carefully controlled to keep the system in a prespecified operating range.

For the regions-mapping technique described above, the goal is to identify the system at a variety of different operating conditions including several different input levels. If a PRBS is used to identify the local dynamics for each operating condition, then the resultant input signal can be thought of as a PRBS superimposed on a series of different pulse functions where the size of the pulse determines the bias of the signal. Each pulse should be long enough to allow the PRBS to effectively

identify the low frequency model response. The use of these two signals will be demonstrated in the next section where they will be applied to the identification of a simple nonlinear system.

5.5 Comparison of Uncertainty Bounds for a Simple Nonlinear System

The identification procedures described in the previous sections are now applied to a simple nonlinear system and their uncertainty bounds compared to the actual bounds of the linearized model. It is shown that the bounds based on a single large PRBS inaccurately describe the true uncertainty and therefore may lead to misleading results.

The system under consideration is a simple first order system in series with a nonlinear gain element.

$$\dot{x}(t) = -x(t) + u(t) \tag{5.41}$$

$$y = \frac{2x}{2-x} \tag{5.42}$$

For this system, the linearized transfer function between Y and U is given by

$$G(s) = \frac{4}{(2-x_o)^2}\frac{1}{s+1} \tag{5.43}$$

where the linearization is performed around $x = x_o$. Confining $x_o \in [-1, 1]$, the upper and lower bounds for the transfer function are given by

$$G_{upper}(s) = \frac{4}{s+1}, \qquad G_{lower}(s) = \frac{0.444}{s+1} \tag{5.44}$$

Ideally, the gain of the identified model should be,

$$|G_{ideal}(\omega)| = \frac{2.222}{\sqrt{\omega^2 + 1}} \tag{5.45}$$

with an associated uncertainty bound of

$$\ell_a(\omega) = \frac{1.778}{\sqrt{\omega^2 + 1}} \tag{5.46}$$

This system is simulated for 102.4 sec at a sampling rate of 10 Hz for a total of 1024 data points. Two different signals are used to identify this system. The first signal is single PRBS with an amplitude of 3. This amplitude is chosen so as to excite the state over the range $x \in [-1, 1]$. The second signal consists of a PRBS with amplitude 0.05 superimposed on a series of four equal length pulses with values of ± 1 and ± 0.333. This system is identified using the various methods presented in Table 5.1.

Figure 5.3 shows the predicted upper bound on the gain of the transfer function for all four test cases. In each case, the spectrum is filtered with a raised cosine lag window [36]. In experiments A-C, relatively poor estimates of the upper bound are obtained. All of these experiments use the single PRBS signal to identify the system, and, therefore, it can be concluded that identification with this signal can lead to inaccurate results when used to determine the uncertainty bounds of nonlinear systems.

Only experiment D, which uses the regions-mapping method, computes an uncertainty bound that is consistent with the true bound, G_{upper}. At low frequencies this bound deviates slightly from the true bound. This deviation is caused by a small amount of biasing that occurs in all of the local transfer function estimates. Figure 5.4 shows the calculated transfer function $\hat{G}^{rm}$ along with both of its uncertainty bounds. As expected, the lower bound fits the theoretical bound well,

too.

5.6 Fixed Bed Methanation Reactor

To verify the effectiveness of this new identification technique for a real system and to point out the steps involved in system identification, the experimental transfer function identification of a fixed bed chemical reactor is performed. A complete description of this reactor can be found in Chapter 3.

The operating conditions used in the reactor identification are presented in Table 5.2, and the steady state axial temperature profiles corresponding to these operating conditions are shown in Figure 4.6. The distinguishing feature in all of the profiles is the presence of the temperature maximum or hot spot. As explained in Section 4.2.4, the location and height of this hot spot are unique functions of the N_2 flow rate.

It is desirable to maintain the hot spot near the entrance of the reactor, since complete conversion of the reactants is assured. If the hot spot temperature is too hot, though, the catalyst will slowly sinter and deactivate. This dichotomy of goals can be reconciled using automatic control of the hot spot temperature. The control objective is to regulate the hot spot temperature for a variety of different operating conditions including different temperature setpoints and inlet concentrations. Regulation of the hot spot temperature is maintained by varying the N_2 flow rate — large flow rates are necessary to keep the hot spot temperature from exceeding a preset upper bound, while lower flow rates are needed to keep the hot spot inside the reactor.

Since the product gases, methane and water, act as inerts, control of the nitrogen flow rate is analogous to control of a mass recycle stream around the reactor. In this control configuration, the product gases are recompressed and recycled back to the reactor inlet. The increased flow rate through the reactor reduces the temperature

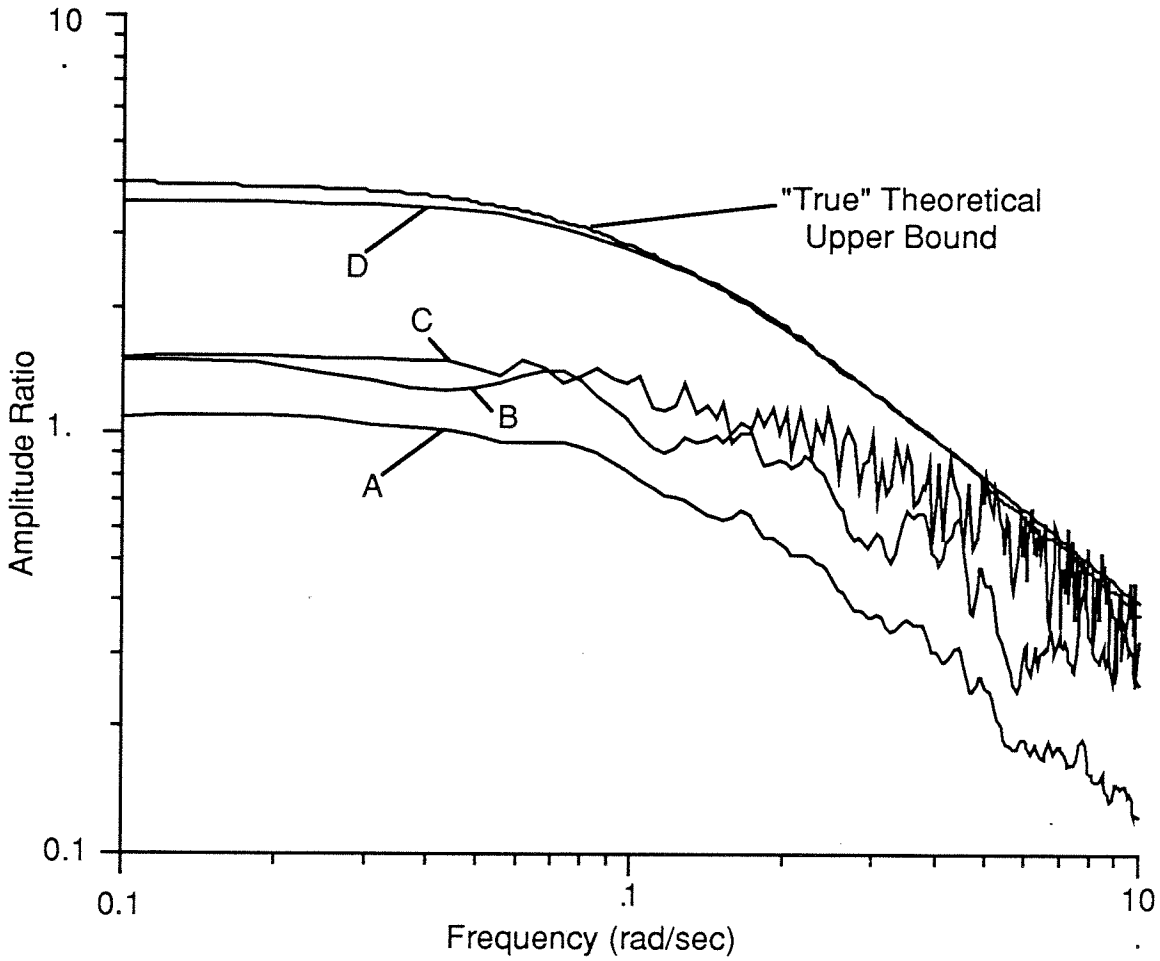

Figure 5.3: Comparison of upper bound on gain of transfer function for nonlinear system

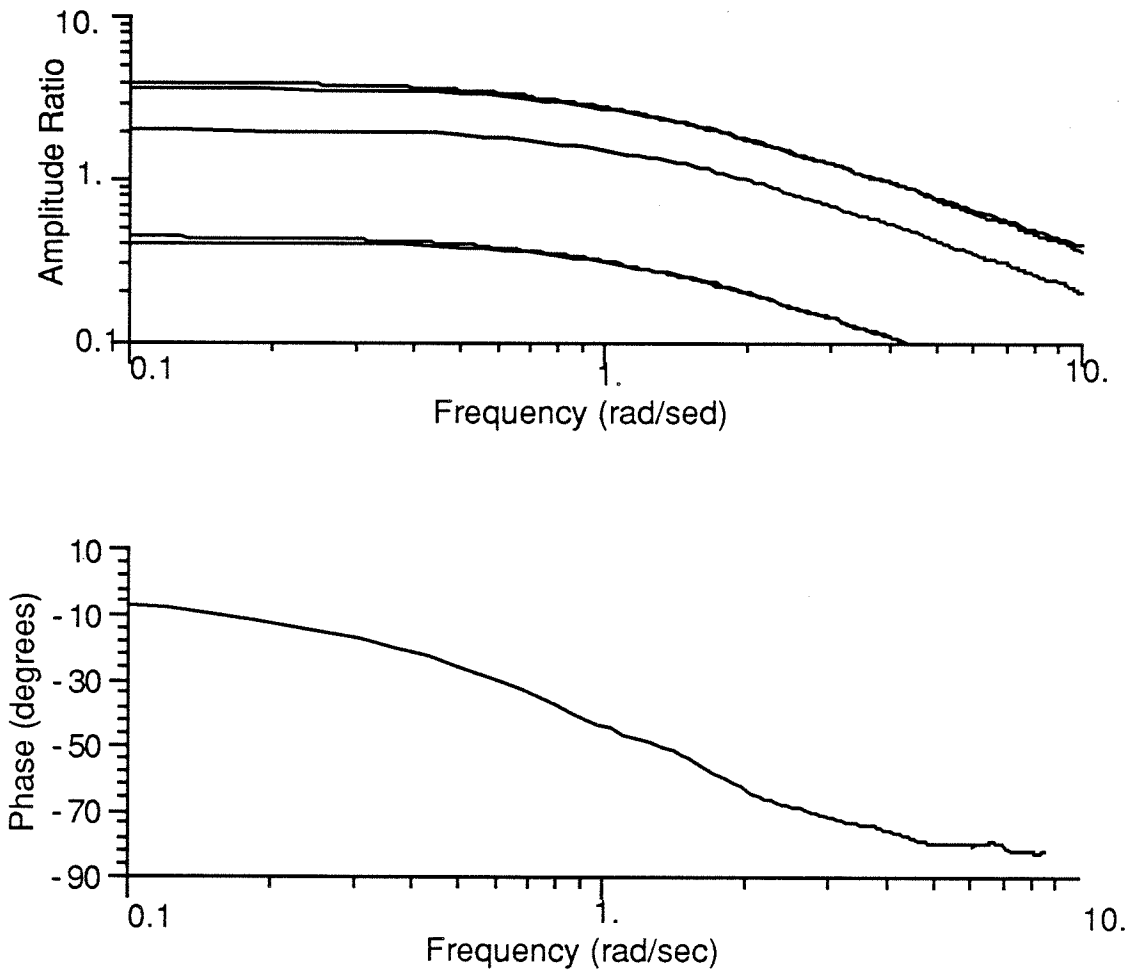

Figure 5.4: Frequency response of nonlinear model identified using regions-mapping technique. Superimposed on the frequency response are the theoretical and computed uncertainty bounds.

of the hot spot. This analogy holds because there is complete conversion inside the reactor, the product gases do not affect the reaction kinetics, and the temperature of the exit stream is approximately equal to the inlet temperature.

To measure the hot spot temperature and position in real time, the single mobile thermocouple used to generate the steady state temperature profiles in Figure 4.6 is replaced with 16 fixed thermocouples. These thermocouples are spaced at irregular intervals and are sampled once every 5 seconds. The hot spot temperature is estimated from these thermocouples by fitting a parabola through the three largest temperatures. The maximum value for the parabola is then computed and used as the hot spot temperature estimate. Likewise, the hot spot position is estimated from the position of parabolic maximum.

Figure 5.5 shows the response of the estimated hot spot temperature to a slow ramp in N_2 flow rate. While it is believed that the true hot spot temperature is a monotonic function of N_2 flow rate, the estimated hot spot exhibits several local minima. These minima, which are a consequence of the hot spot interpolation, place severe limitations on the robust controller because the steady state gain of the local linearized model changes sign as the hot spot passes through a minimum. To avoid these problems, the transfer function relating the hot spot temperature to the N_2 flow rate is identified only over the range 10–16 slpm where the interpolation effects are relatively small. While other means of estimating the hot spot temperatures have been investigated, parabolic fitting is adopted because of its simplicity and relative accuracy.

5.7 Application of Relay Controller

Using the nitrogen flow rate range specified in the previous section, a relay controller is setup which regulates the hot spot temperature at 335°C. For this operating range, the crossover frequency of the plant is 0.016 rad/sec, and the

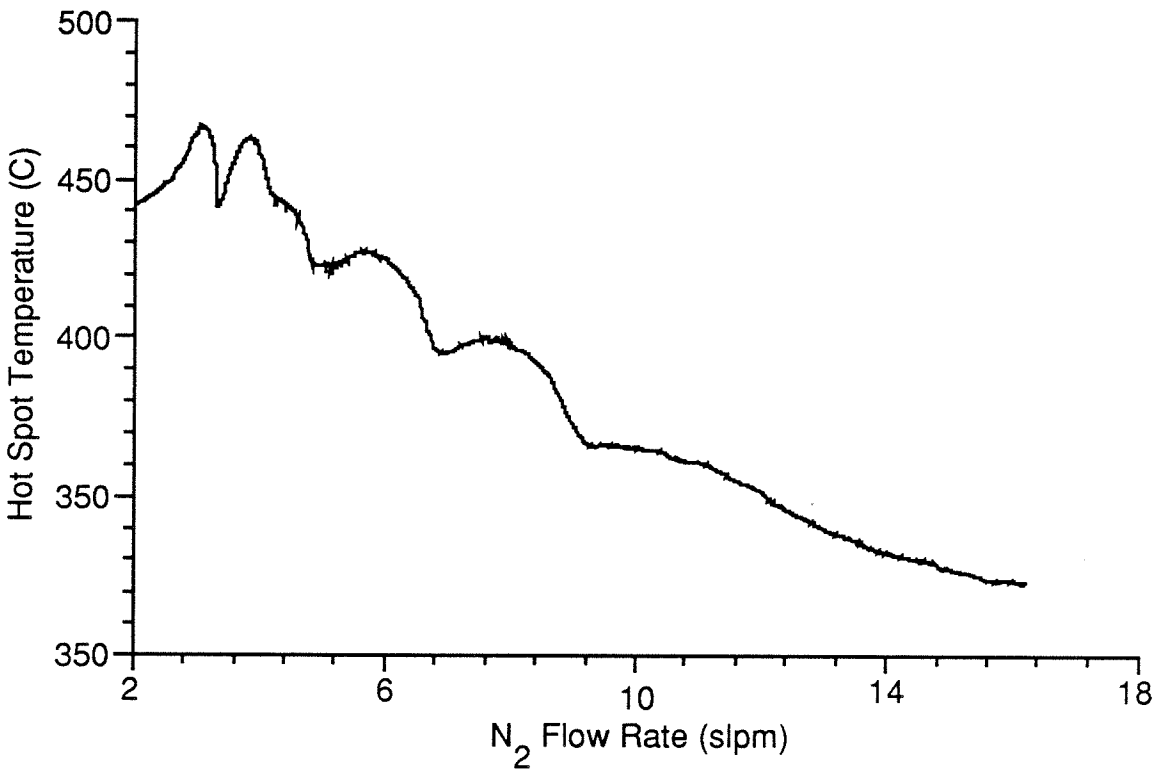

Figure 5.5: Estimated hot spot temperature for a slow ramp in N_2 flow rate

breakdown frequency is approximately 0.17 rad/sec. The hot spot temperature response for these two frequencies is shown in Figure 5.6. No attempt is made to account for the decrease in the magnitude of the output response which naturally occurs due to the rolloff of the transfer function by increasing the nitrogen flow rate range. This range is fixed for all experiments.

To determine whether the breakdown is due to noise or uncertainty, the control loop is opened, and a square wave of frequency 0.28 rad/sec is directly introduced into the reactor. The result of this experiment, Figure 5.6, shows the hot spot temperature to be periodic even though its closed-loop counterpart is not. This implies that the breakdown of the relay experiment is due to noise and not plant uncertainty. This is not surprising since the amplitude of the output is so small.

5.8 Open-Loop Identification

Using a frequency range with an upper limit specified by the breakdown frequency, a PRBS is constructed and implemented for 3 different flow rate ranges. (See Table 5.3.) Each binary sequence contains 1023 points and lasts for 17,885 seconds.

A local transfer function is estimated for each of the three cases in Table 5.3 using spectral analysis. A global model is then obtained by applying the regions-mapping technique to these local estimates. Figure 5.7 shows the resulting non-parametric model. As expected, the estimated crossover frequency of 0.014 rad/sec is very close to that identified using the relay controller.

Surrounding this model are the upper and lower uncertainty bounds. The uncertainty associated with this model is small at low frequencies and remains constant over the range 0.001–0.02 rad/sec. At 0.02 rad/sec, the uncertainty increases in size and remains relatively large for higher frequencies. Because of the inherent trade off between robustness and performance, it is expected that the closed-loop bandwidth

Case	Type of Input	Magnitude of Input	Method used to compute Uncertainty
A	PRBS	-3 to 3	Distribution Theory
B	PRBS	-3 to 3	Probability Distribution
C	PRBS	-3 to 3	Regions-Mapping
D	PRBS at 3 different operating points	PRBS -0.05 to 0.05 superimposed on input of $\pm 1, \pm 0.333$	Regions-Mapping

Table 5.1: Experiments used to identify nonlinear gain model

Variable	Amount	Units
CO_2	0.42	slpm
H_2	2.52	slpm
N_2	10-16	slpm
Inlet Temperature	240	°C
Dowtherm Temperature	256	°C

Table 5.2: Reactor operating conditions

Case	Flow Rate (slpm)	Steady State hot spot Temperature for mean Flow Rate $°C$
A	10 - 12	362
B	12 - 14	338
C	14 - 16	327

Table 5.3: Flow rate ranges used in the reactor identification experiments

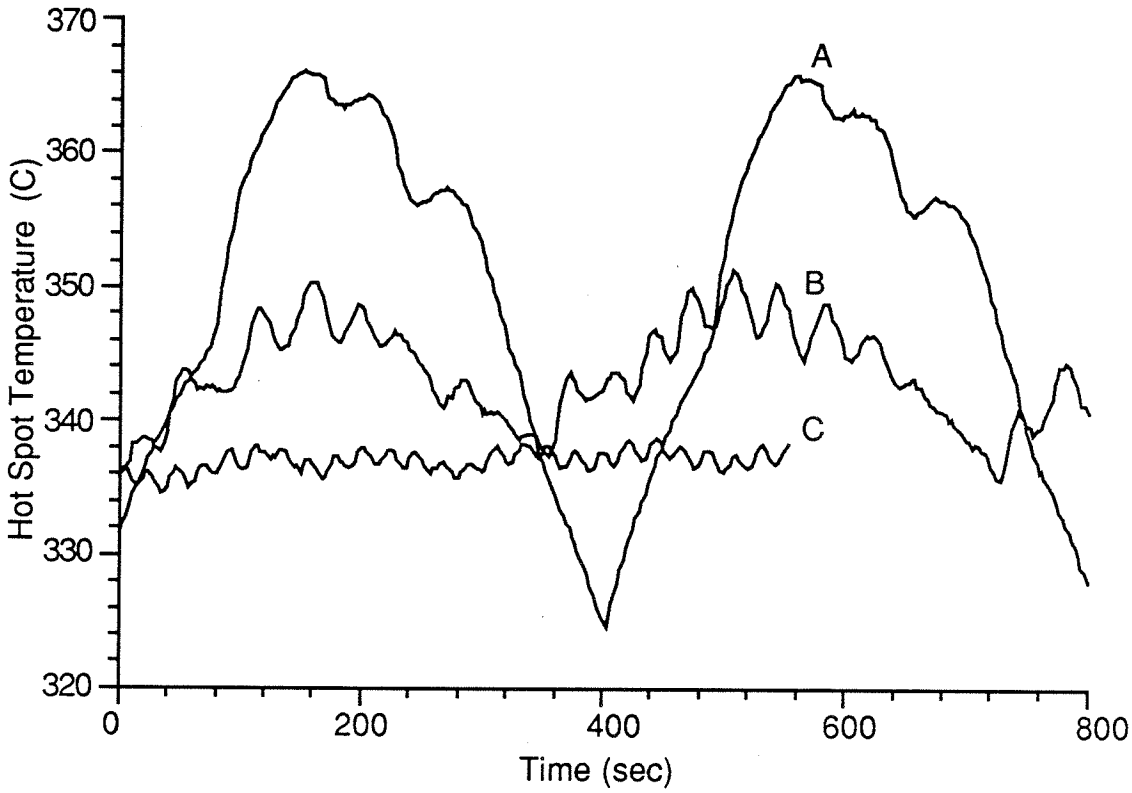

Case A - closed-loop response at crossover frequency
Case B - closed-loop response near breakdown frequency
Case C - open-loop response to a fast square wave input

Figure 5.6: Hot spot temperature response for reactor under closed-loop relay control

will be smaller than 0.02 rad/sec.

5.9 Controller Design and Uncertainty Validation

To check the validity of the uncertainty bound, Internal Model Control, IMC, theory is used to design a robust controller and that controller is then implemented on the reactor. (See [92] for details on the design method.) The first step of the design procedure is to approximate the non-parametric model by a parametric model. A 3 pole - 3 zero model is chosen to represent the non-parametric frequency response and the parameters of this model are fit using linear least squares. This model is ($T_s = 5$ sec) :

$$\tilde{P}(z) = \frac{(z + 0.681)(z - 1.136)(z - 2.241)}{(z - 0.975)(z - 0.809)(z + 0.339)} \tag{5.47}$$

An H_∞ optimal technique for doing the fitting is available in [103,48]. Using a first-order robustness filter,

$$f(z) = \frac{(1 - e^{\frac{-T_s}{\lambda}})z}{z - e^{\frac{-T_s}{\lambda}}} \tag{5.48}$$

and the parametric model, $\tilde{P}(z)$, the controller, $C(z, \lambda)$ then is parameterized as

$$C(z, \lambda) = \frac{\tilde{P}_M^{-1} f}{1 - \tilde{P}_A f} = \frac{N(z, \lambda)}{D_1(z, \lambda) - D_2(z, \lambda)} \tag{5.49}$$

where

$$N(z, \lambda) = 112(1 - e^{\frac{-T_s}{\lambda}})z(z - 0.975)(z - 0.809)(z + 0.339) \tag{5.50}$$

$$D_1(z, \lambda) = (z + 0.681)[(z - 0.880)(z - 0.446)(z - e^{\frac{-T_s}{\lambda}})] \tag{5.51}$$

$$D_2(z, \lambda) = 0.393(z + 0.681)[(1 - e^{\frac{-T_s}{\lambda}})z(z - 1.136)(z - 2.241)] \tag{5.52}$$

Because there is a mismatch between the parametric model, $\tilde{P}$, and the non-

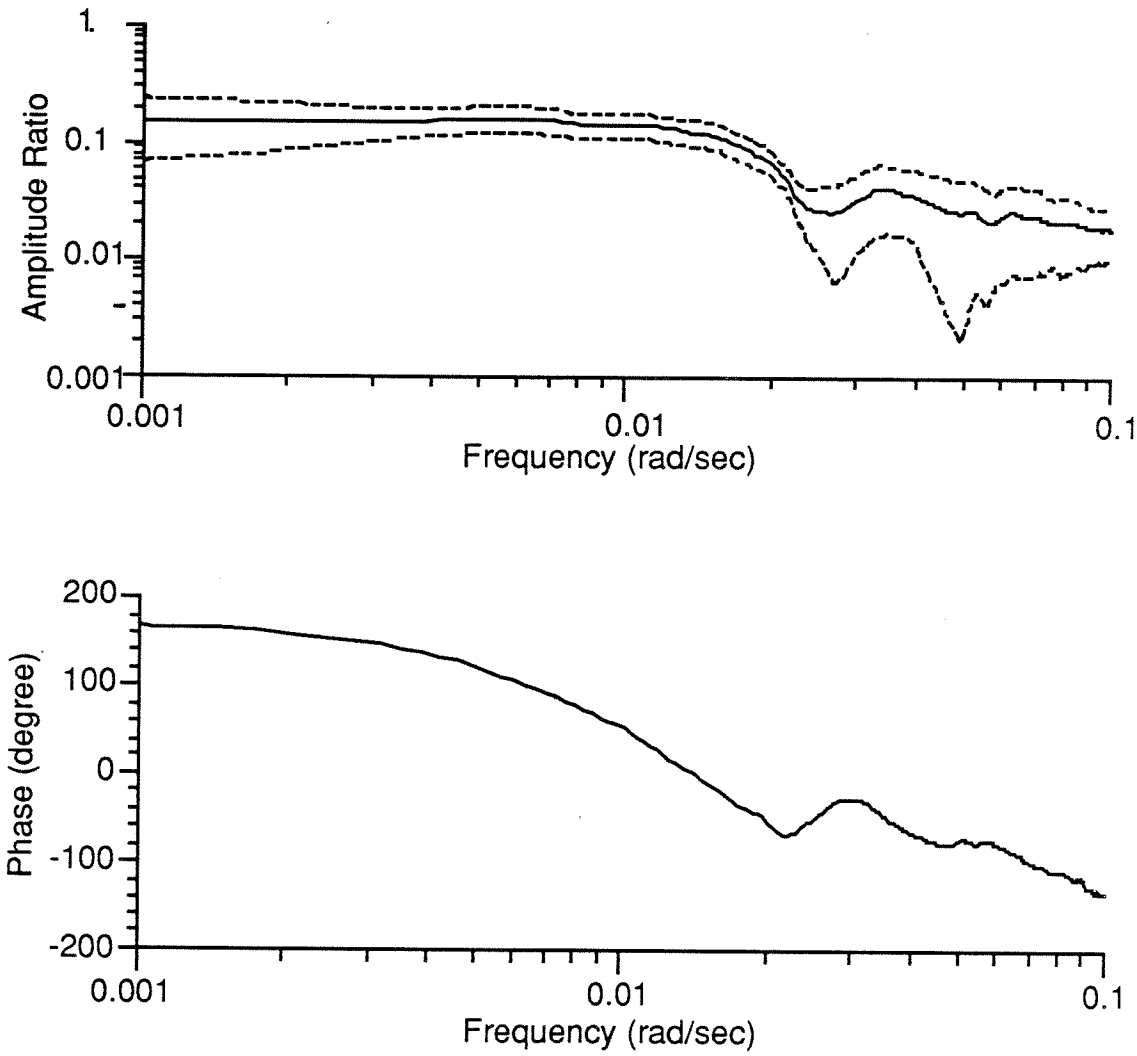

Figure 5.7: Identified frequency response of methanation reactor with uncertainty bounds

parametric model, $\hat{G}^{rm}$, the additive uncertainty, ℓ_a, is recalculated using

$$\ell_a(\omega_k) = \max_i |\hat{G}_i^s(\omega_k) - \tilde{P}(e^{i\omega_k T_s})| \tag{5.53}$$

from which the multiplicative uncertainty, ℓ_m, can be computed.

$$\ell_m(\omega_k) = \tilde{P}^{-1}(e^{i\omega_k T_s})\ell_a(\omega_k) \tag{5.54}$$

Figure 5.8 shows a plot of the complementary sensitivity, η, times the multiplicative uncertainty for three different λ. For a controller to robustly stabilize the plant, $\eta\ell_m$ must be less than 1 at all frequencies [92]. This is true for all $\lambda \geq 164$ sec. Therefore, if the calculated uncertainty bound is a tight bound, $\lambda = 164$ sec should stabilize the reactor over the whole operating window, whereas, $\lambda < 164$ sec will be closed-loop unstable for at least one operating condition.

A number of validation experiments are conducted in which the hot spot temperature setpoint is given either a positive or a negative step change. Several filter parameters in the range 7.2 sec $\leq \lambda \leq$ 497 sec are tested. Initial experiments reveal that it is more difficult to stabilize the system around hotter hot spot temperatures. Therefore, most of the validation experiments are conducted with a final setpoint temperature near 360°C. It is found that for $\lambda \leq 47$ sec the closed-loop system is unstable while for $\lambda \geq 164$ sec the closed-loop system is stable. For the intermediate range 47 sec $< \lambda <$ 164 sec responses resembling limit cycles are obtained and no clear conclusion about stability can be drawn. Typical experimental runs for $\lambda = 47$ sec, $\lambda = 97$ sec, and $\lambda = 164$ sec are shown in Figures 5.9– 5.11, respectively. These experimental results tend to validate the uncertainty bounds obtained with the regions-mapping method.

In addition to the setpoint changes, the system is also examined for disturbances in the CO_2 flow rate. This is an important and often analyzed regulatory problem

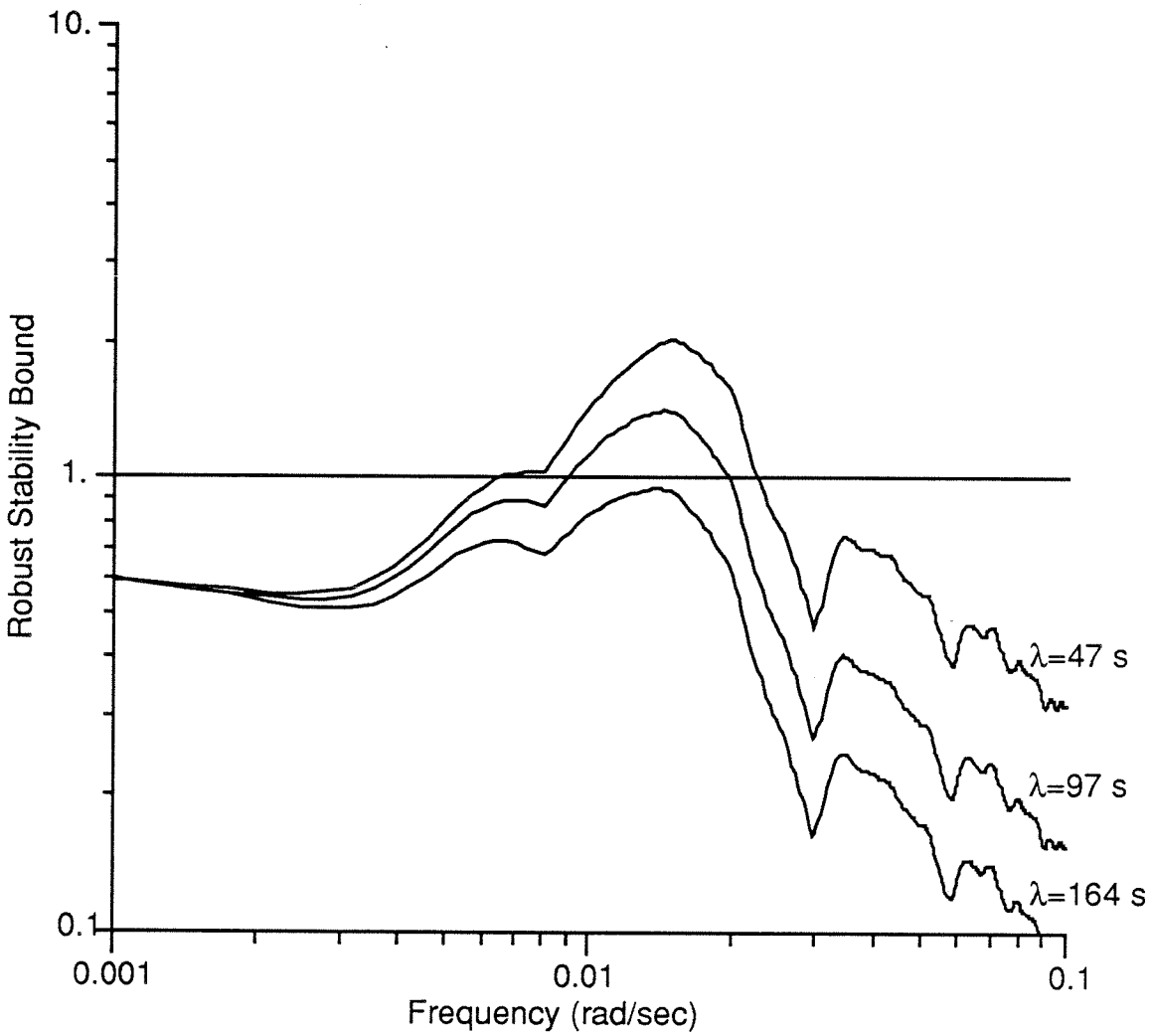

Figure 5.8: Robust stability, $\eta \ell_m$, as a function of frequency for different robustness filters

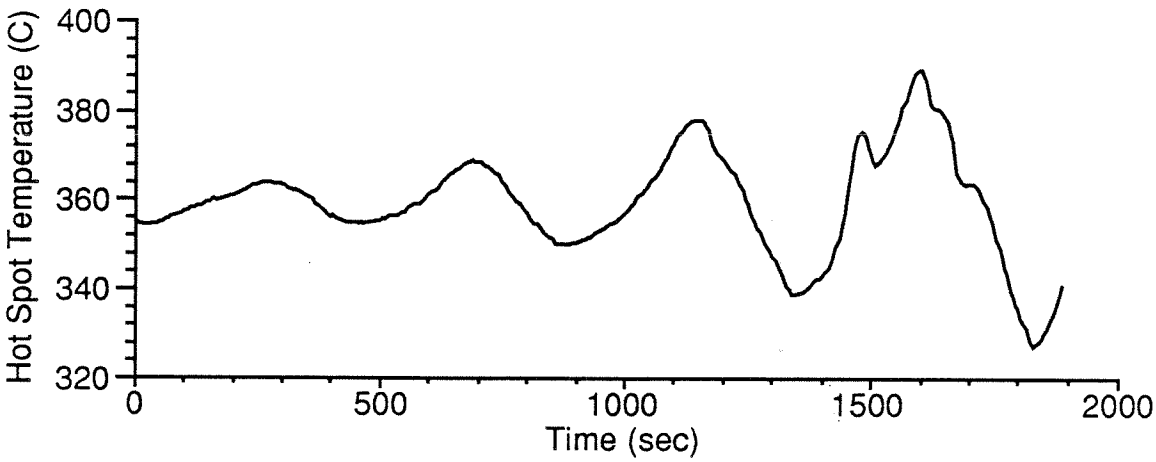

Figure 5.9: Closed-loop response of system to step in hot spot temperature setpoint. Filter time constant is 47 seconds.

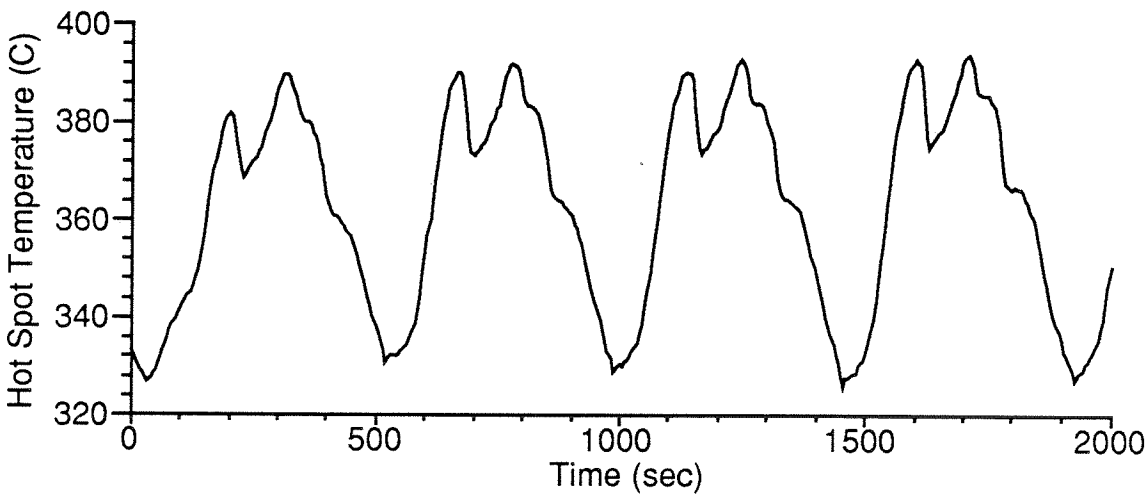

Figure 5.10: Closed-loop response of system to step in hot spot temperature setpoint. Filter time constant is 97 seconds.

since the inlet feed concentrations of an industrial reactor are often fixed by upstream conditions over which the control system has no effect. In this reactor, increases in the reactant concentrations are known to increase the hot spot temperature. The goal of the control system is to maintain the hot spot temperature at its setpoint value in light of these changes.

For this set of experiments, the system is initially brought to steady state at a predefined setpoint. A +15% change in the inlet CO_2 flow rate is made and the closed-loop response of the hot spot temperature is monitored. If left uncorrected, a 15% increase in the CO_2 flow rate raises the steady state hot spot temperature from 10–30°C depending on the total flow rate of gas through the system.

Using the previously designed controller with a filter time constant of 164 seconds, the closed-loop responses of the hot spot are examined around three different operating points: hot spot temperatures of 325, 335, and 365°C. The results of these experiments are shown in Figures 5.12–5.14. From these figures, it is apparent that the controller maintains its robustness even though it has not been explicitly designed around the new operating conditions.

Conclusions

In this chapter, spectral analysis theory is used to identify a non-parametric frequency domain model from input-output data. Three uncertainty bounds for this model are derived: two bounds based on the residual spectrum and a third new bound based on a regions-mapping technique. These uncertainty bounds are examined using Fourier analysis, and it is shown that the uncertainty bounds are composed of two parts: one which measures the deviation of the model from the empirical transfer function estimate, and a second which monitors the noise level.

Next, it is shown how a relay controller preceded by a lead compensator can be used to determine the frequency range over which the control identification exper-

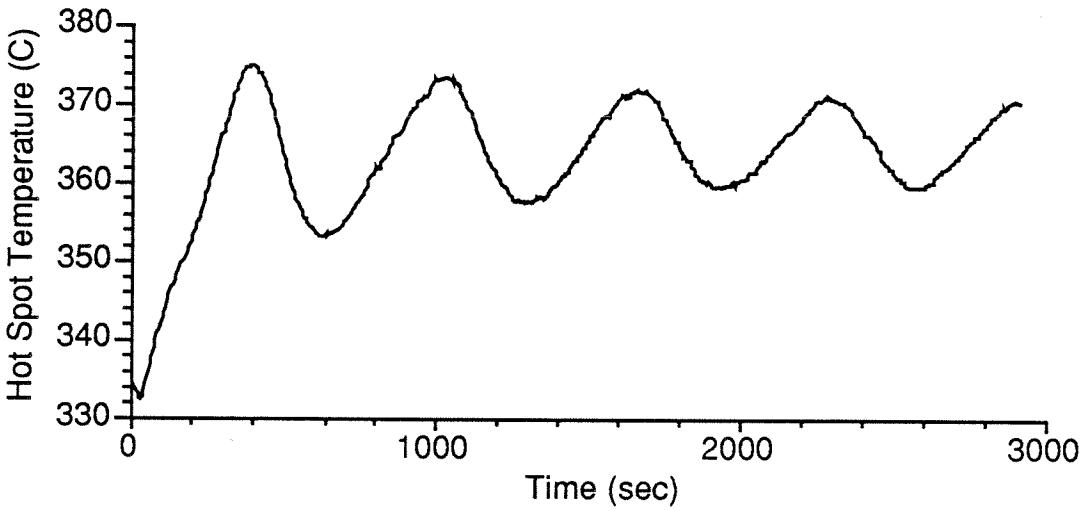

Figure 5.11: Closed-loop response of system to step in hot spot temperature setpoint. Filter time constant is 164 seconds.

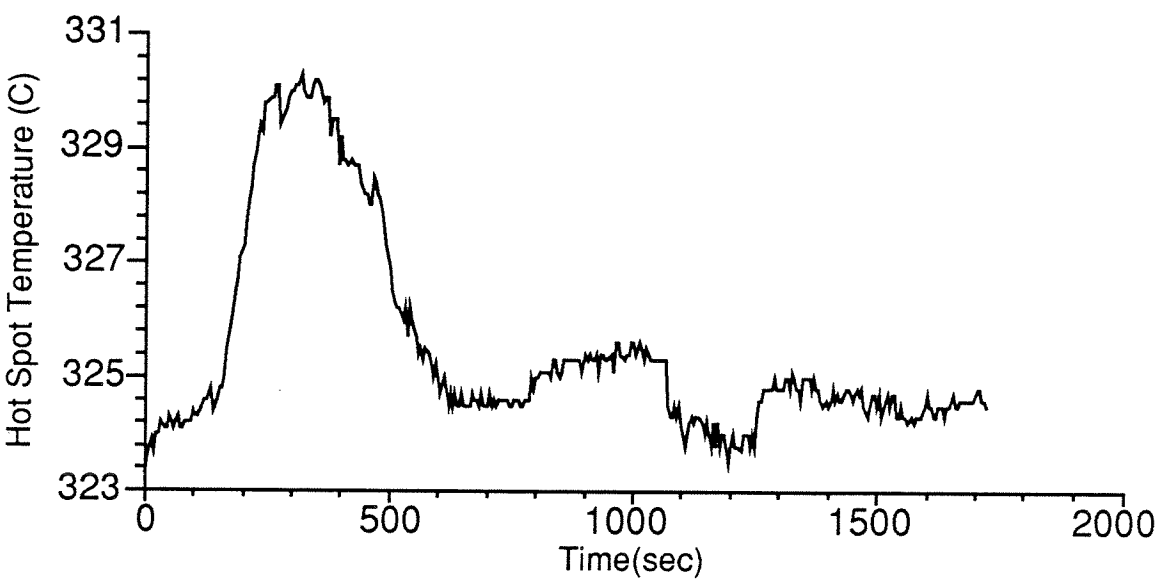

Figure 5.12: Closed-loop hot spot response for +15% increase in CO_2 flow rate. Setpoint temperature is 325°C

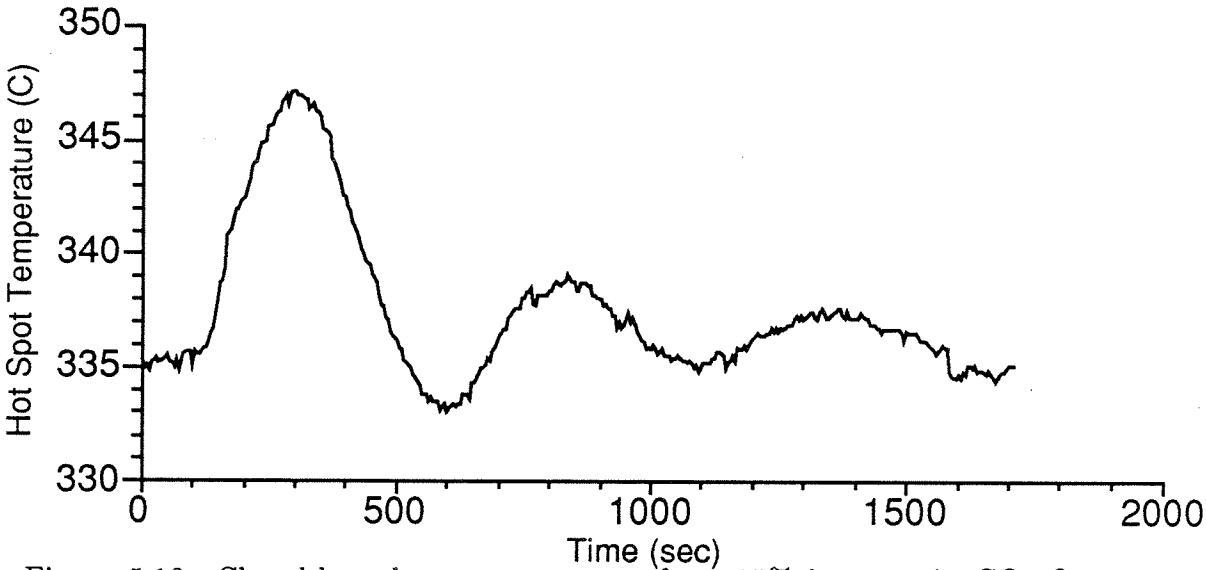

Figure 5.13: Closed-loop hot spot response for +15% increase in CO_2 flow rate. Setpoint temperature is 335°C

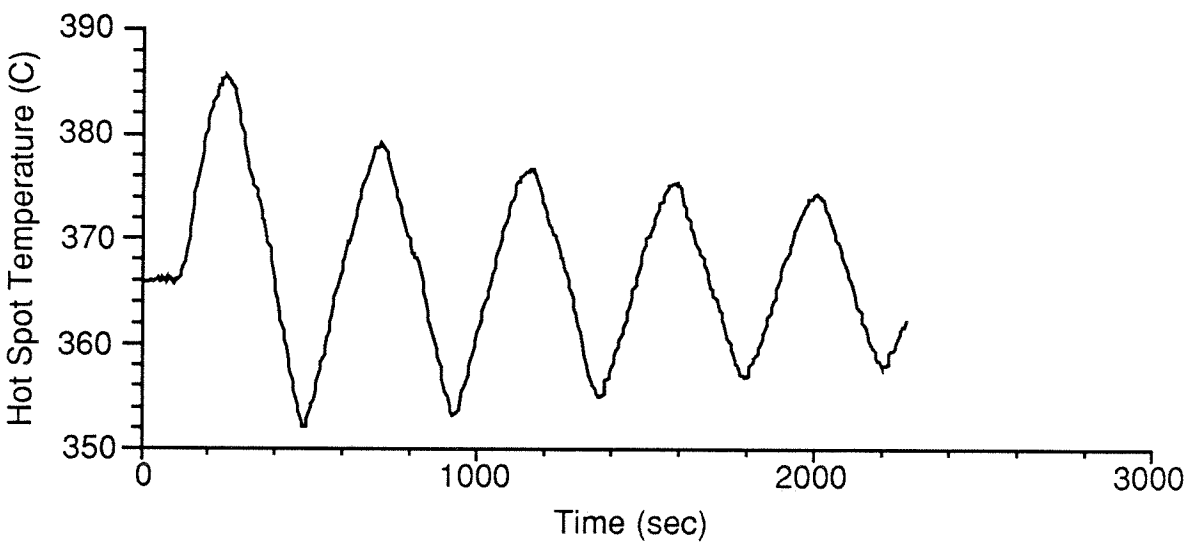

Figure 5.14: Closed-loop hot spot response for +15% increase in CO_2 flow rate. Setpoint temperature is 365°C

iment should be conducted. This relay experiment does not help in locating the uncertainty bounds, though, if the high frequency response is dominated by noise.

Then, a simple nonlinear model is used to test the accuracy of the various identification methods. All three uncertainty bounds are compared to theoretical bounds obtained for the linearized model and the bounds based on the residual spectrum are discarded as being deficient. This result is especially important for systems which need to be identified over a wide range of operating conditions.

Finally, the identification of a fixed bed reactor is performed and the uncertainty bound using the regions-mapping technique is estimated. The transfer function sought is the change in hot spot temperature to a change in inert gas, N_2, flow rate. Using the identified model and computed uncertainty bound, an IMC controller is designed which is shown to be robustly stable if the time constant of the robustness filter, λ, is greater than 164 sec. This agreed with experimental results which showed the closed-loop system to be stable for $\lambda \geq 164$ sec, but unstable for $\lambda \leq 47$ sec. Although the uncertainty description is based on a fixed reactant flow rate, the robust controller effectively regulates the hot spot temperature for a +15% change in the reactant flow rate.

Chapter 6

Robust Inferential Control

Abstract

An inferential robust control technique is applied to an experimental fixed bed reactor. The control variables are the exit concentration and the maximum bed temperature. Since the concentration cannot be measured fast enough for control, it is inferred from a single temperature measurement. The location of this measurement is selected to optimize the performance of the closed-loop system when model uncertainty is allowed. Closed-loop experiments are conducted to test the robustness characteristics of the controller. For these experiments, the operating regions most sensitive to modelling uncertainty are determined. While the controller is designed to account for model uncertainty and to give good performance, a significant steady state offset can occur in the controlled variables. This offset is due to the inherent nonlinearity of the system.

6.1 Introduction

For the problem presented in the previous chapter, the reactor was operated under the condition of full conversion. In the present chapter, we turn our attention to the problem of controlling the reactor under conditions of partial conversion. In this case, the controlled variables are the outlet temperature and the outlet concentration. Again, the control objectives are to obtain stability and good performance over a range of different operating conditions. In contrast to the previous chapter, we have a multiple-input multiple-output problem.

In practice, it is highly problematic to measure concentration in real time. First, gas chromatographs are relatively expensive to operate and maintain. They must be periodically recalibrated, their columns must be reconditioned, and they can have unpredictable and costly down times. In addition, gas chromatographs have relatively slow sampling rates. This slow sampling rate can affect the stability

and deteriorate the performance of the closed-loop control system. Furthermore, if the unit is located an appreciable distance from the reactor, there can also be a significant transportation delay associated with the sampling process. It may require 3–4 samples before an accurate reading of the concentration is obtained. For these reasons, it is decided to infer the concentrations from the temperature measurements (inferential control).

There are two important issues in the design of an inferential control scheme:

- Which measurements should be selected to optimize the closed-loop performance?
- Given a set of measurements, how does one design an inferential controller which is robust to changes in the operating conditions?

In this chapter a measurement selection technique derived from Structured Singular Value analysis [78,77] is implemented on the experimental reactor. The measurements used in the controller design are based on the application of this technique at steady state. A description of closed-loop inferential control experiments is included to demonstrate the advantages of this scheme.

6.2 Measurement Selection for Inferential Control

A number of researchers have examined the measurement selection problem and a number of different approaches have been proposed. Several researchers, including Seinfeld and coworkers [71] and MacGregor and coworkers [47], examined the problem using a stochastic state space framework. Measurements were selected by their ability to minimize a scalar measure of the covariance matrix of the state prediction error. Model uncertainty was accounted for by introducing random disturbances additively into the system equations. The statistical properties of these disturbances are intended to reflect the expected degree of modelling mismatch. In the present

work, we take a different approach by considering norm-bounded uncertainty on the empirical transfer functions which describe the process.

6.2.1 Inferential Control

Inferential control was first proposed by Weber and Brosilow [139] for the design of a static estimator but was later extended by Brosilow and coworkers [60,12,59] to include dynamics. Inferential control uses secondary variables, temperature measurements in the present study, to infer the effects of unmeasured disturbances on the controlled variables. An estimator is constructed which measures the secondary variable and predicts the effective change in the controlled variable. Using this information, a feedback controller can be designed to compensate for the projected changes in the controlled variable.

Assuming that there is no uncertainty in the model,

$$s = G_{sd}d + G_{sm}m \tag{6.1}$$

$$c = G_{cd}d + G_{cm}m \tag{6.2}$$

where s represents the vector of secondary measurements, c the vector of controlled variables, m the vector of manipulated variables, and d the vector of unmeasured disturbances. Assuming G_{sd} is invertible then

$$d = G_{sd}^{-1}(s - G_{sm}m) \tag{6.3}$$

$$c = G_{cd}G_{sd}^{-1}(s - G_{sm}m) + G_{cm}m \tag{6.4}$$

$$= G_{cd}G_{sd}^{-1}s - [G_{cd}G_{sd}^{-1}G_{sm} - G_{cm}]m \tag{6.5}$$

If the transfer function $[G_{cd}G_{sd}^{-1}G_{sm} - G_{cm}]^{-1}G_{cd}G_{sd}^{-1}$ is stable and realizable (proper

and casual) then the controller

$$m = [G_{cd}G_{sd}^{-1}G_{sm} - G_{cm}]^{-1}G_{cd}G_{sd}^{-1}s \tag{6.6}$$

gives an error free response.

At steady state, the above transfer function matrices reduce to a set of constant matrices where each element in a matrix represents a steady state gain. If the number of independent measurements exceeds of equals the number of disturbances, then a perfect steady state estimator can be obtained from

$$E = G_{cd}G_{sd}^{-1} \tag{6.7}$$

where G_{sd} is any invertible set of measurements. If the number of unmeasured disturbances exceeds the number of measured variables, Brosilow [139] suggests the use of a least squares optimal estimator

$$E = G_{cd}G_{sd}^{T}(G_{sd}G_{sd}^{T})^{-1} \tag{6.8}$$

Brosilow points out that in practice, an estimator designed using Equation 6.7 "will more often than not give very poor estimates. This is due to the fact that estimation errors caused by errors in modelling, measurement, and numerical roundoff can be greatly amplified by a poor choice of measurements" [139]. He goes on to point out that measurements should be chosen to minimize two quantities:

- **Relative Error** This is the norm of the error in the steady state estimate of the controlled variables divided by the norm of the controlled variable. This error is caused by having more unmeasured disturbances than measured variables.
- **Condition Number of G_{sd}** This is the condition number of the static gain matrix relating the disturbances to the secondary measurements.

The relative error is a measure of the estimator accuracy whereas the condition number of G_{sd} is a measure of the estimator's sensitivity to model uncertainty. These two quantities are both dependent on the number of measurements used in the inference. Typically, as this number increases the relative error decreases whereas the condition number increases. Therefore, there is a trade-off between these functions. Because the number of combinations of measurements can be extremely large, Brosilow suggests a simple scheme for measurement selection based on the above trade-off.

Brosilow and Tong [12] point out that a feedback control scheme employing the inferential estimates (an inferential control scheme) can be represented by the block diagram shown in Figure 6.1. In this diagram, $\hat{G}_{sm}$ is an estimate of the transfer function between the manipulated variables and the secondary variables and $\tilde{Q}$ is the controller.

If $\hat{G}_{sm} = G_{sm}$, then the signal which enters the estimator is a function of the disturbances only. Furthermore, the control signal, m, is not fed back through the estimator, E, or the controller, $\tilde{Q}$. Under these circumstances, perfect control is obtained when

$$E = G_{cd}G_{sd}^{-1} \tag{6.9}$$

$$\tilde{Q} = G_{cm}^{-1} \tag{6.10}$$

assuming G_{sd}^{-1} and G_{cm}^{-1} are stable and realizable. If they are not, they can be approximated using the techniques found in [59]. While it is true that uncertainty in G_{sd} may lead to steady state errors in control, the closed-loop stability of this scheme is invariant to the amount of uncertainty associated with G_{sd} as long as G_{sd} remains stable (see Lee and Morari [78] for robust stability conditions).

6.2.2 Robust Inferential Control

Using the inferential control framework, Lee and Morari [78,77] propose a new methodology for measurement selection and controller design based on Structured Singular Value theory. This analysis allows for structured norm-bounded uncertainty in any of the system transfer functions as well as frequency domain performance specifications. They show that Brosilow's condition number criterion holds only under specific assumptions on model uncertainty and performance specification.

In the present work, we will implement this measurement selection technique on the experimental reactor. Figures 6.2 and 6.3 shows the block diagram under consideration. In these figures,

$$\Delta^* = \begin{bmatrix} \Delta_1^* & & \\ & \ddots & \\ & & \Delta_\ell^* \end{bmatrix} \tag{6.11}$$

where Δ_i^* are the uncertainties associated with the individual transfer functions. W_d, W_p are frequency dependent performance weights used to normalize the disturbance and controlled variables, respectively. The controller, $Q = \tilde{Q}E$, is chosen so that the nominal system is closed-loop stable. This is true, if and only if Q is stable.

For simplicity, the measurement selection process is performed for steady state conditions. In this way, the number of candidate measurement sets can be reduced. The final selection, however, must be based on dynamic considerations.

The measurement selection is based on the minimization of the worst-possible closed-loop steady state performance. Since this is a difficult optimization problem, the controller is restricted to the following form:

$$E = G_{cd}(G_{sd})_l^{-1} \tag{6.12}$$

$$\tilde{Q} = (G_{cm})_r^{-1} \tag{6.13}$$

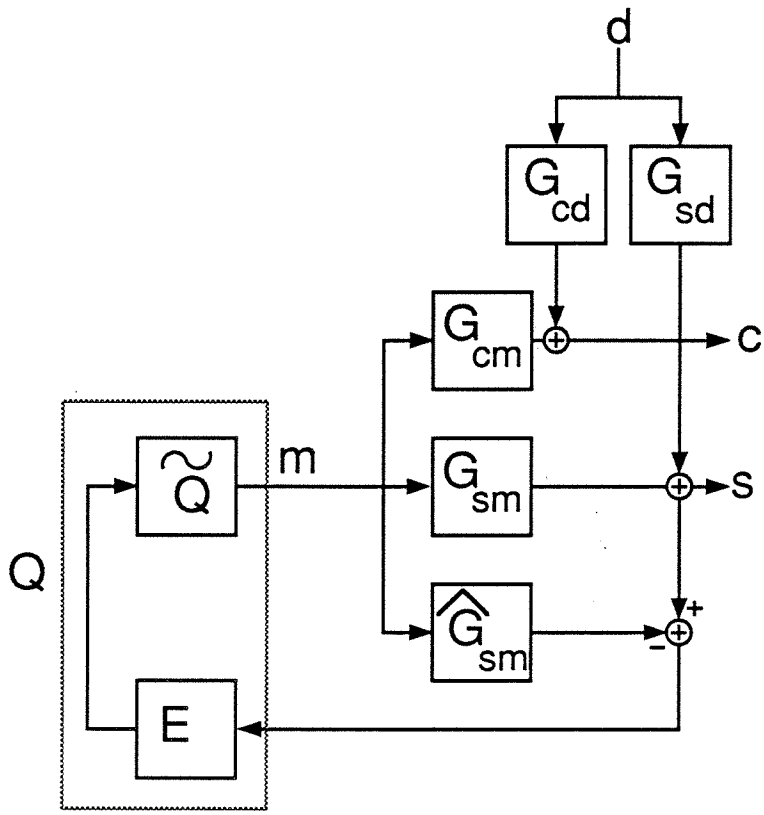

Figure 6.1: Inferential control scheme

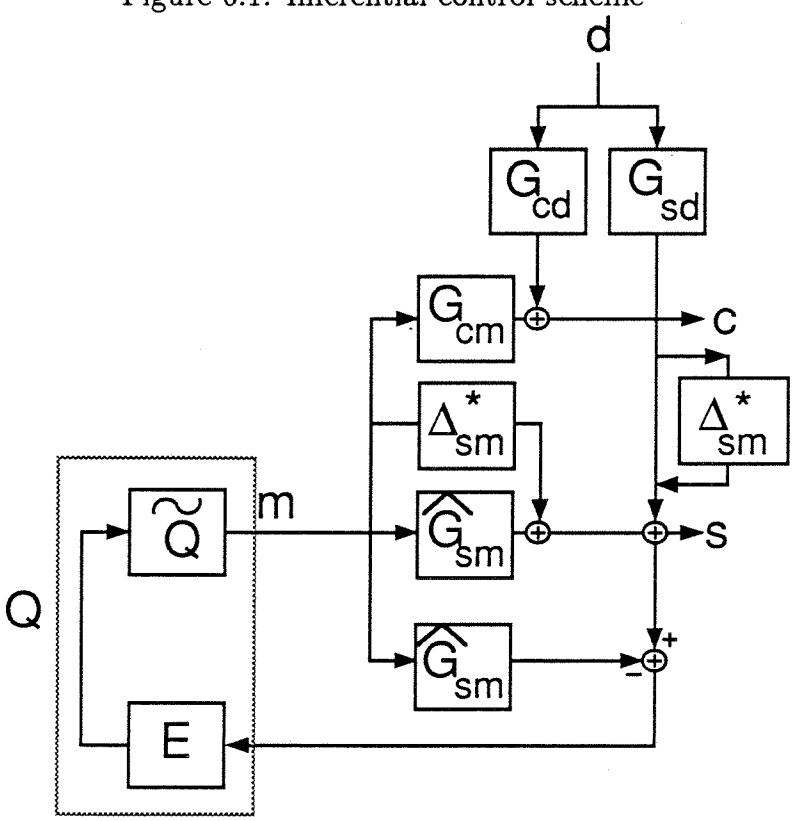

Figure 6.2: Inferential control applied to an uncertain system

where the subscript denotes left or right inverse, respectively. The block diagram of the inferential control scheme is then transformed into the M-Δ form shown in Figure 6.3.

Considering this M-Δ structure and using the Structured Singular Value, the worst-possible closed-loop performance, c_p^*, can be computed from Definition 6.1 and Theorem 6.1.

Definition 6.1 (Structured Singular Value [24]) *Let* $M \in \mathcal{C}^{n\times m}$ *and define the set* $\mathbf{\Delta}$ *as*

$$\mathbf{\Delta} = \left\{ \tilde{\Delta} : \tilde{\Delta} = \begin{bmatrix} \Delta_1^* & & \\ & \ddots & \\ & & \Delta_\ell^* \end{bmatrix} ; \Delta_i^* \in \mathcal{C}^{m_i \times n_i}; \sum_{i=1}^{\ell} m_i = m, \sum_{i=1}^{\ell} n_i = n \right\} \tag{6.14}$$

Then $\mu_{\mathbf{\Delta}}(M)$ *is defined as*

$$\mu_{\mathbf{\Delta}}(M) = \begin{cases} \left[\min_{\tilde{\Delta}\in\mathbf{\Delta}} \left\{\bar{\sigma}(\tilde{\Delta}) : \det(I + M\tilde{\Delta}) = 0\right\}\right]^{-1} \\ 0 \text{ if } \nexists \text{ no } \tilde{\Delta} \in \mathbf{\Delta} \text{ such that } \det(I + M\tilde{\Delta}) = 0 \end{cases} \tag{6.15}$$

Theorem 6.1 (Lee and Morari [77]) *Let* $M_{11} \in \Re^{n\times m}, M_{12} \in \Re^{n\times q}, M_{21} \in \Re^{p\times m}$, *and* $M_{22} \in \Re^{p\times q}$. *Define the set* $\mathbf{\Delta}_u$ *as*

$$\mathbf{\Delta}_u = \left\{ \begin{bmatrix} \Delta_1 & & \\ & \ddots & \\ & & \Delta_\ell \end{bmatrix} : \bar{\sigma}(\Delta_i) \leq 1 \text{ for } 1 \leq i \leq \ell; \Delta_i^{m_i\times n_i}; \sum_{i=1}^{\ell} m_i = m, \sum_{i=1}^{\ell} n_i = n \right\} \tag{6.16}$$

Also define

$$f(c_p) = \mu \begin{bmatrix} \mathbf{\Delta}_u^* & \\ & \mathbf{\Delta}_p \end{bmatrix} \begin{pmatrix} M_{11} & M_{12} \\ c_p M_{21} & c_p M_{22} \end{pmatrix} \tag{6.17}$$

where

$$\mathbf{\Delta}_u^* = \left\{ \tilde{\Delta} = \begin{bmatrix} \Delta_1^* & & \\ & \ddots & \\ & & \Delta_\ell^* \end{bmatrix} : \Delta_i^* \in \Re^{m_i \times n_i}; \sum_{i=1}^{\ell} m_i = m, \sum_{i=1}^{\ell} n_i = n \right\} \tag{6.18}$$

$$\Delta_p = \left\{ \Delta : \Delta \in \Re^{q \times p} \right\} \tag{6.19}$$

Assume that $\mu_{\mathbf{\Delta}_u^*}(M_{11}) < 1$. *Then,*

$$\max_{\Delta_u \in \mathbf{\Delta}_u} \bar{\sigma}[M_{22} + M_{21}\Delta_u(I - M_{11}\Delta_u)^{-1}M_{12}] = \frac{1}{c_p^*} \tag{6.20}$$

where c_p^* *solves the equation* $f(c_p^*) = 1$.

If c_p^* is < 1, then the worst possible closed-loop performance exceeds the performance criterion, as expressed in W_p, and the chosen measurement set should be eliminated from further consideration. On the other hand, if $c_p^* > 1$, robust steady state performance is guaranteed. The measurement set which maximizes c_p^* has the smallest potential steady state error, and should be the first measurement set considered for control design.

Although the steady state criterion provides a simple screening tool for measurement selection, in most cases it must be supplemented with dynamic criteria. This is especially important when the measurements have significant time delays. For each measurement set, $\tilde{Q}$ and E are designed using a simple synthesis procedure. Lee and Morari [77] suggest that the estimator, E, be designed as a Kalman-filter augmented with an appropriate output matrix. If the left inverse of G_{sd} exists, $G_{cd}(G_{sd})_l^{-1}$ is stable and realizable, and measurement noise is insignificant, then the optimal choice for E is $G_{cd}(G_{sd})_l^{-1}$.

The design of $\tilde{Q}$ is slightly more complicated. Using the Internal Model Control design procedure, $\tilde{Q}$ is split into two parts, F and $\tilde{Q}_n$ where F is a simple robustness

filter usually of the form g(s)I and $\tilde{Q}_n$ is either an H_2 or H_∞ optimal controller designed for the nominal conditions. If G_{cm} has a stable right inverse, $\tilde{Q} = (G_{cm})_r^{-1}$ is optimal, otherwise, $\tilde{Q}_n$ is an approximate inverse of G_{cm}.

Using $\tilde{Q}_n$ and E, norm bounds are derived for F and (I–F) using a procedure developed by Skogestad and Morari [110]. These bounds are sufficient conditions such that if $\bar{\sigma}(F) < c_F^*$ or $\bar{\sigma}(I-F) < c_{I-F}^*$ $\forall\omega$ then the filter, F, guarantees robust performance. If no filter can be found to meet these requirements, then a different measurement set should be examined.

This measurement selection/control design procedure can be summarized as follows:

1. Eliminate from consideration those measurement sets that are clearly infeasible. For instance, eliminate those with significant non-minimum phase characteristics.

2. For the remaining sets, compute the worst possible steady state closed-loop performance, $1/c_p^*$. If $c_p^* < 1$ eliminate measurement set.

3. Starting with the measurement set which yields the largest c_p^*, compute $\tilde{Q}_n$ and E.

4. Derive robust performance norm bounds on F and (I–F).

5. Design F to meet these bounds for each frequency. If no F can be found, change measurement sets and go to 3.

6. Implement robust inferential controller, F, $\tilde{Q}_n$, and E, on physical system.

6.3 Application of Robust Inferential Control to a Methanation Reactor

In this section, the robust control methods — measurement selection and control — presented in the previous section are applied to the concentration control of an experimental fixed bed reactor. All aspects of the controller design will be covered including the description of the model uncertainty, steady gain identification of the secondary measurement, robust measurement selection, design of the dynamic compensator, and the implementation of the controller on the reactor.

6.3.1 Control Problem

In the following experiments, we shall control the exit concentration and the maximum bed temperature. The control objective is to regulate these variables over a diverse set of operating conditions. These operating conditions are listed in Table 6.1 and include both partial and complete conversion of the reactant CO_2. Unlike the experiments presented in the previous chapter, partial conversions are obtained by manipulating the flow rate of the product recycle stream. For the partial conversion conditions, the maximum bed temperature occurs at the reactor exit whereas for full conversion a hot spot forms inside the reactor.

The manipulated variables are the recycle flow rate and the power supplied to a series of heaters at the inlet of the reactor. Increasing the recycle flow rate increases the space velocity in the reactor and makes the reactor behave (at least kinetically) more like a continuous stirred tank reactor [50]. Since the methanation reaction has positive order kinetics, the steady state CO_2 exit concentration increases for increasing recycle flow rates. On the other hand, the maximum bed temperature decreases for increasing flow rates. For the power supplied to the heaters, the situation is reversed. Increases in the power tend to increase the maximum temperature

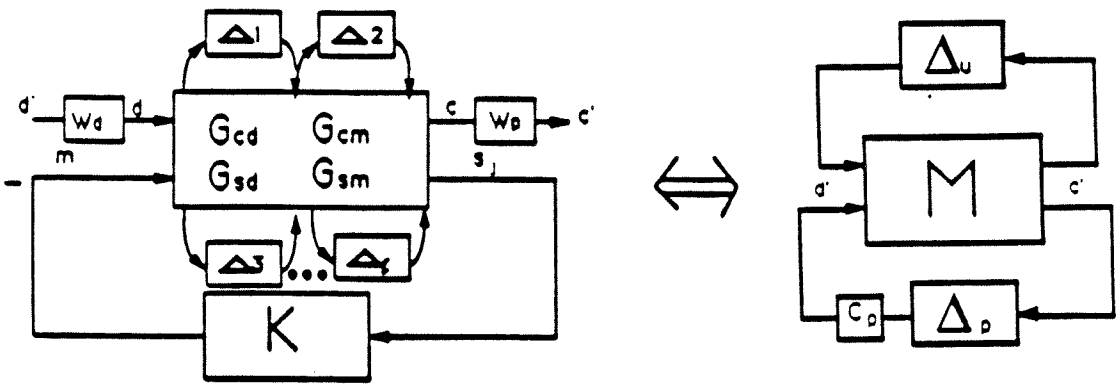

Figure 6.3: M-Δ structure

Variable	Amount	Units
Exit CO_2 Concentration	0-1.5	% vol
Exit Temperature	268-290	°C
Inlet Heating Power	0-30	% of 1800 w capacity
Recycle Flow rate	10-18	slpm
Inlet CO_2 Concentration	3.5	% vol
CO_2 Feed Flow rate	0.44	slpm
H_2 Feed Flow rate	1.96	slpm
N_2 Feed Flow rate	10	slpm
Dowtherm Temperature	253-257	°C

Table 6.1: Operating conditions for inferential control experiments

and decrease the exit reactant concentration.

We considered disturbances in the reactor wall temperature only. Physically, this temperature is equal to the temperature of a boiling Dowtherm fluid which surrounds the reactor. This fluid is contained inside a small pressure vessel. There are two reasons for changes in the Dowtherm temperature:

- pressure changes inside the Dowtherm container
- incomplete boiling of Dowtherm. By incomplete boiling, we mean that the Dowtherm is boiling in some sections of the reactor but not in others.

It will be shown that the steady state bed temperatures and exit concentration change significantly with small changes in the wall temperature. We did not account for disturbances in the feed concentration since for most operating conditions the bed temperatures are only weakly dependent on concentration. This is due in part to the zero order kinetics which are observed for partial conversions.

6.3.2 Steady State Uncertainty Description

In the present work, we consider two types of uncertainty (see Figure 6.2):

- additive uncertainty, Δ_{sm}, in the transfer function G_{sm} relating the manipulated variables (recycle flow rate and heating power) to the temperatures measurements
- output uncertainty, Δ_{sd} in the transfer function G_{sd} relating the disturbance (variation in reactor wall temperature) to the secondary (temperature) measurements

This uncertainty description is chosen for the following two reasons:

- Only uncertainty in G_{sm} can limit the closed-loop stability.

- Since the measurement selection issue is of primary interest at this point, only uncertainty related to the secondary measurements need be considered.

The uncertainty bounds are calculated in the following manner:

1. Static gains in the transfer functions matrices, G_{sm} and G_{sd}, are measured for a variety of different operating conditions.

2. For each element in these matrices, the static gain is bounded using the measured extremes.

3. The nominal model is computed by averaging these two extremes.

4. A bound on the uncertainty is obtained by measuring the distance from the model to either extreme.

This approach is relatively easy to implement experimentally since it is feasible to measure the static gains at different operating conditions. If the uncertainties in the different gains are uncorrelated (independent) with each other a very conservative control design can result. On the other hand if some correlation (dependence) is found, a tighter control design can be obtained.

Theoretically, all possible combinations of the temperatures measurements must be considered when selecting the measurement set. Since this can result in a very time-consuming search, it was decided to limit our search to one temperature measurement. The measurement selection problem is reduced to the selection of the single temperature measurement that will give the best closed-loop robust performance.

Uncertainty in G_{sm}

G_{sm} is a 1×2 transfer function composed of the elements:

- G_{T_xR} - The transfer function between the recycle and the selected temperature measurement, T_x

- G_{T_xH} - The transfer function between the heating power and the selected temperature measurement, T_x

The gains, G_{T_xR} and G_{T_xH}, are identified for different operating points within the selected window of operation (see Table 6.1). These gains are identified by exciting the system with a small step in either of the two manipulated variables while holding the other variable constant. Two sets of experiments are run:

1. changes in heating power holding flow constant — steps from 0–30% in the heating power for recycle flow rates of 10, 12, 15, and 17 slpm

2. changes in flow rate holding power supplied to heaters constant — steps from 10–12, 12–15, and 15–17 slpm for 15% power

For complete identification of the process, the system should also be excited with steps in recycle for different values in the heating power. This is not done in the present work since it is recognized that within the window of operation, the process has a stronger dependence on the recycle flow rate than on the inlet heating power.

The uncertainty in the function G_{sm} is taken as the individual uncertainty in each of the gains G_{T_xR} and G_{T_xH}. Mathematically,

$$G_{sm} = \hat{G}_{sm} + \Delta^*_{sm} \tag{6.21}$$

where

$$\hat{G}_{sm} = \begin{pmatrix} \hat{G}_{T_xR} \\ \hat{G}_{T_xH} \end{pmatrix} \tag{6.22}$$

$$\Delta^*_{sm} = W_{e_2} \Delta_{sm} W_{e_1} \tag{6.23}$$

$$W_{e_1} = \begin{pmatrix} W_{T_xR} & 0 \\ 0 & W_{T_xH} \end{pmatrix} \tag{6.24}$$

$$W_{e_2} = [1 \quad 1] \tag{6.25}$$

$$\Delta_{sm} = \begin{pmatrix} \Delta_1 & 0 \\ 0 & \Delta_2 \end{pmatrix} \tag{6.26}$$

$$\bar{\sigma}(\Delta_1) \leq 1 \qquad \bar{\sigma}(\Delta_2) \leq 1 \tag{6.27}$$

The nominal gains, $\hat{G}_{T_xR}$ and $\hat{G}_{T_xH}$, with their associated uncertainty bounds, W_{T_xR} and W_{T_xH}, are computed as explained above and are presented in Table 6.2.

As mentioned earlier, a tighter control design can result when there is a correlation between the uncertainty elements of G_{sm}. Specifically, if $\Delta_2 = \alpha\Delta_1$ for some constant scalar α then from Equations 6.21–6.27

$$G_{T_xH} = \alpha\frac{W_{T_xH}}{W_{T_xR}}\left(G_{T_xR} - \hat{G}_{T_xR}\right) + \hat{G}_{T_xH}$$

Based on the experimental results, it is possible to derive such a correlation for some of the thermocouples along the reactor bed. For example, it is observed that for thermocouples 13, 14, and 15, for decreasing recycle flow rate, G_{T_xR} increases while G_{T_xH} decreases indicating a negative correlation.

Uncertainty in G_{sd}

G_{sd} is a single-input single-output transfer function relating the reactor wall temperature to the selected measurement, T_x. In this case the uncertainty was measured by imposing steps of -3°C in Dowtherm temperature for 2 different operating points:

- 15% power 10 slpm recycle
- 15% power 17 slpm recycle

With these two experiments the system is excited at the extremes of the selected operation window. As is done for G_{sm}, the steady state gain and the uncertainty associated with that gain are computed from the results of these experiments. These results are listed in Table 6.2.

6.3.3 Measurement Selection

Based on the information in Table 6.2, we can select the thermocouple to be used in the inferential control scheme. Equation 6.28 gives the M matrix for the assumed uncertainty description. It is assumed for Equation 6.28 that G_{cm} and G_{sd} are invertible. Table 6.3 shows the values of μ for robust stability and the scalar c_p^* for robust performance for each of the available thermocouples along the reactor. The results of this table are displayed in Figure 6.4. It is observed that c_p^* increases as the selected thermocouple approaches thermocouple 13. After this thermocouple, a drastic deterioration in c_p^* occurs. This deterioration, can be explained by the strong nonlinearity associated with the formation of a hot spot at the exit of the reactor.

$$M = \left[\begin{array}{c|c} M_{11} & M_{12} \\ \hline M_{21} & M_{22} \end{array}\right] = \left[\begin{array}{cc|c} -W_{e_1}\tilde{Q}EW_{e_2} & -W_{e_1}\tilde{Q}EW_{sd} & W_{e_1}\tilde{Q}EG_{sd}W_d \\ 0 & 0 & G_{sd}W_d \\ \hline -W_pEW_{e_2} & -W_pEW_{sd} & 0 \end{array}\right] \tag{6.28}$$

Even though correlations are accounted for between the elements of G_{sm}, there is only a slight difference in c_p^* between the correlated and uncorrelated cases ($< 1\%$). This is due to the fact that the compensator Q weights the heat input much more heavily than the recycle flow rate. At steady state,

$$Q = \tilde{Q}E = \left[\begin{array}{c} G_{T_{13}R} \\ G_{T_{13}H} \end{array}\right] = \left[\begin{array}{c} 0.07 \\ 5 \end{array}\right]$$

Thermocouple	$\hat{G}_{T_xR}$	W_{T_xR}	$\hat{G}_{T_xH}$	W_{T_xH}	$\hat{G}_{T_xT_w}$	$W_{T_xT_w}$	Correlation between W_{T_xR} and W_{T_xH}
1	-2.875	0.125	1.2	0.12	2.16	0.5	-
2	-3.00	0.5	1.1	0.1	2.16	0.5	0
3	-3.08	0.08	0.96	0.08	2.33	0.33	0
4	-2.75	0.25	0.84	0.08	2.33	0.33	0
5	-2.58	0.08	0.7	0.06	2.5	0.195	0
6	-2.625	0.375	0.66	0.06	2.58	0.25	0
7	-2.75	0.25	0.64	0.04	2.91	0.08	0
8	-2.75	0.75	0.6	0.04	2.74	0.08	0
9	-2.75	0.75	0.56	0.04	2.74	0.08	0
10	-3.125	0.875	0.53	0.05	3.16	0.16	+
11	-3.25	0.75	0.5	0.02	3.16	0.16	+
12	-3.375	1.125	0.44	0.04	3.33	0.33	0
13	-3.125	0.875	0.36	0.04	3.5	0.16	-
14	-3.00	0.5	0.21	0.13	3.5	0.16	-
15	-2.75	0.25	0.13	0.17	3.33	0.33	-

Table 6.2: Average steady state gain with corresponding uncertainty for transfer functions G_{T_xR}, G_{T_xH}, and $G_{T_xT_w}$

Thermocouple	μ	c_p^*
1	0.910	4.25×10^{-2}
2	0.825	0.104
3	0.579	0.432
4	0.596	0.405
5	0.407	0.95
6	0.421	0.83
7	0.249	2.27
8	0.307	1.773
9	0.307	1.773
10	0.328	1.349
11	0.181	2.59
12	0.279	1.148
13	0.131	2.971
14	0.584	0.538
15	0.831	0.122

Table 6.3: Steady state robust stability and robust performance measures, μ and c_p^* for various thermocouples

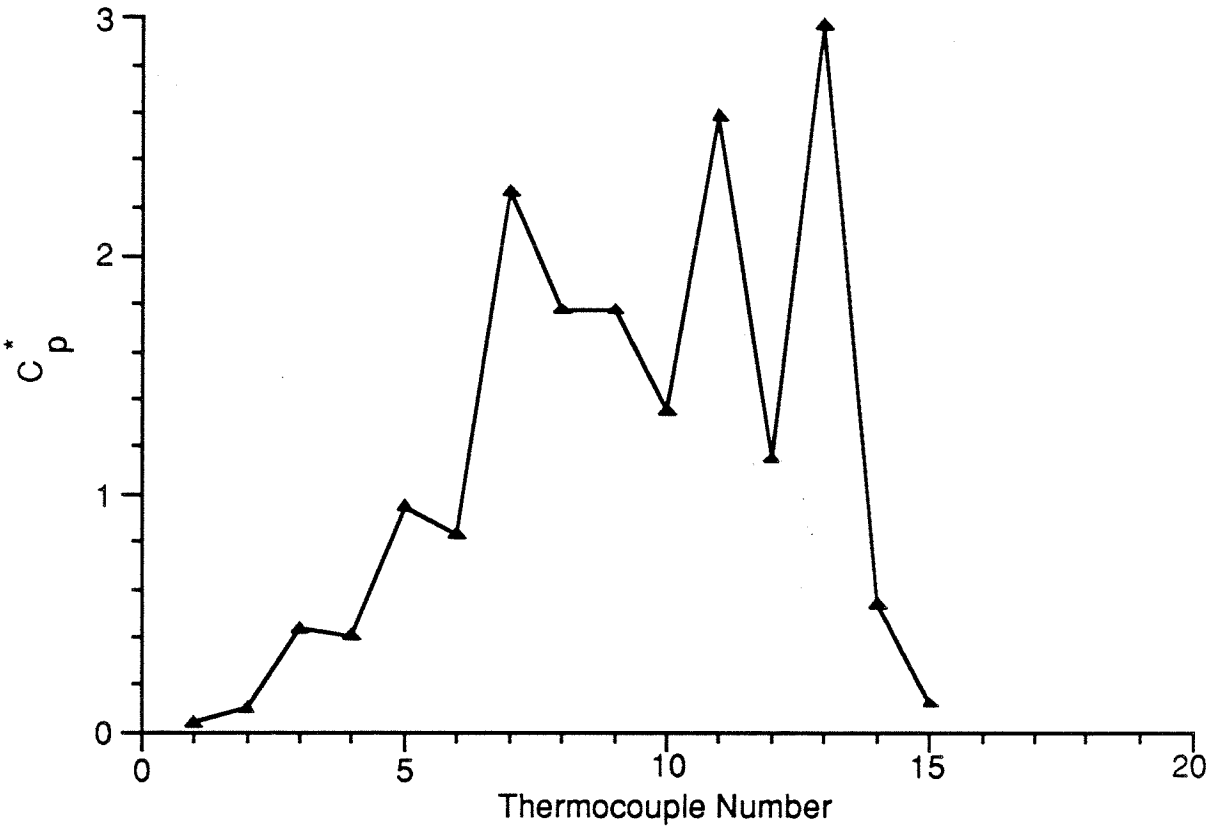

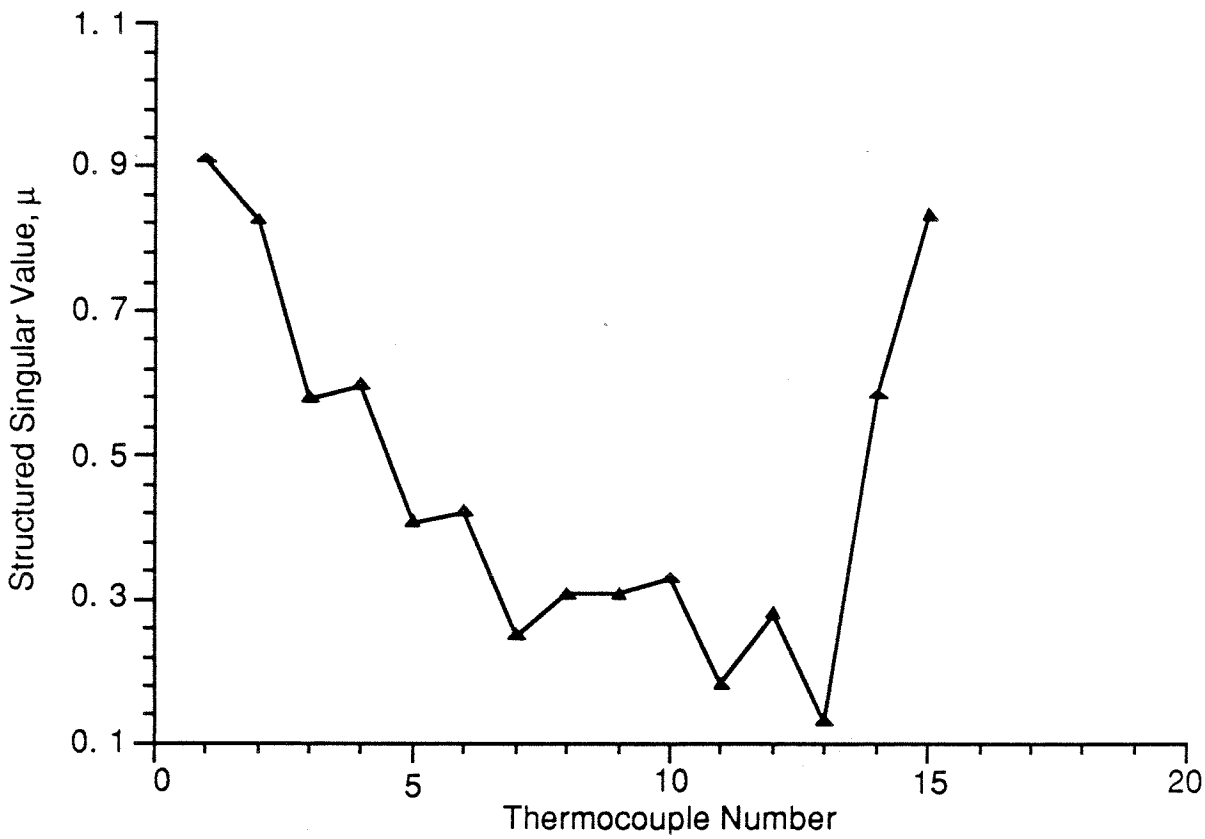

Figure 6.4: μ and c_p^* as a function of thermocouple position

Therefore, the uncertainty associated with $G_{T_{13}H}$ dominates. For comparison, c_p^* was computed for a different nominal operating point (12 slpm recycle and 15% power). In this case, the product

$$\tilde{Q}E = \begin{bmatrix} 0.5 \\ 2 \end{bmatrix}$$

and correlations in G_{sm} were found to drastically lower the value of c_p^*.

6.3.4 Dynamic Compensator Design

Using thermocouple 13 and the nominal operating conditions of 15 slpm recycle and 15% power, transfer functions are identified for the nine elements shown in Table 6.4. These transfer functions relate the controlled and measured variables to the manipulated and disturbance variables. From the input-output time histories, it was recognized that every transfer function can be adequately modelled as a first order system with dead time. The sampling time for all experiments is 40 seconds.

Using these models, the estimator is chosen as

$$E = G_{cd}G_{sd}^{-1} = \begin{bmatrix} -0.3437\frac{1-0.8528z^{-1}}{1-0.2125z^{-1}} \\ 0.8513\frac{1-0.8528z^{-1}}{1-0.8612z^{-1}} \end{bmatrix} \tag{6.29}$$

While the transfer function $G_{sd}^{-1} = G_{T_{13}T_w}^{-1}$ is predictive and therefore not realizable, E is realizable owing to the time delay in G_{cd}.

Ideally, the compensator, $\tilde{Q}_n$, should invert G_{cm}. However, since all four elements of G_{cm} contain time delays, one can only approximate this inverse. While H_2 or H_∞ optimal control theory can be used to do this inversion, we relied instead on the IMC factorization approach presented in Holt and Morari [54]. Using this factorization,

the matrix G_{cm} is divided into an all-pass part and a minimum phase part.

$$G_{cm} = G^A_{cm} G^M_{cm} \tag{6.30}$$

The all-pass matrix, G^A_{cm}, is a diagonal matrix containing only dead time elements. These dead times are the minimum dead times necessary to make $(G^M_{cm})^{-1}$ non-predictive. Using this factorization,

$$G^A_{cm} = \begin{bmatrix} z^{-13} & 0 \\ 0 & z^{-4} \end{bmatrix} \tag{6.31}$$

$$\tilde{Q}_n = (G^M_{cm})^{-1} = \begin{bmatrix} \frac{0.0186z^{-10}}{1-0.919z^{-1}} & \frac{0.0083z^{-4}}{1-0.4444z^{-1}} \\ \frac{0.444}{1-0.8431z^{-1}} & \frac{0.0901}{1-0.3947z^{-1}} \end{bmatrix} \frac{1}{D} \tag{6.32}$$

$$D = \frac{0.001675z^{-6}}{(1-0.3947z^{-1})(1-0.919z^{-1})} - \frac{0.00368}{(1-0.8431z^{-1})(1-0.4444z^{-1})} \tag{6.33}$$

The zeros of D are inside the unit circle, and, therefore, $\tilde{Q}_n$ is stable. While this choice of $\tilde{Q}_n$ leads to a sub-optimal controller, the two controlled variables are decoupled.

Finally, $\tilde{Q}_n$ is augmented with a robustness filter of the form

$$F = \frac{(1-e^{-T_s/\lambda})z}{(z-e^{-T_s/\lambda})} I \tag{6.34}$$

By adjusting λ different controllers can be designed each with a different speed of response.

6.3.5 Closed-Loop Experiments

In a formal robust control design, the filter F is based on a description of the model uncertainty. However, in the present work, we opted to tune the filter on-line.

In this manner, we can determine the minimum time constant necessary to maintain stability. Since this time constant is a function of the operating conditions, we can determine the operating conditions for which the controller is most sensitive to plant-model mismatch. Furthermore, we can also test the efficiency of the inferential controller for maintaining exit concentration.

To meet these goals, we studied the disturbance rejection problem for different operating points in the system. These experiments are conducted in the following manner:

1. The pressure in the Dowtherm container is increased resulting in the slow increase in wall temperature.

2. The controller is activated at a predefined operating point.

3. Pressure inside Dowtherm container is released causing a step disturbance in wall temperature.

4. The manipulated and controlled variables are monitored and stability of the closed-loop determined.

The operating conditions for which the experiments are performed and the resulting closed-loop stability are presented in Table 6.5. The time histories of the manipulated variables for these four experiments are shown in Figures 6.5–6.8. As is apparent for these figures, it is more difficult to stabilize the system for lower recycle flow rates. For these operating condition, the system appears to be most sensitive to model mismatch. By increasing the filter time constant, we are able to maintain stability at low flow rates, but at the expense of a significantly reduced speed of response (Experiment 1).

The time history of the controlled variables associated with Experiment 3 are presented in Figure 6.9. Also shown in this figure are the setpoints and the expected deviation for open-loop conditions. It is apparent from these figures that the

	R	H	T_w
C_o	$\frac{0.0901Z^{-9}}{1-0.3947Z^{-1}}$	$\frac{-0.0083Z^{-13}}{1-0.4444Z^{-1}}$	$\frac{-0.1771Z^{-2}}{1-0.2125Z^{-1}}$
T_{max}	$\frac{-0.444}{1-0.8431Z^{-1}}$	$\frac{0.0186Z^{-10}}{1-0.9190Z^{-1}}$	$\frac{0.4386Z^{-2}}{1-0.8612Z^{-1}}$
T_{13}	$\frac{-0.547}{1-0.8301Z^{-1}}$	$\frac{0.0195Z^{-10}}{1-0.9430Z^{-1}}$	$\frac{0.552Z^{-2}}{1-0.8528Z^{-1}}$

Table 6.4: Transfer function models based on nominal operating conditions

Experiment	Initial Operating Conditions	Robustness Filter Time Constant	Magnitude of Disturbance	Stability Results
1	15% Power 11 slpm Recycle 256°C Wall Temp.	140 sec	-1°C	Stable
2	15% Power 11 slpm Recycle 256°C Wall Temp.	38 sec	-1°C	Unstable
3	5% Power 15 slpm Recycle 257°C Wall Temp.	38 sec	-3°C	Stable
4	15% Power 17 slpm Recycle 256°C Wall Temp.	38 sec	-1°C	Stable

Table 6.5: Closed-loop inferential control experiments

inferential control scheme rejects the disturbance in wall temperature although with significant steady state offset.

6.4 Conclusions

In conclusion, a robust inferential controller has been successfully implemented on an experimental fixed bed methanation reactor. This controller uses a robust measurement selection technique to determine which thermocouple or set of thermocouples gives the smallest potential steady state error due to model mismatch. Once the measurements are selected, the controller is designed based on Internal Model Control theory. By design, the controller contains a single adjustable tuning parameter. This parameter is used to achieve robustness in the presence of plant-model mismatch.

When this control methodology is applied to an experimental reactor, some interesting conclusions can be drawn:

- For the operating conditions chosen, the measurement selected for use in inferential control is the one with smallest associated uncertainty, Δ_{T_xH}. This corresponds to the thermocouple which is just upstream from the hot spot.

- For the selected nominal operating conditions, correlation between uncertainty blocks, Δ_{T_xH} and Δ_{T_xR}, did not significantly improve the worst possible steady state performance, c_p^*. This is due in part to the large sensitivity of the controller to changes in G_{T_xH}. As demonstrated, this does not hold for other operating points.

- Using a controller designed from Internal Model Control Theory, the system is identified for regions which are highly sensitive to modelling mismatch. The methanation reactor is most sensitive to mismatch at lower total flow rates. Under these conditions, a hot spot forms inside the reactor. If it is desired to

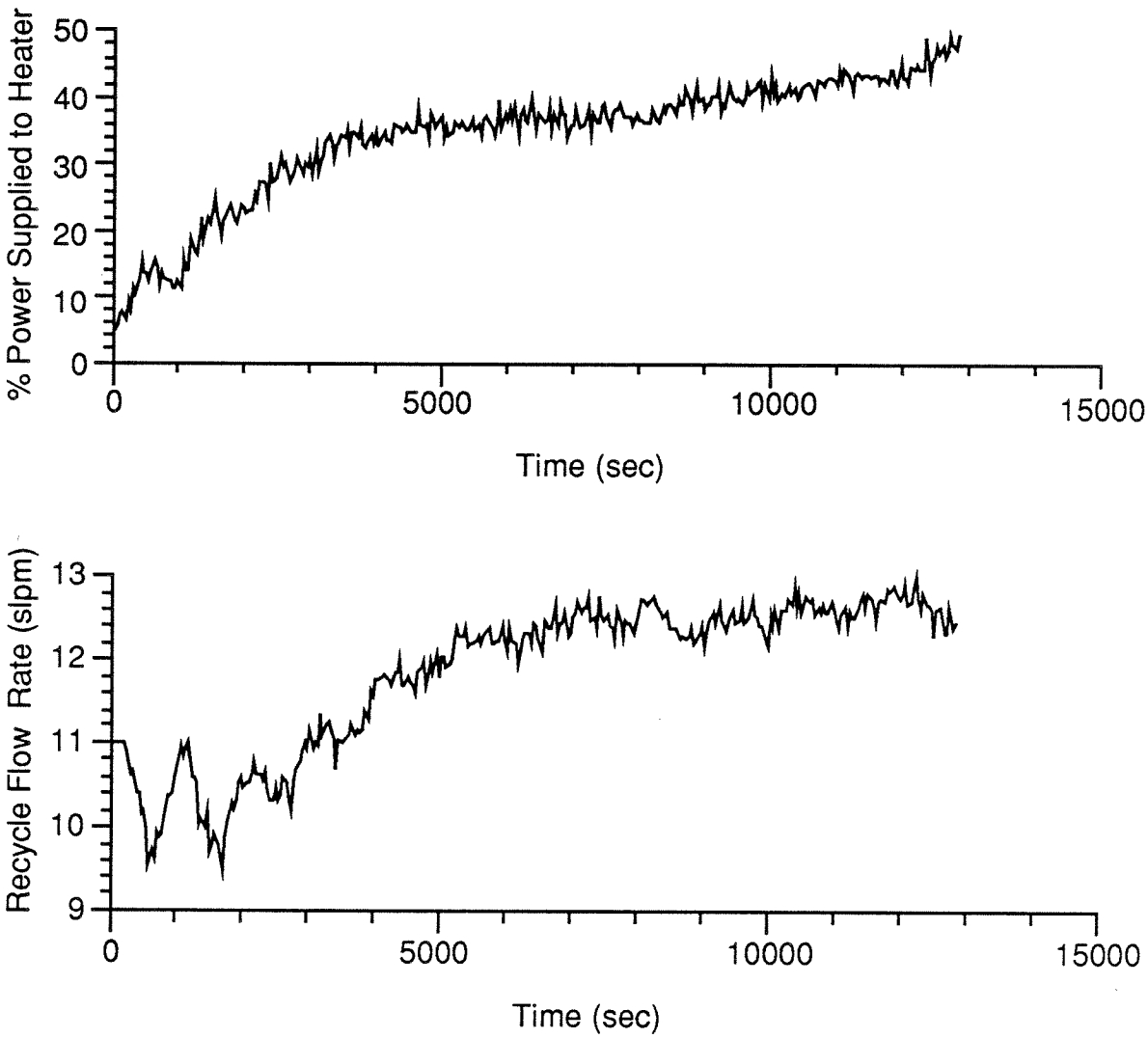

Figure 6.5: Response of manipulated variables to step decrease in wall temperature — Experiment 1

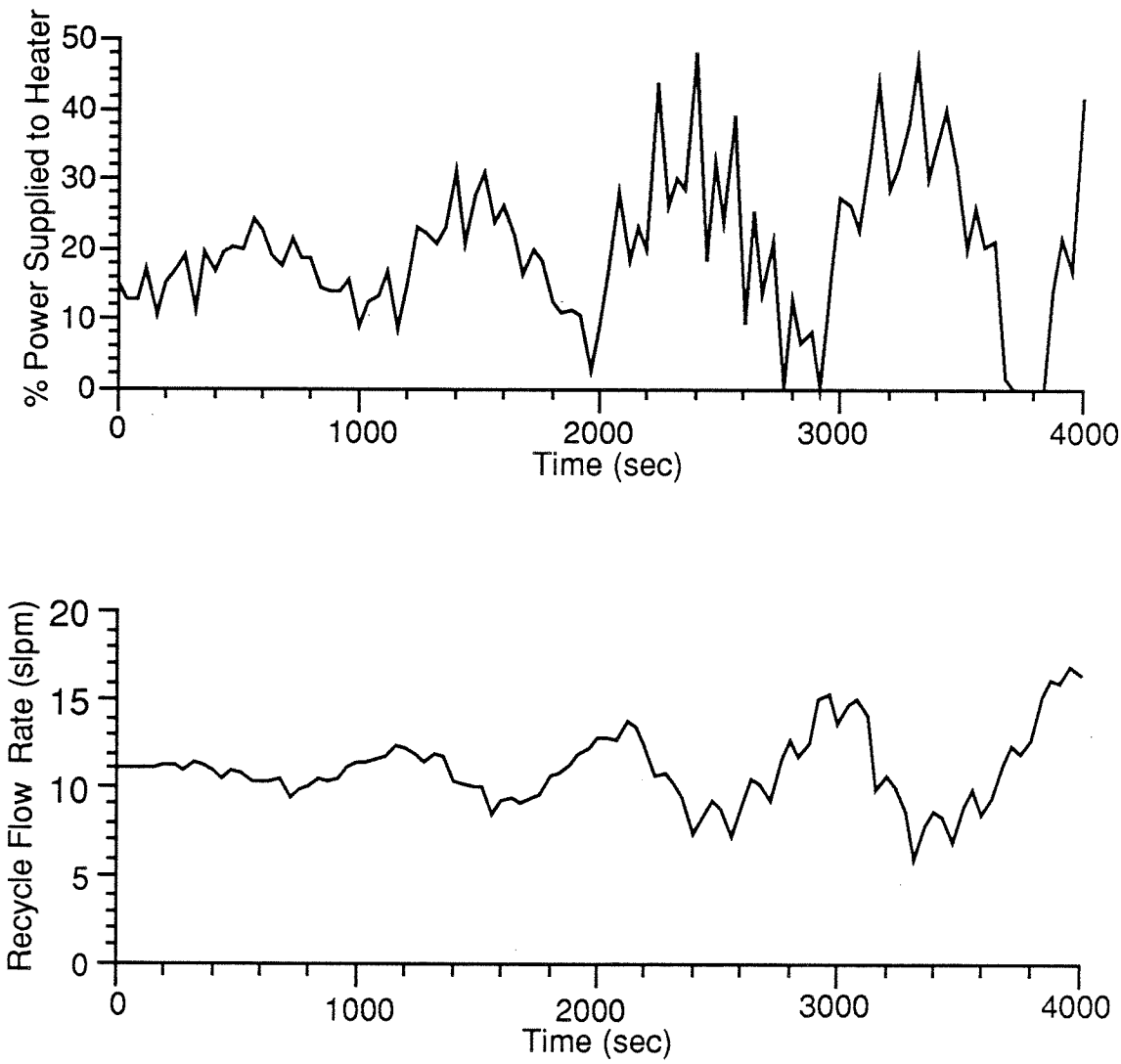

Figure 6.6: Response of manipulated variables to step decrease in wall temperature — Experiment 2

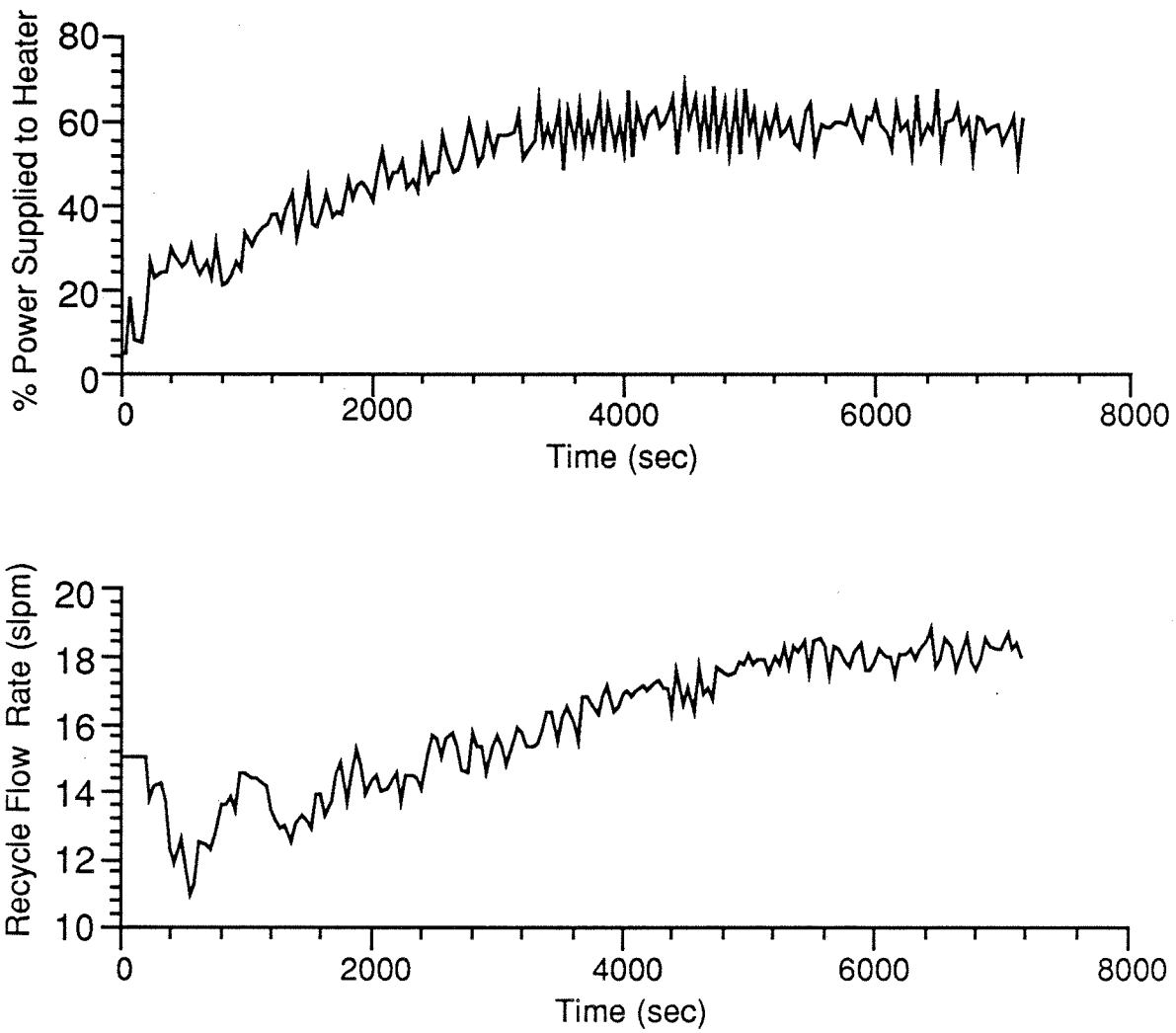

Figure 6.7: Response of manipulated variables to step decrease in wall temperature — Experiment 3

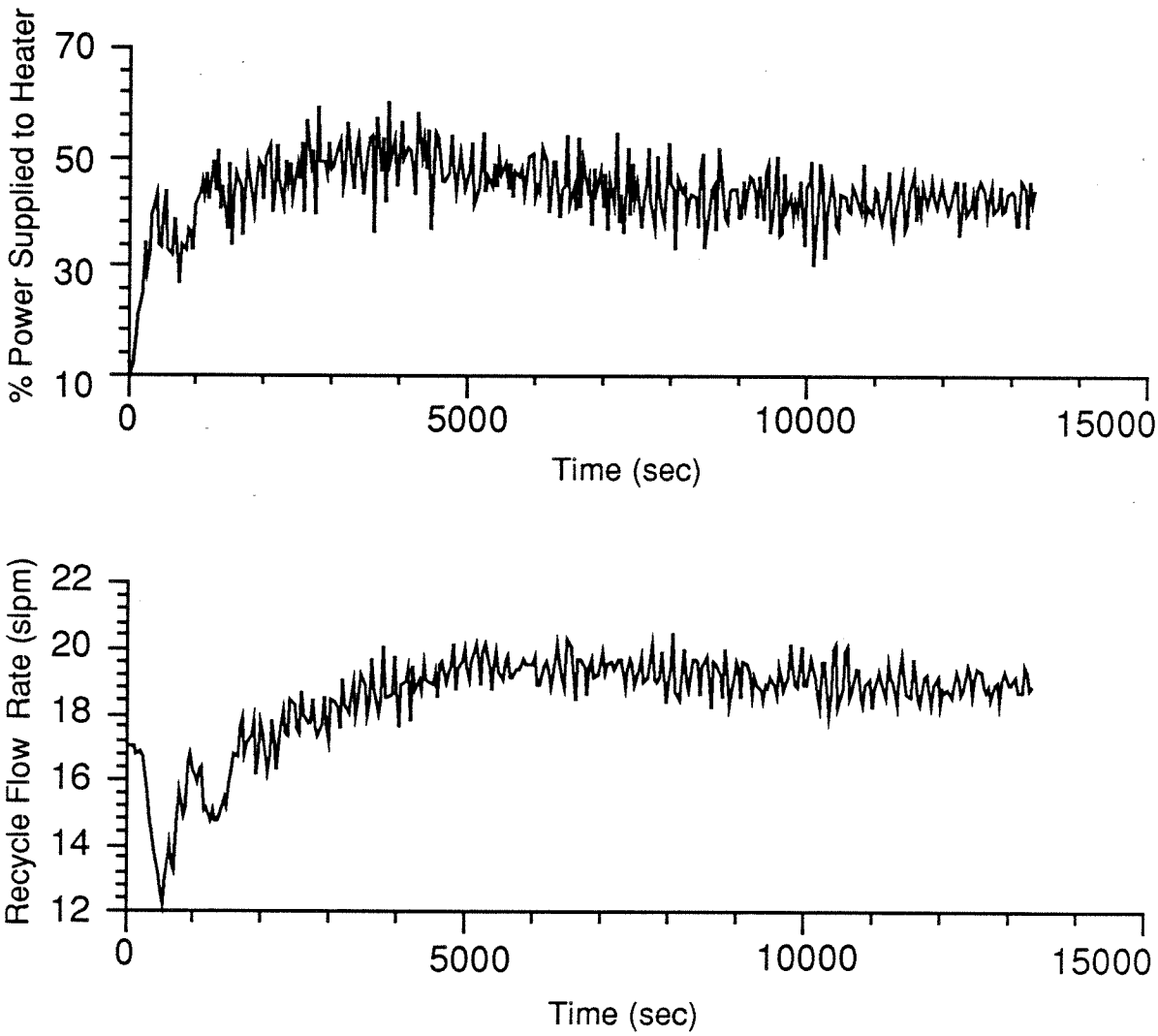

Figure 6.8: Response of manipulated variables to step decrease in wall temperature — Experiment 4

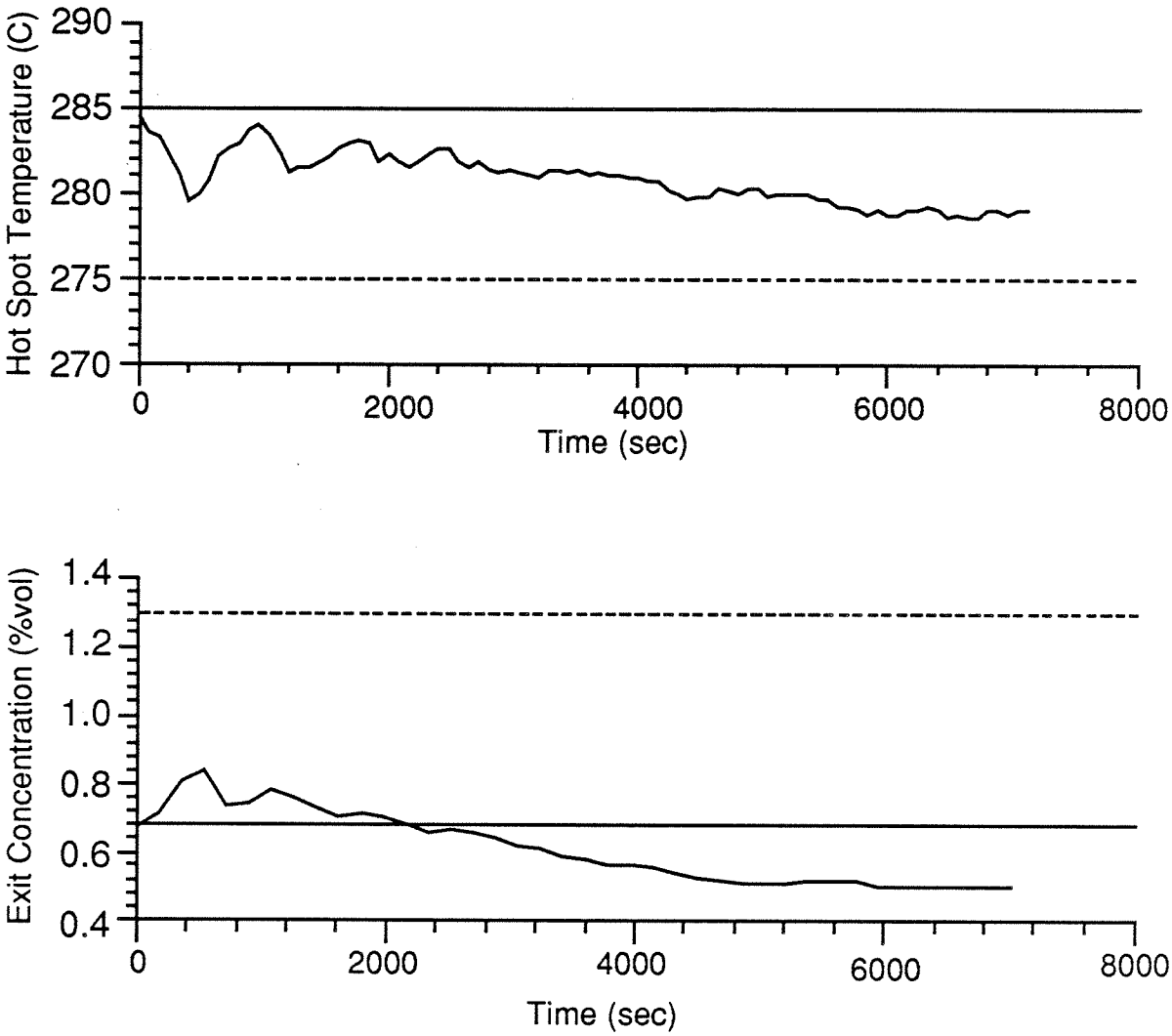

Figure 6.9: Response of controlled variables to step decrease in wall temperature — Experiment 3. The straight solid line is the setpoint and the dashed line is the expected open loop offset.

operate the system near these operating points, it is important to get accurate information on the system dynamics in this region.

- Because of the inherent system nonlinearities, the inferential controller produces a significant steady state offset in the controlled variables. This offset even occurs for the nominal operating condition around which the system was originally identified. For this reason, future efforts in controller design should concentrate on robust nonlinear or adaptive control schemes.

Chapter 7

Conclusions and Future Research

7.1 Conclusions

The following conclusions can be drawn from this research:

- A fully automated fixed bed chemical reactor is constructed to examine the applicability of recently developed control theory, especially robust control theory, to a chemical process which has been traditionally difficult to control. Due to its modular design, this system is highly flexible and can adapt to several different operating configurations with the potential for either mass or energy recycle. It incorporates several features often found in industrial reactors including: a feed-effluent heat exchanger, a recycle stream, an axial thermowell, and a reactor cooling jacket.

- The reaction under study is the methanation of CO_2. This reaction is chosen for its industrial importance and many desirable properties. These properties include a large heat and free energy of reaction, practically non-existent side reactions, and well documented kinetics. Unfortunately, these same properties limit the scope of the control studies by removing any selectivity issues.

- Several different schemes are proposed for the control of this reactor of which two are further investigated.

    1. The reactor hot spot temperature is regulated using the flow rate of an inert gas. Setpoint changes as well as changes in the flow rates of the reactants are studied.

    2. The outlet concentration and temperature are controlled by manipulating the inlet temperature and the flow rate of the recycle stream. In this configuration, the controlled variables must be inferred from internal reactor temperatures. Disturbances in the reactor wall temperature are examined.

- Mathematical models for the feed-effluent heat exchanger and the methanation reactor are developed. Both of these models grew out of three needs: to explain phenomena which could not be quantified using standard chemical engineering design calculations, to predict the system output for new operating conditions, and to better understand the significance of various physical interactions which occur in the system. The complexity of the model depends on the needs of the designer. In the case of the feed-effluent heat exchanger, the model simply explains the steady state relationship between heat transfer in the heat exchanger and heat loss to the environment; in the case of the reactor, the model explains the complex dynamical relationships between heat and mass transport in the presence of an exothermic chemical reaction for a two phase reactor. This reactor model predicts the effects of changes in various operating parameters, such as the inlet temperature and flow rate, on the reactor profiles. Although not explicitly done in this thesis, this model can be used to estimate the transfer functions between various manipulated and controlled variables.

- The parameters used in the reactor model are estimated from a series of steady state experiments. The parameter estimation is performed using a divide and conquer procedure in which specific experiments are run to identify small subsets of the general parameter set. Once all parameters have been identified, the model is compared to new experimental data obtained from more general experiments, and the most sensitive parameters, the pre-exponential rate constant and the heat transfer coefficient between the gas and the cooling jacket wall, are re-estimated. The final model is in good agreement with the temperature profiles obtained experimentally. This model correctly predicts the size, shape, and position of the hot spot inside the reactor for various operating conditions.

- The mathematical model of the reactor is reduced to a set of ordinary differential equations using finite difference methods. This model is able to describe the sharp gradients found in the concentration profile and for this reason is preferred to a similar model reduced using orthogonal collocation. To optimize the speed and storage requirements of the finite difference scheme and still retain a high degree of accuracy, a variable mesh spacing is allowed and the model is rewritten so that the Jacobian is banded.

- A new black-box method is proposed for identifying a single-input single-output non-parametric frequency domain model from a given set of input-output time data. As part of the identification procedure, this method automatically computes a bound on the amount of uncertainty associated with the model. The identification proceeds in three steps.

    1. An operating window is defined over which the manipulated and controlled variables are allowed to vary.

    2. A number of local identification experiments are conducted at various points in this operating window.

    3. The set of local models is bounded, and from this bound, a global model with its associated uncertainty is defined.

  This new method uses spectral analysis theory to identify the local models and a regions-mapping method to bound them.

- To test the integrity of this method, it is used to identify a mathematical model representing a simple nonlinear system. The uncertainty bound obtained is compared to the true bound and to the uncertainty bounds predicted by two different methods. The bounds obtained from these other methods are inaccurate because these methods do not properly capture the nonlinearity associated

with changes in the operating conditions. Since the regions-mapping approach overcomes this problem, its bound is nearly identical to the true bound.

- The identification of the fixed bed reactor is performed. The transfer function sought is the change in hot spot temperature to a change in inert gas, N_2, flow rate. The operating range for the inert gas flow rate is divided into three parts, and a series of local identification experiments is performed for each part using a pseudo random binary signal as the input signal. Using the new identification technique, a global model and uncertainty bound are obtained from which a robust controller is designed. This controller contains one adjustable parameter — the time constant of a robustness filter, λ. Using robust control theory, it is predicted that the closed-loop system will be stable for all operating conditions if $\lambda \geq 164$ sec and unstable for at least one operating condition otherwise. This agreed with experimental results which showed the closed-loop system to be stable for $\lambda \geq 164$ sec, but unstable for $\lambda \leq 47$ sec. For λ between these values, responses resembling limit cycles are obtained.

- A robust inferential controller has been successfully implemented on an experimental fixed bed methanation reactor. This controller uses a robust measurement selection technique to determine which thermocouple or set of thermocouples gives the smallest potential steady state error due to model mismatch. Once the measurements are selected, a controller is designed based on Internal Model Control theory. By design, this controller contains a single adjustable tuning parameter. This parameter is used to achieve robustness in the presence of plant-model mismatch.

- For the operating conditions chosen, the measurement selected for use in inferential control is the one with smallest associated uncertainty in the transfer function relating the measured variable to the heat input. This corresponds

to a thermocouple which is just upstream from the hot spot. Since there is a significant increase in uncertainty near the hot spot, it is important to know the position of the hot spot in the reactor.

- Using closed-loop experiments, the system is identified for regions which are highly sensitive to modelling mismatch. The methanation reactor is most sensitive to mismatch at lower total flow rates. Under these conditions, a hot spot forms inside the reactor. If it is desired to operate the system near these operating points, it is important to get accurate information on the system dynamics in this region.

7.2 Future Research

Future research on this reactor should concentrate in two areas.

1. The practical implementation of existing robust control methods to new, and potentially more interesting, operating conditions should be investigated. These new operating conditions can be obtained by

   Reducing Cooling Jacket Temperature As pointed out in Chapter 4, the current operating regime admits only a single highly reactive steady state. This is due in part to the modulation of the catalyst bed temperature by the cooling jacket. Because of the results reported by other researchers [140], it is believed that by lowering the cooling jacket temperature, a more interesting operating region containing multiple steady states will be reached. This new operating region presents additional control problems including the operation of the system at an unstable operating point, and the rejection of large and potentially destabilizing disturbances. Practically, this requires the replacement of the current cooling medium, Dowtherm A, by a fluid with a much lower boiling point.

Modifying the Catalyst Loading A potentially simpler way to obtain the same results as above is to thin the catalyst with more inert material. This will also help to reduce the steep gradients found in the concentration and temperature profiles.

Operating with Energy Recycle By operating the reactor in conjunction with the feed-effluent heat exchanger, the system may admit multiple steady states.

Using a More Precise Concentration Measurement As pointed out in Richards and Schnelle [102], one of the latest trends in industrial control is the move toward continuous on-line gas analyzers. Use of such an analyzer in this reactor would remove the need for inferential control of the outlet concentration and effectively decouple the temperature measurements from the concentration measurements allowing for more advanced control strategies.

Using a Different Reaction As a long range goal, the methanation reaction should be replaced by a more complex set of gas phase reactions. By choosing a chemical system with multiple reactions, a number of new control objectives arise including optimization of the product yield, reactant conversion, or reaction selectivity. A number of well documented series-parallel reactions including the partial oxidation of xylene to phthalic anhydride, the partial oxidation of n-butane to maleic acid, the partial oxidation of methanol to formaldehyde, and the hydrogenolysis of butane fit in this category.

2. Practical methods for the identification of uncertain models should be further developed. Areas of practical interest include:

Parametric Identification Two questions are pertinent. The most obvious question is "What is the uncertainty associated with the parameters of the model?" While the answer to this question may appear to be straightforward, it is complicated by correlations which may exist between various model parameters. To have the least conservative controller design, these correlations must be accounted for. The second and more fundamental question is "Which model captures uncertainty in the least conservative manner?"

Multiple-Input Multiple-Output Identification While the single-input single-output identification techniques presented in Chapter 5 can be extended to the element by element identification of a multiple-input multiple-output system, the uncertainty correlation between the elements is unaccounted for. It is the identification of these correlations which brings the largest advances in robust control, and hence more intuitive ways of identifying this correlation is needed.

Nonlinear Modelling In addition to the identification of a linear model, a more ambitious goal is the identification of an uncertain nonlinear model. Such a model could make use of recent advances in the robust control of a nonlinear system [23,94].

Bibliography

[1] Milton Abramowitz and Irene A. Stegun. *Handbook of Mathematical Functions.* Dover Publications, 1964.

[2] K.J. Astrom and T. Hagglund. Automatic tuning of simple regulators. In *Proceeding from IFAC 9th World Congress*, pages 1867–1872, 1984.

[3] K.J. Astrom and T. Hagglund. Automatic tuning of simple regulators with specifications on phase and amplitude margins. *Automatica*, 20:645–651, 1984.

[4] M.S. Bartlett. Smoothing periodograms from time-series with continuous spectra. *Nature (London)*, 161:686–687, 1948.

[5] A. Bhattacharya and B. Joseph. Simulation of fixed-bed gas-solid reactors using an adaptive-spline collocation method. *Computers and Chemical Engineering*, 12:351–353, 1988.

[6] R. Byron Bird, Warren E. Stewart, and Edwin N. Lightfoot. *Transport Phenomena.* John Wiley and Sons, 1960.

[7] R.B. Blackman and J.W. Tukey. *The Measurement of Power Spectra.* Dover Publications, 1959.

[8] D. Bonvin, R.G. Rinker, and D.A. Mellichamp. On controlling an autothermal fixed bed reactor at an unstable state — II: Discrimination among rival models

to achieve suitable internal structure. *Chemical Engineering Science*, 38:245–255, 1983.

[9] D. Bonvin, R.G. Rinker, and D.A. Mellichamp. On controlling an autothermal fixed-bed reactor at an unstable state — III Model reduction and control strategies which avoid state estimation. *Chemical Engineering Science*, 38:607–618, 1983.

[10] D. Bonvin, R.G. Rinker, and D.A. Mellichamp. On controlling an autothermal fixed-bed reactor at an unstable state — I: Steady state and dynamic modeling. *Chemical Engineering Science*, 38:233–244, 1983.

[11] David R. Brillinger. *Time Series - Data Analysis and Theory.* Holt, Rinehart and Winston, 1975.

[12] Coleman Brosilow and Martin Tong. Inferential control of processes: part II The structure and dynamics of inferential control systems. *AIChE Journal*, 24:492–500, 1978.

[13] B. Bussemeier, C.D. Frohning, and B. Cornils. Lower olefins via Fishcer-Tropsch. *Hydrocarbon Processing*, 105–112, 1976.

[14] M. Caracotsios and W.E. Stewart. Sensitivity analysis of initial value problems with mixed ODE's and algebraic equations. *Comput. and Chem. Engng*, 9:359–365, 1985.

[15] G.F. Carey and B.A. Finlayson. Orthogonal collocation of finite elements. *Chemical Engineering Science*, 30:587–596, 1975.

[16] G. Clifford Carter and Albert H. Nuttall. Analysis of a generalised framework for spectral estimation - part 1: The technique and its mean value. *IEE Proceedings Part F*, 130:239–241, 1983.

[17] David N. Chiang. *CO Methanation over a Nickel Catalyst.* Master's thesis, California Institute of Technology, 1983.

[18] Richard W. Chylla and Ali Cinar. Experimental control of a multi-bed tubular autothermal reactor. In *Proceeding of the American Control Conference*, 1987.

[19] K. Clement and S. Bay Jorgensen. Experimental investigation of a fixed bed chemical reactor control system designed by the Direct Nyquist Array method. *IFAC Control Science and Technology*, 1981.

[20] P.J. Daniell. Discussion following "On the theoretical specification and sampling properties of autocorrelated time series" by M.S. Bartlett. *Journal of the Royal Statistical Society*, 8:88, 1946.

[21] A.P. De Wasch and Froment G.F. A two dimensional heterogeneous model for fixed bed catalytic reactors. *Chemical Engineering Science*, 26:629–634, 1971.

[22] M.M. Denn. Chemical reaction engineering — optimization, control, and stability. *Industrial and Engineering Chemistry*, 61:46–50, 1969.

[23] Francis J. Doyle, Andrew K. Packard, and Manfred Morari. Robust controller design for a nonlinear CSTR. *Chemical Engineering Science*, 44, 1989.

[24] J.C. Doyle. Analysis of feedback systems with structured uncertainties. *IEE Proceedings Part D*, 129:242–250, 1982.

[25] J.C. Doyle. Lecture notes, ONR/Honeywell workshop on advances in multivariable control. *Minneapolis, MN*, 1984.

[26] J.C. Doyle. Robustness of multiloop linear feedback systems. *Proceedings of the IEEE Conference on Decision and Control*, 1978.

[27] J.C. Doyle and G. Stein. Multivariable feedback design: concepts for a classical/modern synthesis. *IEEE Trans. Automat. Contr.*, AC-26:4–16, 1981.

[28] B.A. Finlayson. *The Method of Weighted Residuals and Variational Principles.* Academic Press, 1972.

[29] B.A Finlayson. *Nonlinear Analysis in Chemical Engineering.* McGraw-Hill, 1980.

[30] Alan S. Foss, John M. Edmunds, and Basil Kouvaritakis. Multivariable control system for two bed reactors by the characteristic locus method. *Industrial and Engineering Chemistry Fundamentals*, 19:109–117, 1980.

[31] Alan S. Foust, Leonard A. Wenzel, Curtis W. Clump, Maus Louis, and L. Bryce Andersen. *Principles of Unit Operations.* John Wiley and Sons, 1960.

[32] Bruce A. Francis, J. William Helton, and George Zames. H^{∞}- optimal feedback controllers for linear multivariable systems. *IEEE Transactions on Automatic Control*, AC-29:888–900, 1984.

[33] K.B. Froment, G.F. Bischoff. *Chemical Reactor Analysis and Design.* John Wiley and Sons, New York, 1979.

[34] C.E. Garcia and M. Morari. Internal Model Control — 1 A unifying review and some new results. *Industrial Engineering Chemistry Process Design Development*, 21:308–323, 1982.

[35] L. Gardini, A. Servida, M. Morbidelli, and S. Carra. Use of orthogonal collocation on finite elements with moving boundaries for fixed-bed catalytic reactor simulation. *Computers and Chemical Engineering*, 9:1–17, 1985.

[36] W.A. Gardner. *Statistical Spectral Analysis - A Nonprobabilistic Theory.* Prentice-Hall, 1988.

[37] O. Garza-Garza and M.P. Dudukovic. Solution of models for gas-solid non-catalytic reactions by orthogonal collocation on finite elements with moving boundary. *Computers and Chemical Engineering*, 6:131–139, 1982.

[38] K.R. Godfrey. Theory of the correlation method of dynamics analysis and its applications. *Measurement Control*, 2:65, 1969.

[39] L. Goldschmidt, L. Hallager, and S.B. Jorgensen. Dynamics and control of an adiabatic fixed bed reactor with varying catalyst activity. *IFAC Control of Distillation*, 1986.

[40] N.R. Goodman. Statistical analysis based on a certain multivariate complex Gaussian distribution (an introduction). *Ann. Math. Statist.*, 34:152–177, 1963.

[41] L. Hallager and S. Bay Jorgensen. Experimental investigation of self-tuning control of a gas phase fixed bed catalytic reactor with multiple inputs. *IFAC Control Science and Technology*, 1981.

[42] E.J. Hannan. *Multiple Time Series.* John Wiley and Sons, 1970.

[43] Knud Waede Hansen and Sten Bay Jorgensen. Dynamic modelling of a gas phase catalytic fixed-bed reactor — II Results from dynamic experiments. *Chemical Engineering Science*, 31:587–598, 1976.

[44] Knud Waede Hansen and Sten Bay Jorgensen. Dynamic modelling of a gas phase catalytic fixed-bed reactor — I: Experimental apparatus and determination of reaction kinetics. *Chemical Engineering Science*, 31, 1976.

[45] Knud Waede Hansen and Sten Bay Jorgensen. Dynamic modelling of a gas phase catalytic fixed-bed reactor — III Identification using binary pulse sequence test signals. *Chemical Engineering Science*, 31, 1976.

[46] T.J. Harris, J.F. MacGregor, and J.D. Wright. An application of self-tuning regulators to catalytic reactor control. In *Joint Automatic Control Conference*, 1978.

[47] T.J. Harris, J.F. MacGregor, and J.D. Wright. Optimal sensor location with an application to a packed bed tubular reactor. *AIChE Journal*, 26, 1980.

[48] A.J. Helmicki, C.A. Jacobson, and C.N. Nett. H_∞ identification of stable lsi systems: a scheme with direct application to controller design. In *Proceedings from the American Control Conference*, pages 1428–1434, 1989.

[49] Joris Herten and Gilbert F. Froment. Kinetics and product distribution in oxidatation of o-xylene. *Industrial Engineering Chemistry Process Design and Development*, 7:516–526, 1968.

[50] Charles J. Hill. *Chemical Engineering Kinetics and Reactor Design.* John Wiley and Sons, 1977.

[51] Sa Van Ho and Peter Harriot. The kinetics of methanation on nickel catalysts. *Journal of Catalysis 64*, 1980.

[52] J.A. Hoiberg, B.C. Lyche, and A.S. Foss. Experimental evaluation of dynamic models for a fixed bed catalytic reactor. *AlChE Journal*, 17, 1971.

[53] B. Holt and et al. CONSYD — integrated software for computer-aided control system design and analysis. *Computers and Chemical Engineering*, 11:187–203, 1987.

[54] B.R. Holt and M. Morari. Design of resilient processing plants — V The effect of deadtime on dynamic resilience. *Chemical Engineering Science*, 40:1229–1237, 1985a.

[55] I.M. Horowitz. History of personal involvement in feedback control theory. *IEEE Control Systems Magazine*, 1984.

[56] Gwilym M. Jenkins and Donald G. Watts. *Spectral Analysis and Its Applications.* Holden-Day, 1968.

[57] O.K. Jensen and B.A. Finlayson. Solution of the transport equations using a moving coordinate system. *Advances in Water Resources*, 3:9–18, 1980.

[58] S.B. Jorgensen. Fixed bed reactor dynamics and control — a review. In *Proceedings IFAC Control of Distillation Columns and Chemical Reactors*, pages 11–24, 1986.

[59] Babu Joseph and Coleman Brosilow. Inferential control of processes: part III Construction of optimal and suboptimal dynamic estimators. *AIChE Journal*, 24:500–509, 1978.

[60] Babu Joseph and Coleman B. Brosilow. Inferential control of processes: part I Steady state analysis and design. *AIChE Journal*, 24:485–492, 1978.

[61] Arthur Jutan, J.P. Tremblay, J.F. MacGregor, and J.D. Wright. Multivariable computer control of a butane hydrogenolysis reactor: part I State space reactor modeling. *AlChE Journal 23*, 1977.

[62] Arthur Jutan, J.D. Wright, and J.F. MacGregor. Multivariable computer control of a butane hydrogenolysis reactor: part II Design and on-line implementation of a stochastic controller using an identified multivariable noise model. *AIChE Journal*, 30, 1984.

[63] Arthur Jutan, J.D. Wright, and J.F. MacGregor. Part III On-line linear quadratic stochastic control studies. *AlChE Journal*, 23:751–758, 1977.

[64] Steven M. Kay and Stanley Lawrence Marple. Spectrum analysis - a modern perspective. *Proceedings of the IEEE*, 69:1380–1418, 1981.

[65] Rohit Khanna. *Control Model Development for Packed Bed Chemical Reactors.* PhD thesis, California Institute of Technology, 1984.

[66] Rohit Khanna and John H. Seinfeld. Mathematical modeling of packed bed reactors: numerical solutions and control model development. *Advances in Chemical Engineering*, 13:113–191, 1987.

[67] Raymond E. Kirk and Donald E. Othmer, editors. *Encyclopedia of Chemical Technology.* Interscience Encyclopedia, 1974.

[68] J. Klose and M. Baerns. Kinetics of the methanation of carbon monoxide on an alumina-supported nickel catalyst. *Journal of Catalysis*, 85, 1984.

[69] L.H. Koopmans. *The Spectral Analysis of Time Series.* Academic Press, 1974.

[70] D.J. Kozub, J.F. MacGregor, and Joseph D. Wright. Multivariable control of a catalytic tubular reactor using both Wiener-Hopf controller design and internal model controller design approaches. *IFAC Control of Distillation and Fixed Bed Reactors*, 1986.

[71] S. Kumar and J.H. Seinfeld. Optimal location of measurements in tubular reactors. *Chemical Engineering Science*, 33:1507–1516, 1978.

[72] Leon Lapidus and George F. Pinder. *Numerical Solution of Partial Differential Equations in Science and Engineering.* Wiley-Interscience, 1982.

[73] Alvin Lappinga and Alan Foss. Rapid set point attainment of reactor feed preheat system and coordination with reactor control. In *Proceeding of American Control Conference*, pages 1602–1607, 1984.

[74] Daniel Lee Laughlin. *Control System Design for Robust Performance Despite Model Parameter Uncertainties: Application to Cross-Direction Response Control in Paper Manufacturing.* PhD thesis, California Institute of Technology, 1988.

[75] D.L. Laughlin, K.G. Jordan, and M. Morari. Internal model control and process uncertainty: mapping uncertainty regions for SISO controller design. *International Journal of Control*, 44:1675–1698, 1986.

[76] D.L. Laughlin and M. Morari. Graphical stability analysis for control systems with model parameter uncertainties. *Computer Vision Graphics and Image Processing*, 47:59–76, 1989.

[77] Jay Lee and Manfred Morari. Robust control of nonminimum-phase systems through the use of secondary measurements: inferential and inferential cascade control. *Submitted to Automatica*, 1989.

[78] Jay Lee and Manfred Morari. Robust measurement selection. *Submitted to Automatica*, 1989.

[79] K.S. Lee and Won-Kyoo Lee. On-line optimizing control of a nonadiabatic fixed bed reactor. *AlChE Journal*, 31:667–675, 1985.

[80] K.L Levien, C. Chapat, and M. Morari. RTCP — a software package for experiments in process-control research. *Computers and Chemical Engineering*, 11:227–232, 1987.

[81] Lennart Ljung. On the estimation of transfer functions. *Automatica*, 21:677–696, 1985.

[82] Lennart Ljung. *System Identification - Theory for the User.* Prentice-Hall, 1987.

[83] A.P. Loh, G.O. Corrêa, and I. Postlethwaite. Estimation of uncertainty bounds for robustness analysis. *IEE Proceedings, Pt. D*, 134:9–16, 1987.

[84] Peter J. Lunde and Frank L. Kester. Carbon dioxide methanation on a ruthenium catalyst. *Industrial Engineering Chemistry Process Design and Development*, 13:27–33, 1974.

[85] D. Luss and N.R. Amundson. *AIChE J*, 13:279, 1967.

[86] Jorge Anibal Mandler. *Robust Control System Design for a Fixed-Bed Catalytic Reactor.* PhD thesis, California Institute of Technology, 1987.

[87] P.E. McDermott, D.A. Mellichamp, and R.G. Rinker. Pole-placement self-tuning control of a fixed-bed autothermal reactor, part II: multivariable control. *AlChE Journal*, 32:1015–1024, 1986.

[88] P.E. McDermott, D.A. Mellichamp, and R.G. Rinker. Pole-placement self-tuning control of a fixed-bed autothermal reactor, part I: single variable control. *AlChE Journal*, 32, 1986.

[89] David E. Mears. On criteria for axial dispersion in nonisothermal packed-bed catalytic reactors. *Industrial and Engineering Chemistry Fundamentals*, 15:20–23, 1976.

[90] S.G. Metchis and A.S. Foss. Averting extinction in autothermal catalytic reactor operations. *AIChE Journal*, 33, 1987.

[91] M.L. Michelsen and J. Villadsen. A convenient computational procedure for collocation constants. *Chemical Engineering Journal*, 4:64, 1972.

[92] Manfred Morari and Evanghelos Zafiriou. *Robust Process Control.* Prentice Hall, 1989.

[93] D. Onderwater and J.F. MacGregor. Use of nonlinear transformations and a self-tuning regulator to develop an algorithm for catalytic reactor temperature control. *The Canadian Journal of Chemical Engineering*, 66, 1988.

[94] Andrew K. Packard. *What's New with μ: Structured Uncertainty in Multivariable Control.* PhD thesis, University of California, Berkeley, 1987.

[95] L. Padmanabhan and L. Lapidus. *Chemical Reactor Theory — A Review*, pages 314–399. Prentice Hall, 1974.

[96] Ahmet Palazoğlu and Scott E. Owens. Robustness analysis of a fixed-bed tubular reactor: impact of modeling decisions. *Chemical Engineering Communications*, 59:213–227, 1987.

[97] Stephen C. Paspek, Arvind Varma, and James J. Carberry. Utilization of the recycle reactor in determining kinetics of gas-solid catalytic reactions. *Chemical Engineering Education*, 78, 1980.

[98] S.I. Pereira Duarte, G.F. Barreto, and N.O. Lemcoff. Comparison of two-dimensional models for fixed bed catalytic reactors. *Chemical Engineering Science*, 39:1017–1024, 1984.

[99] Linda R. Petzold. *A Description of DASSL: a Differential/Algebraic System Solver.* Technical Report 82-8637, Sandia National Laboratory, 1982.

[100] I. Postlethwaite, S.D. O'Young, D.W. Gu, and J. Hope. H^{∞} control system design: a critical assessment based on industrial applications. In *10th Triennial World Congress*, pages 301–306, IFAC, 1987.

[101] W.H. Ray. Fixed-bed reactors; dynamics and control. In *Proceedings Second Internation Symposium Chemical Reaction Engineering*, pages 1–19, 1972.

[102] John R. Richards and Phillip D. Schnelle. Perspectives on industrial reactor control. *Chemical Engineering Progress*, October:32–36, 1988.

[103] D.E. Rivera and M. Morari. Control-relevant model reduction problems for SISO H_2, H_∞, and μ-controller synthesis. *International Journal of Control*, 46:505–527, 1987.

[104] D.E. Rivera, C. Webb, and M. Morari. A control-relevant identification methodology. In *Proceedings from Annual Meeting*, AIChE, 1987.

[105] R.B. Root and R.A. Schmitz. An experimental study of steady state multiplicity in a loop reactor. *AIChE J*, 15:670–679, 1969.

[106] P.D. Schnelle and J.R. Richards. A review of industrial reactor control: difficult problems and workable solutions. In *Proceedings of the Third International Conference on Chemical Process Control*, pages 749–802, 1986.

[107] Marvin J. Schwedock, Larry C. Windes, and W. Harmon Ray. Steady state and dynamic modelling of a packed bed reactor for the partial oxidation of methanol to formaldeyde — ii. experimental results compared with model predictions. *Chemical Engineering Communications*, 78:45–71, 1989.

[108] James M. Silva, P. Henrik Wallman, and Alan S. Foss. Multi-bed catalytic reactor control systems: configuration development and experimental testing. *Industrial and Engineering Chemistry Fundamentals*, 18:383–391, 1979.

[109] Jeffrey l. Silverstein and Reuel Shinnar. Effect of design on the stability and control of fixed bed catalytic reactor with heat feedback. 1. Concepts. *Industrial and Engineering Chemistry Process Design and Development*, 21:241–256, 1982.

[110] S. Skogestad and M. Morari. Some new properties of the structured singular value. *IEEE Transaction on Automatic Control*, AC-33:1151–1154, 1988.

[111] Roy Smith. Personal Communication, 1989.

[112] Roy S. Smith and John C. Doyle. Model invalidation: a connection between robust control and identification. *Proceedings from American Control Conference*, 1435–1440, 1989.

[113] Jan P. Sorensen. Experimental investigation of the dynamics of a fixed-bed reactor. *Chemical Engineering Science*, 31:719–725, 1976.

[114] Jan P. Sorensen. Experimental investigation of the optimal control of a fixed-bed reactor. *Chemical Engineering Science*, 32, 1977.

[115] Jan P. Sorensen, Sten Bay Jorgensen, and Karsten Clement. Fixed-bed reactor Kalman filtering and optimal control — I Computational comparison of discrete vs. continuous time formulation. *Chemical Engineering Science 35*, 1980.

[116] B.E. Stangeland and A.S. Foss. Control of a fixed-bed reactor. *Industrial and Engineering Chemistry Fundamentals*, 9:38–48, 1970.

[117] David M. Strand. *Design and Construction of a Fixed Bed, Non-Adiabatic Methanator for Multi-Variable Computer Control Studies.* PhD thesis, California Institute of Technology, 1984.

[118] H. Terndrup, K. Clement, and S. Bay Jorgensen. Multivariable fixed bed reactor control using frequency domain methods. *ACT*, 1983.

[119] Brian Thompson. *Fundamentals of Gas Analysis by Gas Chromatography.* Varian Associated, 1977.

[120] J.P. Tremblay and J.D. Wright. Computer control of a butane hydrogenolysis reactor. *The Canadian Journal of Chemical Engineering*, 52, 1974.

[121] H.B. Vakil, M.L. Michelsen, and A.S. Foss. Fixed bed reactor control with state estimation. *Industrial and Engineering Chemistry Fundamentals*, 12:328–335, 1973.

[122] H. Van Doesburg and W.A. De Jong. Transient behavior of an adiabatic fixed-bed methanator- I: Experiments with binary feeds of CO or CO_2 in hydrogen. *Chemical Engineering Science*, 31:45–51, 1976.

[123] H. Van Doesburg and W.A. De Jong. Transient behavior of an adiabatic fixed-bed methanator- II: methanation of mixtures of carbon monoxide and carbon dioxide. *Chemical Engineering Science*, 31:53–58, 1976.

[124] C. Van Heerden. Autothermic processes: properties and reactor design. *Industrial and Engineering Chemistry*, 45:1242, 1953.

[125] C. Van Heerden. The character of the stationary state of exothermic processes. *Chemical Engineering Science*, 8:133, 1958.

[126] T. Van Herwijnen, H. Van Doesburg, and W.A. De Jong. Kinetics of the methanation of CO and CO_2 on a nickel catalyst. *Journal of Catalysis*, 28:391–402, 1973.

[127] R.Z.C. Van Meerten, J.G. Vollenbroek, M.H.J.M. De Croon, P.F.M.T. Van Nisselrooy, and J.W.E. Coenen. The kinetics and mechanism of the

methanation of carbon monoxide on a nickel-silica catalyst. *Applied Catalysis*, 3, 1982.

[128] M.A. Vannice. The catalytic synthesis of hydrocarbons from H_2/CO mixtures over the group VIII metals: IV The kinetics behavior of CO hydrogenation over Ni catalysts. *Academic Press, Inc.*, 1976.

[129] Sorab Rustom Vatcha. *Analysis and Design of Methanation Processes in the Production of Substitute Natural Gas from Coal.* PhD thesis, California Institute of Technology, 1976.

[130] M. Vidyasagar. *Nonlinear Systems Analysis.* Prentice-Hall, 1978.

[131] J.V. Villadsen and M.L. Michelsen. *Solution of Differential Equation Models by Polynomial Approximation.* Prentice Hall, 1978.

[132] J.V. Villadsen and W.E. Stewart. Solution of boundary-value problems by orthogonal collocation. *Chemical Engineering Science*, 22:1483–1501, 1967.

[133] P. Henrik Wallman and Alan S. Foss. Experiences with dynamic estimators for fixed bed reactors. *Industrial and Engineering Chemistry Fundamentals*, 20:234–239, 1981.

[134] P. Henrik Wallman, James M. Silva, and Alan S. Foss. Multivariable integral controls for fixed bed reactors. *Industrial and Engineering Chemistry Fundamentals*, 18:392–399, 1979.

[135] S-Y Wang, S.H. Moon, and M. Albert Vannice. The effect of SMSI (Strong Metal-Support Interaction) behavior on CO absorption and hydrogenation on Pd catalysts. *Journal of Catalysis 71*, 1981.

[136] Robert C. Weast, editor. *Handbook of Chemistry and Physics.* Chemical Rubber Company, 1975.

[137] Gordon D. Weatherbee and Calvin H Bartholomew. Hydrogenation of CO_2 on group VIII metals: II. Kinetics and mechanism of CO_2 hydrogenation on nickel. *Journal of Catalysis 77*, 1982.

[138] Christopher Webb. *Technical Reference Guide to Experimental Methanation Reactor.* October 1989.

[139] Richard Weber and Brosilow Coleman. The use of secondary measurements to improve control. *AIChE Journal*, 18:614–622, 1972.

[140] Stig Wedel and Dan Luss. Steady-state multiplicity features of an adiabatic fixed- bed reactor with Languir-Hinshelwood kinetics; CO or CO_2 methanation. *Industrial and Engineering Chemistry Fundamentals*, 23:280–288, 1984.

[141] P.B. Weisz and J.S. Hicks. *Chemical Engineering Science*, 17:265, 1962.

[142] G.A. White, T.R. Roszkowski, and D.W. Stanbridge. *Hydrocarbon Processing*, 54:130, 1975.

[143] Larry C. Windes, Marvin J. Schwedock, and W. Harmon Ray. Steady state and dynamic modelling of a packed bed reactor for the partial oxidation of methanol to formaldeyde — i. model development. *Chemical Engineering Communications*, 78:1–43, 1989.

[144] C. Wong, D. Bonvin, D.A. Mellichamp, and R.G. Rinker. On controlling an autothermal fixed-bed reactor at an unstable state — IV Model fitting and control of the laboratory reactor. *Chemical Engineering Science*, 38:619–633, 1983.

[145] J.D. Wright, J.F. MacGregor, A. Jutan, J.P. Tremblay, and A Wong. Inferential control of an exothermic packed bed tubular reactor. In *Proceeding of the American Control Conference*, 1977.

[146] R.E. Young and D.A Mellichamp. Frequency domain estimation of uncertainty descriptions. In *Proceedings from American Control Conference*, 1989.

[147] G. Zames. Feedback and optimal sensitivity: model reference transformations, multiplicative seminorms, and approximate inverses. *IEEE Transactions on Automatic Control*, AC-26:301–320, 1981.